ABSTRACT

Title of Document: CHARACTERISTICS AND CHEMICAL KINETICS OF HYDROGEN SULFIDE COMBUSTION IN THERMAL CLAUS REACTOR

Hatem Mohamed Mohiy Elden Selim, Doctor of Philosophy, 2012

Directed by: Professor Ashwani K. Gupta,
Department of Mechanical Engineering

Hydrogen sulfide is a hazardous gas from both environmental safety and human health perspectives. Hydrogen sulfide presence in any combustion application results in the formation of acidic gases that affects ozone layer and causes acidic precipitation. Exposure to H_2S levels at 100 ppm or higher can endanger human life. Hydrogen sulfide is commonly found to exist in crude natural gas and oil wells. With the decrease in fossil fuels reserves around the world, we will have to rely on extracting energy from wells that contain higher amounts of H_2S. In addition, environmental regulations strictly regulate the H_2S discharge into the atmosphere. Subsequently, efficient hydrogen sulfide treatment becomes of increasing importance with time.

Hydrogen sulfide treatment is typically a chemical reaction process (Claus process) in which hydrogen sulfide is combusted to end-products of sulfur and water. Hydrogen sulfide combustion in thermal Claus reactor has been investigated in this research. A reduced reaction mechanism for H_2S oxidation has been developed using a novel error-propagation-based approach for reduction of detailed reaction mechanisms.

The reduced mechanism has been used for detailed investigation of chemical kinetics mechanistic pathways in Claus process.

Experimental examination of H_2S combustion in different flames, methane/air and hydrogen/air, is provided. Chemical kinetics pathways and reaction conditions responsible for sulfurous compounds formation (SO_2, CS_2, and COS) are addressed. Hydrogen sulfide flame emissions have been investigated for intermediate species identification using chemiluminescence flame spectroscopy. Effect of acid gas composition (H_2S, CO_2 and N_2) on hydrogen sulfide combustion and Claus process efficiency is also provided. Finally, examination of the quality of captured sulfur with respect to reactor conditions is presented.

CHARACTERISTICS AND CHEMICAL KINETICS OF HYDROGEN SULFIDE COMBUSTION IN THERMAL CLAUS REACTOR

By

Hatem Mohamed Mohiy Elden Selim

Dissertation submitted to the Faculty of the Graduate School of the
University of Maryland, College Park, in partial fulfillment
of the requirements for the degree of
Doctor of Philosophy
2012

Advisory Committee
Professor Ashwani K. Gupta, Chair
Professor Ahmed S. Al Shoaibi, The Petroleum Institute, Abu Dhabi
Professor Nam S. Wang
Professor Bao Yang
Professor Kenneth H. Yu, Dean's Representative

DEDICATION

To my parents, my beloved wife, and my children

ACKNOWLEDGMENTS

My experience as a student in The Combustion Laboratory at The University of Maryland has been very fruitful. One result of this experience is the five-year research effort presented in this dissertation. Throughout these years I have also met so many amazing persons. I would like firstly to thank my advisor, Dr. Ashwani Gupta for his sustained support. I have learned from Dr. Gupta the true meaning of hard work and perseverance. I am also grateful to Dr. Ahmed Al Shoabi for his insightful input on my research. I also will never forget the sincere friendship and great memories I have had with all the Lab. members.

I, also, am dearly thankful to my family who gave me nothing but support and belief. I am especially thankful to my father, Dr. Mohiy Selim for his support and inspiration, and my mother, Mrs Hala El Halwagy for all her love. I am also sincerely thankful to my beloved wife, Mai Omar for all the support and all what she sacrificed to company me along in this journey. Also my daughter Farida and my son Malek for all the love and euphoria they filled my life with.

Finally, I would like to express my deep gratitude to The Petroleum Institute, Abu Dhabi and ADNOC for their financial support of this project. I am also grateful to Reaction Design for their support to the numerical part of this research by providing a free license of CHEMKIN-PRO software.

TABLE OF CONTENTS

LIST OF TABLES

LIST OF FIGURES

NOMENCLATURE

A	Major species in the reaction mechanism
B	Minor species in the reaction mechanism
$DERE_{A.i}$	Direct elementary reaction error of species A associated with the removal of elementary reaction *i*
d_o	Outer diameter
d_{in}	Inner diameter
D_{jet}	Burner inner jet diameter
E_{ϕ}	Equivalence ratio uncertainty range
$FA)_{th}$	Theoretical fuel to air ratio
i	Any elementary reactions
j	Any species in reaction mechanism
k_i	Reaction rate coefficient of elementary reaction *i*
N	Total number of species in reaction mechanism
n_R	Total number of elementary reactions
R	Dimensionless radial distance
r_{AB}	Direct interaction coefficient between species A and B
W	Dimensionless axial distance
Y	Mole fraction
ε	Error threshold
δ_B^i	Equal to 1 if reaction *i* contains species B, otherwise equals to zero
$\delta\phi$	Equivalence ratio uncertainty

Φ	Equivalence ratio
Δ	Flow controller error
$\nu'_{i,A}$	Stoichiometric coefficient of species A in reaction *i* in reactants side
$\nu''_{i,A}$	Stoichiometric coefficient of species A in reaction *i* in products side
$\omega_{f,i}$	Forward reaction rate of reaction *i*
$\omega_{b,i}$	Backward reaction rate of reaction *i*
ω_i	Net reaction rate of reaction *i*
$\forall$	Volumetric flow rate

Superscripts

i	Index for elementary reactions
'	Reactants side of an elementary reaction
''	Products side of an elementary reaction

Subscripts

A	Species A
AB	Effect of species B on A
b	backward reaction
f	forward reaction
H_2S	Hydrogen sulfide
i	Index for elementary reactions
in	Inner
jet	burner inner jet
N_2	Nitrogen
O_2	Oxygen

o	Outer
R	Elementary reactions
th	Theoretical
ϕ	Equivalence ratio

CHAPTER 1: INTRODUCTION

This chapter discusses firstly the causes of hydrogen sulfide existence (H_2S) in combustion applications and its hazardous effects on both environment and human health. Secondly, a brief description of H_2S treatment process is provided. Moreover, the motivations and objectives of this research are addressed. Finally, research frame work and approach are briefly presented.

1.1 Hazards of Hydrogen Sulfide

Hydrogen sulfide is known to be present in different quantities in crude natural gas extracted from wells. Hydrogen sulfide poses several hazardous effects on both environment and human health. From the environmental side, H_2S represents an extreme threat on the safety of earth environment. For instance, the use of crude natural gas in any chemical to thermal energy transformation process, e.g. combustion, results in the formation of acid gases such as SO_2 and SO_3. These gases enhance the chances of corrosive acids formation, e.g., H_2SO_4 and H_2SO_3. The formed acids are considered major source of acidic precipitation [1]. Moreover, H_2S combustion can form sulfurous-carbonaceous compounds, for examples, COS and CS_2. These compounds reach stratosphere and generate sulfate aerosol layer [2] which might affect the ozone concentration negatively [3].

On the other hand, hydrogen sulfide causes several hazardous effects on the human health. For instance, H_2S poses irritant and toxic effects on nose, eyes, skin, and respiratory and nervous systems. These effects, attributed to H_2S, depend on H_2S concentration in air and duration of exposure. Low concentrations of H_2S can cause burning and tearing of eyes, headache, dizziness, dyspnea, and skin and throat irritations. Exposure of higher concentrations

of H_2S can cause asphyxiation, loss of consciousness, and death. The US Occupational Safety & Health Administration (OSHA) classified the low-hazard H_2S exposure of 10 ppm or less [4]. The medium-hazard H_2S exposure was considered greater than 10 ppm and less than 30ppm. Higher than 30 ppm was designated as high-risk H_2S exposure. They also stated that exposure to H_2S levels at 100 ppm or higher can endanger human life immediately. It is also worthy mentioning that the foul odor of H_2S, it has the odor of rotten egg, should not be used as means of H_2S detection. This is attributed to the fact that H_2S can disable the olfactory nerves in case of prolonged exposure.

1.2 Hydrogen Sulfide Treatment

The hazardous effects of hydrogen sulfide posed on both environment and human health makes it regulated for discharge into the atmosphere by very strict environmental regulations. Subsequently, crude natural gas must undergo H_2S separation process before it becomes available for utilization. Moreover, separated hydrogen sulfide can not be discharged into the atmosphere; hence it must yield a very effective process of treatment. Separation of pure natural gas occurs in so called amine extraction [5-9] process, while hydrogen sulfide treatment is typically demonstrated in so called Claus process [10-14].

1.2.1 Amine Extraction process

Amine extraction process is used for the separation of H_2S and any other contaminants (mostly carbon dioxide) from crude natural gas. Aqueous solutions of alkaline-based organic compounds are used to absorb H_2S and CO_2 from the fuel stream. The alkaline-based organic compounds are typically alkanolamines which consist of at least one hydroxyl group and one amino group as shown in figure 1-1. Separation process starts with the ionization of H_2S and

CO_2, alkanolamine protonation, and formation of sulfur and bicarbonate salts. Formed salts are cracked thermally to regenerate the alkanolamines and decouple both H_2S and CO_2. Stream of H_2S and CO_2 is called acid/sour gas stream, i.e., it contains acids-forming gases. The following set of reactions describes the amine extraction process of both hydrogen sulfide and carbon dioxide from crude natural gas stream [5]:

$H_2O \leftrightarrow H^+ + OH^-$	(Ionization of water)
$H_2S \leftrightarrow H^+ + HS^-$	(Ionization of dissolved H_2S)
$CO_2 + H_2O \leftrightarrow HCO_3^- + H^+$	(Hydrolysis & ionization of dissolved CO_2)
$RNH_2 + H^+ \leftrightarrow RNH_3^+$	(Protonation of alkanolamine)
$RNH_3^+ + HS^- \rightarrow (RNH_3)HS$	(Formation of alkanolammonium sulfide salt)
$RNH_3^+ + HCO_3^- \rightarrow (RNH_3)HCO_3$	(Formation of alkanolammonium bicarbonate salt)
$(RNH_3)HS \xrightarrow{\text{heat}} RNH_2 \downarrow + H_2S \uparrow$	(Thermal cracking of alkanolammonium sulfide salt to regenerate alkanolamine and release H_2S gas)
$(RNH_3)HCO_3 \xrightarrow{\text{heat}} RNH_2 \downarrow + H_2O + CO_2 \uparrow$	(Thermal cracking of alkanolammonium carbonate salt to regenerate alkanolamine and release CO_2 gas)

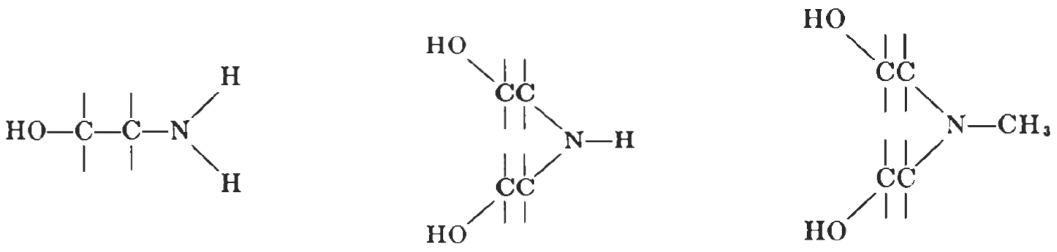

Figure 1-1. Structural composition of primary, secondary, and tertiary alkanolamines [5].

In addition to hydrogen sulfide and carbon dioxide, acid gas can contain nitrogen existing as part of ammonia in the aqueous solution, which is converted into nitrogen and water. Amine extraction process is typically followed by the Claus process for hydrogen sulfide treatment.

1.2.2 Claus Process

Collected hydrogen sulfide undergoes treatment in Claus process wherein reaction between H_2S and O_2 occurs under rich conditions (Φ =3) to form elemental sulfur (S_2). During this reaction one third of H_2S is burned to form SO_2, reaction (1-1). The reaction continues between SO_2 and non-reacted H_2S to form sulfur, reaction (1-2), which is then captured in liquid or solid form. Practically, Claus process is divided into thermal stage followed by catalytic stage. Same chemical reactions take place in both stages. However, catalysts are used in the catalytic stage that possesses significantly lower concentrations of H_2S. The catalytic stage is normally a series of catalytic reactors work successively to enhance efficiency of H_2S treatment process.

$$3H_2S + 1.5O_2 \rightarrow H_2O + SO_2 + 2H_2S, \Delta Hr = -518 \text{ KJ/mol} \quad (1\text{-}1)$$

$$2H_2S + SO_2 \rightarrow 1.5\ S_2 + H_2O, \Delta Hr = 47 \text{kJ/mol} \quad (1\text{-}2)$$

1.3 Motivations and Objectives

Treatment of hydrogen sulfide is of pivotal importance in order to hinder its deleterious effects on both environment and human health. With the shrinking reserves of fossil fuels around the world, we must place increased emphasis on extracting energy from wells that contain higher amounts of hydrogen sulfide.

Since hydrogen sulfide treatment relies primarily on H_2S combustion, better understanding of H_2S reaction chemistry will lead into considerable improvement of the thermal

reactor (stage) of Claus process. This improvement of Claus process thermal stage can reduce the number of catalytic reactors used in the catalytic stage (immense cost savings).

During the process of hydrogen sulfide treatment other sulfur compounds might be formed, such as sulfur dioxide (SO_2), carbonyl sulfide (COS), and carbon disulfide (CS_2). All these compounds are extremely harmful, thus H_2S decomposition does not mean that all its effects have been terminated. Consequently, understanding the conditions under which other sulfur compounds are formed is of pinnacle significance.

Acid gas can contain several contaminants other than hydrogen sulfide. Carbon dioxide and nitrogen are common contaminants to exist in the acid gas stream. Even though these gases might not have the hazardous effects of H_2S, their presence in the acid gas stream might affect H_2S treatment negatively. Accordingly, determination of the effect of these contaminants on H_2S combustion is of acmic importance.

All of sulfur gaseous compounds reflect significantly malignant effects on the environment and the human health. Therefore, the sole means to inhibit H_2S effects is to extract sulfur out of it. Extracted sulfur will have a commercial value, but presence of other contaminants, e.g., CO_2, in acid gas might deteriorate the purity of sulfur. Subsequently, determination of the quality of sulfur collected from H_2S treatment is substantial.

All of the abovementioned motivations have shaped the objectives of our research. Our major research objectives are, firstly, to understand the chemical kinetics of H_2S combustion under different reaction conditions both numerically and experimentally. Understanding the most significant elementary reactions and intermediate species of H_2S reaction will allow us to pinpoint the expected outcome of H_2S combustion. Our second objective is to examine the effect of contaminants other than hydrogen sulfide, mainly CO_2 and N_2, on H_2S reaction. On the other

hand, this will allow us to determine the efficiency of H_2S treatment according to the concentration of other contaminants in the acid gas stream. Our last objective is to examine the quality of captured sulfur with respect to the introduced reactants which are likely to exist in a typical Claus reactor.

1.4 Research Framework

Framework of research presented in this dissertation comprises several approaches in order to achieve the targeted objectives. The first approach was numerical and it aimed to develop a comprehensive reduced reaction mechanism that can successfully represent H_2S combustion. Assumptions, reduction strategy, and error threshold have been defined or chosen to suit the case of study. Aptitude and fidelity of the reduced mechanism have been examined over a wide range of conditions. The reduced mechanism has been used, then, to understand chemistry of H_2S combustion in Claus process.

The second approach was experimental and its target was to determine the behavior of H_2S combustion in different flames, i.e., H_2S is injected in trace amounts into main flame. This approach was subdivided into two steps. Firstly, combustion of H_2S in CH_4/air and H_2/air flames has been explored in order to determine stable combustion products under all examined conditions. Secondly, investigation of H_2S intermediate species has been conducted via H_2S flames spectroscopy.

The third approach was to investigate the effect of contaminants in acid gas (CO_2 and N_2) on sulfur recovery from hydrogen sulfide. This also was an experimental approach wherein carbon dioxide and nitrogen effects on H_2S combustion have been examined. Different concentrations of both gases were used in order to broaden the scope of the study.

The final approach was concerned with the examination of the quality of captured sulfur with respect to reaction conditions. In this approach we have explored experimentally effect of reaction conditions on the allotrope as well as purity of captured sulfur.

CHAPTER 2: LITERATURE REVIEW

This chapter includes an overview of the available literature related to the research presented in this dissertation. Summary of previous approaches, conclusions, and findings are reported. Available literature lies within the scope of our research has been categorized into three sections. The first section covers the contributions of investigators in the development of detailed/reduced reaction mechanisms for hydrogen sulfide combustion. The second section summarizes the previous efforts by researchers exerted to understand the chemistry of hydrogen sulfide combustion both numerically and experimentally. This section comprises the available previous attempts to study and elucidate hydrogen sulfide combustion under any reaction conditions. The third section addresses the hydrogen sulfide flame spectroscopy investigations. Findings and main conclusions about emissions spectra of H_2S flames are listed. It is also vital to emphasize that this chapter sheds light only on the available previous work that has been found, from our point of view, related to the research presented in this dissertation. However, if the readers are interested in finding more details about sulfur chemistry in general, they need to look up other references. For that purpose a good start can be: Levy et al. [15], Cullis et al. [16], Schofield [17], and Hynes et al. [18]. These references cover a considerable amount of the work that has been done previously on sulfur chemistry.

2.1 Development of H_2S Reaction Mechanisms

The hazardous effects of dealing with H_2S combustion experimentally in laboratories forced some researchers to count on numerical simulations for H_2S combustion. In addition, the availability of a reaction mechanism capable of representing H_2S chemical kinetics successfully might make H_2S experiment, ni some cases, dispensable. Subsequently, a lot of attention has

been given to the development of a reaction mechanism that can represent hydrogen sulfide oxidation. One of the early efforts that have been exerted in this regard was by Norrish et al. [19]. They defined a reaction mechanism of H_2S combustion using kinetic spectroscopy and flash photolysis. They found that SH and OH radicals have the most important role in the reaction of H_2S. They divided the reaction into several stages starting with initiation, chain propagation and branching, and chain termination. They defined a group of reactions for each stage of H_2S combustion. The entire reaction mechanism consisted of 13 elementary reactions. Levy et al. [20] built on the work of Norrish and co-workers where they studied $H_2S/O_2/N_2$ combustion in a flat flame burner. Their contribution extended the reaction mechanism to become 18 elementary reactions. They highlighted that radical-radical reactions such as reactions (2-1) and (2-2) should not be neglected.

$$SH + SH \leftrightarrow H_2S + S \qquad (2\text{-}1)$$

$$SH + SH \rightarrow S_2 + H_2 \qquad (2\text{-}2)$$

Muller III et al. [21-23] studied sulfur chemistry in fuel-rich $H_2/O_2/N_2$ flames with 0.25, 0.5 and 1% of H_2S in the mixture. They measured concentrations of SH, S_2, SO, SO_2, and OH using quantitative laser fluorescence measurements. With the help of the aforementioned radical measurements they were able to provide kinetics parameters for various possible intermediate chemical reactions of sulfur compounds. They integrated their work with previous findings to develop a detailed reaction mechanism that included 36 elementary reactions.

Frenklach et al. [24] investigated experimentally the oxidation of H_2S and ignition delay using reflected shock waves. Different concentrations of H_2S in air were tested. They defined formula for the calculation of ignition delay as a function in H_2S concentration and reflected shock temperature. They also developed numerically a reaction mechanism for H_2S oxidation that

reasonably satisfied the experimental results. The reaction mechanism they produced consisted of 17 species and 57 elementary reactions.

Bernez-Cambot et al. [25] studied hydrogen sulfide diffusion-air flame. They divided the reaction into three distinct zones. The first zone is near the fuel-side where H_2S pyrolysis occurs and SO_2 diffuses back from the flame front. The second zone they named it the oxygen-rich zone where H_2 and S are the dominant species of the localized reactions. They defined each zone by a group of chemical reactions. The entire reaction mechanism contained 28 elementary reactions. The third zone is the flame front where both chemical reaction groups overlap.

On the other hand, some researchers did not study H_2S combustion directly, but they contributed into the development of H_2S detailed reaction mechanisms. For instance, Smith et al. [26] investigated the fate of trace amounts of SO_2 introduced into $CO/O_2/Ar$ flame. They investigated the net formation rate of sulfur trioxide using mass spectrometer. They also determined the chemical kinetics parameters of SO_3 elementary reactions as follows:

$$SO_2 + O + M \leftrightarrow SO_3 + M \qquad (2\text{-}3)$$

$$SO_3 + O \rightarrow SO_2 + O_2 \qquad (2\text{-}4)$$

$$K_{2\text{-}3} = 4.4 \times 10^{14} \exp[3163/T] \text{ cm}^6/\text{mol}^2.\text{ s}$$

$$K_{2\text{-}4} = 1.32 \times 10^{12} \exp[-3070/T] \text{ cm}^3/\text{mol.}\text{ s}$$

Zachariah et al. [27] examined the structure of low-pressure-rich H_2/O_2 flames doped with SO_2 both numerically and experimentally. Range of equivalence ratios from 1.35 to 2.4 was discussed. The numerical predictions were conducted using a reaction mechanism that consisted of 44 chemical reactions and 17 species. They defined mechanistic pathways of the dominant reactions as function of the axial distance. The reaction mechanism successfully captured the

details of the reaction. However, hydrogen sulfide was under predicted by ~35% and SH was overpredicted by ~ 60%.

Chernysheva et al. [28] investigated hydrogen sulfide reaction with oxygen under stoichiometric conditions. They developed a detailed reaction mechanism of H_2S combustion that contained 201 reactions and 23 species. They compared the numerical results of their reaction mechanism with experimental data in the literature in order to assure the fidelity of the suggested mechanism. Their mechanism reasonably agreed with most of the experimental data, qualitatively. They highlighted that, H_2S oxidation under stoichiometric conditions is dominated by the following reactions:

$$H_2S + O_2 \leftrightarrow SH + HO_2 \quad (2\text{-}5)$$

$$SH + O_2 \leftrightarrow OH + SO \quad (2\text{-}6)$$

$$SH + O_2 \leftrightarrow SO_2 + H \quad (2\text{-}7)$$

$$SH + O_2 + M \leftrightarrow HSO_2 + M \quad (2\text{-}8)$$

$$SO + O_2 \leftrightarrow SO_2 + O \quad (2\text{-}9)$$

$$H_2S + O \leftrightarrow SH + OH \quad (2\text{-}10)$$

$$H_2S + OH \leftrightarrow SH + H_2O \quad (2\text{-}11)$$

Tsuchiya et al. [29] studied H_2S oxidation using laser photolysis in a shock tube with the atomic resonance absorption spectroscopy as the detection system. They worked on the investigation of three elementary reactions that have important role on H_2S oxidation:

$$SH + O_2 \rightarrow \text{products} \quad (2\text{-}12)$$

$$S + O_2 \rightarrow SO + O \quad (2\text{-}13)$$

$$SO + O_2 \rightarrow SO_2 + O \quad (2\text{-}14)$$

Reaction (2-12) had a lot of controversy in the literature regarding its products. They mentioned that, it has several products channels (HSO+O, SO+OH, SO_2+H, and HO_2+S). They calculated the kinetics parameters of the three reactions (2-12) (considering HSO+O as the products), (2-13), and (2-14). A comparison of Arrhenius plot of those reactions with the literature was conducted. They finally adopted a reaction mechanism that contained 30 elementary reactions to predict H_2S/O_2 combustion numerically.

Glarborg et al. [30-32] have studied in a series of experimental and numerical investigations the effect of SO_2 addition on CO oxidation and recently CO-H_2 mixture [32]. The main conclusion of their work was the negative effect of SO_2 on CO and CO-H_2 mixture oxidation. It was found that SO_2 inhibits CO and CO-H_2 mixture oxidation under the conditions they investigated. It was also proved that under fuel-rich conditions the rate of oxidation inhibition increases. They attributed this to the fact that SO_2 acts as radical sink into the reaction pool where it helps radicals to recombine forming stable species. Reactions (2-15) and (2-16) give a metaphorical example of SO_2 effect on radicals X and Y.

$$X + SO_2 + M \rightarrow XSO_2 + M \quad (2\text{-}15)$$

$$Y + XSO_2 \rightarrow XY + O_2 \quad (2\text{-}16)$$

As a matter of fact reactions (2-3) and (2-4) represent a real case of SO_2 acts as a radical sink. They also compared their experimental results with numerical modeling. The reaction mechanism they adopted consisted of 67 elementary reactions and 23 species. It is also important to mention that they adjusted the reactions parameters of their mechanism along the years.

Sendt et al. [33] constructed a detailed mechanism for H_2–S_2–H_2S system. The reaction mechanism contained 21 reactions and it was developed analytically. They validated their mechanism over a wide range of temperatures (873-1723 K) and pressures (0.04-3 bar). They

also mentioned that the reaction mechanism was extremely sensitive to any changes in the chemical kinetics parameters of reactions responsible for S–S bond:

$$HS_2 + H \leftrightarrow 2\ SH \quad (2\text{-}17)$$

$$H_2S_2 + M \leftrightarrow 2\ SH + M \quad (2\text{-}18)$$

$$H_2S_2 + H \leftrightarrow H_2S + S \quad (2\text{-}19)$$

A detailed sulfur species reaction mechanism was developed by Leeds University research group through a series of studies [34–36]. Blitz et al. [34] studied the reaction between two important intermediate species of H_2S combustion (OH and SO). They calculated the reaction rate coefficient of OH reaction with SO over temperature range of 295-703 K using laser flash photolysis coupled with laser-induced fluorescence (LIF). They defined the reaction rate constant of SO + OH reaction as follows:

$$K = (8.28\pm0.37) \times 10^{-11}\ (T/295)^{-1.35\pm0.11}\ cm^3/mol.s$$

In addition, they stated that reaction of OH/SO is most likely to produce SO_2 and H. However, the reaction occurs on several steps starting with the formation of HOSO. Isomerization of HOSO leads to the formation of HSO_2 which decomposes rapidly to form H and SO_2. The steps that OH/SO proceeds to reach the end-products were ambiguous and needed further work for clarification. In their following study [35] they determined numerically the reaction rate coefficients of all the intermediate steps that were ambiguous:

$$SO_2 + H \rightarrow HSO_2 \quad (2\text{-}20)$$

$$K = 1.76 \times 10^{-15}\ (T^{1.48})\ \exp(-594.6/T)\ cm^3/mol.s$$

$$SO_2 + H \rightarrow HOSO \quad (2\text{-}21)$$

$$K = 5.18 \times 10^{-16}\ (T^{1.61})\ \exp(-3606/T)\ cm^3/mol.s$$

$$SO_2 + H \rightarrow OH + SO \quad (2\text{-}22)$$

$$K = 1.12 \times 10^{-2} (T^{-2.22}) \exp(-15467/T) \text{ cm}^3/\text{mol.s}$$

$$HOSO \rightarrow OH + SO \qquad (2\text{-}23)$$

$$K = 1.92 \times 10^{22} (T^{-9.02}) \exp(-26647/T) \text{ cm}^3/\text{mol.s}$$

They tested the reaction rate coefficients under a wide range of temperatures (300-2000 K) and pressures (10^{-3}-10^{6} atm). They also collaborated with the research group of Dr. Glarborg at The Technical University of Denmark. Glarborg used the reaction rate constants in [35] in one of the studies discussed earlier [31]. In addition, the research group of Leeds University used the developed reaction parameters in their next study of premixed methane flames doped with sulfur and nitrogen [36]. Experimental evaluation of mononitrogen monosulfide (NS) and nitric oxide (NO) was performed using laser induced fluorescence (LIF). The experimental results were compared with numerical simulations which successfully predicted the general trends of both NS and NO. However, significant uncertainties were observed on the results magnitudes. In modification to the reaction mechanism they used, reactions sensitivity analysis had been performed as well as pressure and temperature dependence. Moreover, Arrhenius plots for the elementary reactions were compared with other mechanisms. Several modifications were performed to the mechanism until it reached its final version [37]. The final version of this mechanism included 111 reactions and 41 species.

Cerru et al. [38-39] proposed a detailed reaction mechanism for hydrogen sulfide pyrolysis and oxidation in both laminar and turbulent flames. The mechanism consisted of twelve species and seventy elementary reactions. Comparison of the mechanism with experimental data from the literature revealed that, the mechanism under predicted SO_2 by ~ 31%, and ignition delay time by ~ 35%. On the other hand, they suggested a reduction of the detailed mechanism using sensitivity analysis approach, and implemented steady state

assumption for minor species of HSO, HOSO, $HOSO_2$, H_2S_2, and S. They managed to reduce the reaction mechanism to a six-step reduced mechanism. They compared the 6-step mechanism with their detailed mechanism, experimental data from the literature, and the mechanism of Leeds University. The comparison of the detailed and reduced mechanisms showed good agreement under most of the reaction conditions.

2.2 Hydrogen Sulfide Flame Chemistry

As we mentioned previously H_2S is a very dangerous gas to the surrounding environment. Not only it threats lives and instruments robustness, but also it is a very chemically dominant gas, i.e., it affects the chemical kinetics of any chemical reaction drastically. In addition, taking all the precautious measures to avoid H_2S presence in a reaction might not be sufficient. This is because that, presence of any sulfur compounds such as elemental sulfur or sulfur dioxide will affect the flame chemistry as they are (sulfur and sulfur dioxide) major products of H_2S reaction. In fact, hydrogen sulfide is being formed unintentionally in different chemical [40-44] as well as biological [45-47] applications. Subsequently, presence of hydrogen sulfide can sometimes be inevitable, even though it might not be the target of the application. Furthermore, hydrogen sulfide treatment applications require solid understanding of its chemical kinetics. Because of all these facts a lot of studies were dedicated to the understanding and clarification of hydrogen sulfide chemistry. Investigations started so early in the twentieth century aiming to quantify the basic characteristics of H_2S flame. Along the years, a lot of H_2S flame major features were fully understood, e.g., flammability limits [48,49], ignition delay [24,50], chemical equilibrium [51,52], and flame speed [53,54]. General consensus was observed from the accumulated efforts on a lot of H_2S flame characteristics. However, the pressing need to

thoroughly understand H_2S chemistry forced the researchers to explore more details about H_2S flames.

Levy and Merryman research group studied extensively both hydrogen sulfide and carbonyl sulfide flames in a series of publications [55-59]. Their major focus throughout their work was to track down the formation of different types of sulfur oxides (SO, S_2O, SO_2 and SO_3). For instance, they examined the oxidation of hydrogen sulfide in a flat flame burner under low pressures (0.1 and 0.05 atm). They have modified the sampling procedure from the one they used in previous studies [20,55]. The sampling probe was a quartz tube drawn to a fine tip where an orifice located in the sampled gas passage to assure immediate freeze of the hot gases. This modification allowed the active intermediate species to reach the mass spectrometer without reacting. Sulfur monoxide was not affected by the change in equivalence ratio from stichometric to oxygen-rich conditions. Sulfur dioxide, on the contrary, increased significantly with the increase in oxygen. They highlighted also that S_2O is formed slightly before SO is formed under oxygen-rich conditions. They also suggested possible channels for sulfur monoxide formation in the reaction pool:

$$S + O_2 \rightarrow SO + O \quad (2\text{-}24)$$

$$S_2O + O \rightarrow 2SO \quad (2\text{-}25)$$

$$SH + O \rightarrow SO + H \quad (2\text{-}26)$$

They attributed the formation of S_2O to sulfur monoxide recombination, and the reaction of SO with sulfur:

$$SO + SO \rightarrow S_2O + O \quad (2\text{-}27)$$

$$3\ SO \rightarrow S_2O + SO_2 \quad (2\text{-}28)$$

$$SO + S_n \rightarrow S_2O + S_{n-1} \quad (2\text{-}29)$$

They also dedicated a considerable part of their investigations to the formation of sulfur trioxide in hydrogen sulfide and carbonyl sulfide flames [57-58]. They attributed the formation and depletion of sulfur trioxide in both H_2S and COS flames to reactions (2-30) and (2-31), respectively [57]:

$$SO_2 + O + M \rightarrow SO_3 + M \quad (2\text{-}30)$$

$$SO_3 + O \rightarrow SO_2 + O_2 \quad (2\text{-}31)$$

Moreover, they determined the reaction rate constant of reaction (2-31) for both hydrogen sulfide and carbonyl sulfide flames

$$K_{H2S\ flame} = 6.5 \times 10^{14} \exp(-10800/T)\ cm^3/mol.s$$

$$K_{COS\ flame} = 2.8 \times 10^{14} \exp(-12000/T)\ cm^3/mol.s$$

They stated that reaction (2-31) might not be the only reaction responsible for the SO_3 depletion; reaction (2-32) might pose a significant role as well:

$$SO_3 + H \rightarrow SO_2 + OH \quad (2\text{-}32)$$

Increase in oxygen addition into H_2S and COS flames proved to increase the concentration of SO_3. Similarly, increase in reaction pressure enhanced sulfur trioxide rate of formation. In all cases, SO_3 rate of formation was significantly higher in carbonyl sulfide flames as compared to hydrogen sulfide flames. They ascribed this to the fact that COS flames have lower quantities of hydrogen-containing species; hence reaction (2-32) is marginalized. In addition, having lower quantities of hydrogen-containing species allows higher concentrations of oxygen to exist in the reaction pool, thus reaction (2-30) is maximized.

In a following study [58] they examined the formation of sulfur trioxide in staged combustion of CH_4/H_2S mixture. Staged combustion technique was used to lower NO_x levels in combustion. However, a common setback is the high levels of CO produced in the first stage due to the lack

of oxygen or low reaction temperatures. This might enhance SO_3 formation in the second stage [60]. However, they found that sulfur trioxide enhancement is not significant as compared to single stage combustion. Moreover, controlling time delay of secondary air injection can reduce SO_3 formation drastically. In other words, delay of secondary air injection to the point where temperature is below the required temperature for O-atom formation can minimize SO_3 considerably.

Levy and Merryman also investigated carbonyl sulfide combustion under low pressures [59]. The results revealed that COS flame is divided into two distinct reaction zones. In the first zone, carbon monoxide and sulfur dioxide are formed. In the second zone, carbon monoxide oxidation to carbon dioxide takes place. They suggested a global reaction mechanism that represents the first reaction zone as follows:

$$COS + O_2 \rightarrow CO + SO_2 \qquad (2\text{-}33)$$

Reaction rate constant for reaction (2-33) is:

$$K = 8.2 \times 10^{14} \exp(-29100/T)\ cm^3/mol.s$$

However, they also postulated that reactions (2-34) through (2-36) represent both reaction zones in more details:

$$COS + O \rightarrow CO + SO \qquad (2\text{-}34)$$

$$SO + O_2 \rightarrow SO_2 + O \qquad (2\text{-}35)$$

$$CO + O \rightarrow CO_2 \qquad (2\text{-}36)$$

The research group of Nalbandyan and co-workers has contributed remarkably in clarifying several issues about sulfur chemistry in flames. They have summarized their work on sulfur chemistry in one publication [61] where they discussed their investigations on hydrogen sulfide flames [62-66], carbon disulfide flames [67], vapor sulfur flames [68], and carbonyl

sulfide flames [61] all under low-pressure conditions. Throughout all these studies they used electron spin resonance (ESR) and gas chromatography (GC) in analyzing all the aforementioned flames. For hydrogen sulfide flame, their results revealed that first stage of H_2S combustion includes the formation of H_2, SO_2 and SO. They mentioned that SO consumption and SO_2 formation occurs simultaneously where SO_2 formation ceases with the deletion of SO. By the end of the first stage, hydrogen oxidation coupled with hydroxyl group formation starts to have a more prominent role. They suggested that the presence of H_2S is considered an inhibitor of H_2 oxidation, thus rate of H_2 oxidation is negligible in the first stage. They credited the formation of OH radicals and oxidation of hydrogen to several reactions:

$$H_2 + O \rightarrow OH + H \quad (2\text{-}37)$$

$$H + O_2 \rightarrow OH + O \quad (2\text{-}38)$$

$$H_2 + OH \rightarrow H_2O + H \quad (2\text{-}39)$$

These results agree with the findings of Bernez-Cambot et al. [25], but the major contradiction was the lack of OH presence in the first stage of the reaction.

On the other hand, examination of CS_2 flames revealed that carbon disulfide combustion releases large quantities of atomic oxygen and sulfur monoxide. The addition of trace amount of hydrogen reduced the presence of atomic oxygen considerably. It was also noticed that, under stoichiometric conditions SO mole fraction reaches its maximum, while CS and atomic oxygen are minimal. They studied this phenomenon and found that formation of intermediate compounds such as COS can be the reason. Carbonyl sulfide reacts with atomic oxygen to form sulfur monoxide [69,70]:

$$COS + O \leftrightarrow SO + CO \quad (2\text{-}40)$$

Nalbandyan and co-workers studies also sulfur flames under low pressure conditions. They have dedicated a separated reactor to generate sulfur vapor that can be used in their experiments. Flame analysis using ESR revealed that sulfur vapor oxidation produces significant amounts of atomic oxygen and sulfur monoxide in the reaction pool. Under some conditions, amount of atomic sulfur was about one third of the introduced molecular oxygen. Addition of trace amounts of methane reduced the formed atomic oxygen significantly.

The same research group also investigated the combustion of carbonyl sulfide under low pressure conditions. The results assured that COS combustion produced high amounts of atomic oxygen and sulfur monoxide. It is worthy mentioning that our discussion about the efforts of Nalbandyan research group has been drawn from reference [61]. References [62] to [68] are Russian references, but we cited them in case the reader has an access to their English translation.

Dowling et al. [71] investigated the reaction between sulfur (S_2) and hydrogen to form hydrogen sulfide, reaction (2-41):

$$H_2 + ½\ S_2 \rightarrow H_2S \qquad (2\text{-}41)$$

This reaction represents practically the recombination of hydrogen and sulfur formed in Claus reactor to form hydrogen sulfide. This is unfavorable because it decreases Claus process performance drastically. Therefore, they have studied the rate of recombination of hydrogen and sulfur in Claus process under wide range of temperatures (602-1290 °C) and residence times (0.03-1.5 s). They provided a definition of the rate of recombination reaction (2-41) as follows:

$$-d[H_2]/dt = k_1\ [H_2][S_2] - K_2\ [H_2S]$$

As expected, formation of hydrogen sulfide increased with the increase of reactor temperature and residence time. They recommended the suggestion of Chen et al. [72] that introducing Claus

process effluent gases early enough into a waste heat boiler will freeze the recombination reaction of H_2 and sulfur instantaneously.

Research group of Hawboldt et al. paid a lot of attention to hydrogen sulfide chemistry under Claus process conditions. They first investigated the reaction between hydrogen sulfide and sulfur dioxide which is a pivotal reaction in Claus process [73]. They investigated the reaction in isothermal reactor under wide range of temperatures (850-1150 °C) and residence times (0.05-1.2 s). They developed a kinetic rate expression for SO_2 reaction with H_2S:

$$r = A_f \exp^{E_{af}/RT} P_{H_2S} P_{SO_2}^{0.5} - A_r \exp^{E_{ar}/RT} P_{H_2O} P_{S_2}^{0.75}$$

where,

A_f = 15762 (±1200) mole/cm^3.s atm$^{-1.5}$

E_{af} = 49.9 (± 0.3) kcal/mol

A_r = 506 (±50) mole/cm^3.s atm$^{-1.75}$

E_{ar} = 44.9 (±0.5) kcal/mol

They also studied the rate of hydrogen sulfide pyrolysis in Claus reactor isothermally under wide range of temperatures (850-1150 °C) and residence times (0.5-1.5 s) [74]. They developed a kinetic rate expression for SO_2 reaction with H_2S:

$$r = A_f \exp^{-E_{af}/RT} P_{H_2} P_{S_2}^{0.5} - A_r \exp^{-E_{ar}/RT} P_{H_2} P_{S_2}^{0.75}$$

where,

A_f = 5260 (±260) mole/cm^3.s/atm$^{1.5}$

E_{af} = 45 (± 0.3) kcal/mol

A_r = 14 (±1) mole/cm^3.s/atm^2

E_{ar} = 23.4 (±0.2) kcal/mol

They similarly investigated the rate of pyrolysis and oxidation of ammonia in Claus process [75]. The expressions of rate of ammonia pyrolysis and oxidation respectively are as following:

$$r = A \exp^{-E_a / RT} P_{NH_3}^{1.25}$$

where,

A = 0.00421 mole/cm^3.s/atm$^{1.25}$

E_a = 16.5 kcal/mol

$$r = A \exp^{-E_a / RT} P_{NH_3} P_{O_2}^{0.75}$$

where,

A = 4430 mole/cm^3.s/atm$^{1.75}$

E_a = 40 kcal/mol

In addition to Hawboldt research team, other researchers dedicated a lot of effort to investigate hydrogen sulfide pyrolysis. The importance this topic gained recently is attributed to the potential of H_2S to become an energy source along with the hindrance of its harmful effects. Several research groups derived chemical kinetics rate of dissociation of H_2S under wide range of temperatures, residence times, and pressures [76-77]. Others examined hydrogen sulfide dissociation in presence of catalysts that reduces the required temperatures for high dissociation rates of H_2S. Several catalysts were used for this aspect such as alumina [78] and molybdenum sulfide [79-80].

Slimane at al. [81] investigated numerically partial combustion of hydrogen sulfide under super-adiabatic conditions. The have examined different acid gas compositions and oxidizers (20% H_2S, 80% N_2)/air, (20% H_2S, 80% N_2)/O_2, 100% H_2S/air, 100% H_2S/O_2, (25% H_2S, 75% N_2)/air, and (25% H_2S, 75% N_2)/O_2. The focus of the study was to optimize the hydrogen yield under all examined conditions. The results revealed that high H_2 and low SO_2 yield were

achieved under ultra fuel-rich conditions (equivalence ratios above 6). Using oxygen as an oxidizer shifts the favorable conditions of high H_2 yield to higher equivalence ratios above 12.

Montoya et al. [82] have conducted quantum chemical calculations in order to study the interaction between hydrogen sulfide and molecular oxygen. They defined the possible channels of H_2S reaction with O_2 as follows:

$$H_2S + O_2 \leftrightarrow HO_2 + SH \quad (2\text{-}42)$$

$$H_2S + O_2 \leftrightarrow HSO + OH \quad (2\text{-}43)$$

$$H_2S + O_2 \leftrightarrow SO + H_2O \quad (2\text{-}44)$$

$$H_2S + O_2 \leftrightarrow SO_2 + H_2 \quad (2\text{-}45)$$

They presented the possible isomers from $[H_2,S,O_2]$ that might be formed during the interaction of H_2S and O_2. They defined seven isomers based on lengths of the chemical bonds. With the help of previous findings [83-84] they successfully determined the energy level of each isomer. Based on the energy levels they determined the most favorable reaction path of H_2S/O_2 interaction. They found that reaction (2-42) is the most favorable and dominant reaction of H_2S/O_2 interaction.

2.3 Hydrogen Sulfide Flame Spectroscopy

Even though all the previously discussed efforts have provided extensive knowledge about H_2S combustion, the role of intermediate species is still controversial. The main reason is that all experimental gas analyzers (gas chromatograph, FTIR and mass spectrometer) can only give the analysis of stable combustion byproducts. The deficiency of gas analyzers to detect intermediate species substantiated the use of flame spectroscopy techniques in H_2S/O_2 combustion so as to track the behavior of intermediate spices and to give full interpretation of

H_2S combustion. All flame spectroscopy techniques rely on the analysis of different flame spectra. The basic flame spectra [85] are line spectra (emitted or absorbed), band spectra, and continuous spectra (continuum). Generally, spectra are emanated from transition of an electron from one energy level to another. It has been found that, each flame has its own characteristic spectrum which is generated by species in this flame. Knowing the species (intermediate or stable) that responsible for each line/band/continuum spectrum will augment the understanding of flame chemistry. Subsequently, several studies have been dedicated to the investigation of flame spectroscopy, generically, and hydrogen sulfide flame spectroscopy in specific.

Numerous researchers have investigated the absorption bands of sulfurous compounds in flames. One of the early studies in this regard was conducted by Lewis et al. [86]. They investigated the presence of SH absorption bands. The radical of SH was obtained by giving pulses of radiofrequency current to hydrogen sulfide. The radiofrequency pluses were synchronized to immediately precede the flashlight to be absorbed by SH. They were successfully able to find one band of SH absorption at 323.7nm.

Fuwa et al. [87] investigated the presence of sulfur dioxide ultraviolet absorption bands. They designed and fabricated atomic absorption instrument which is fully described in a previous paper of theirs [88]. The setup consisted of a light source, absorption cell, burner, light dispersing elements, and detectors. Their results revealed that sulfur dioxide has a strong absorption band with 200-230 nm, and a less important absorption band within 250-300 nm.

Ding et al. [89] investigated the absorption spectrum of hydrogen sulfide between 1000 and 1048.2 nm. The strongest absorption bands of H_2S were found between 1015.7 nm and 1021.97 nm. They have compared their results with previous work [90-91] and their results

showed good agreement with the available data in the literature. On the other hand, Syty et al. [92] found a strong absorption band of H_2S within 180-220 nm.

Other researchers paid a lot of attention to the non-intrusive investigation of excited species chemiluminescence in flames which was verified to be an efficient technique for qualitative detection of radicals in flames.

Toyoda et al. [93] studied the emission spectra of carbon disulfide and hydrogen sulfide along with other non-sulfurous compounds. The species of interest were being excited using controlled electron beam. A heated tungsten filament was used as electron source. Emission spectrum of carbon disulfide showed the most intense bands at 282 nm and 285 nm. Hydrogen sulfide emission spectrum showed strong bands at 486, 434, 410, 397, and 389 nm which are attributed to the hydrogen Balmer series [94-95].

Folwer et al. [96] studied the spectrum of carbon disulfide, sulfur and hydrogen sulfide flames. They found that CS_2 flame emissions extend from ultraviolet to blue wavelength. They attributed the formation of bands primarily to the presence of S_2 and SO. Sulfur bands were found to be absorption bands, but they were obtained as emitting bands when a stream of oxygen was directed into the flame. Sulfur monoxide emission bands were feebly obtained as compared to S_2 bands. The examination of sulfur and hydrogen sulfide flame spectra showed similar patterns as compared to CS_2 flame spectrum. They only highlighted that hydrogen sulfide flame spectra showed observable OH bands.

Gaydon et al. [97] studied the spectra and characteristics of hydrocarbon flames containing small amounts of SO_2 and SO_3. The results showed band systems for S_2, CS, SO, and SH and they discussed the mechanisms of the formation of these radicals. A strong ultraviolet

emission band was also observed and they attributed this to the reaction between SO_2 and atomic oxygen to form SO_3.

$$SO_2 + O \leftrightarrow SO_3 + 81 \text{ kcal} \quad (2\text{-}46)$$

Other research groups dedicated their efforts to the investigation of continuum emissions from sulfur compounds in flames. The most famous continuum spectrum in flames of sulfur compounds is sulfur dioxide afterglow.

Gaydon research group was one of the first groups to investigate the phenomenon of sulfur dioxide afterglow [98]. They generated the SO_2 afterglow by subjecting purified liquid sulfur dioxide to intense discharge of two aluminum electrodes. They obtained strong violet-blue afterglow in the range of 260-470 nm. They found SO_2 absorption bands superimposed on the continuum within 280-315 nm. They also considered the series of peaks superimposed on the afterglow continuum in the range of 382.8-469.9 nm are emanated from different excited species. The most prominent species responsible for those peaks were sulfur monoxide, sulfur dioxide, oxygen, and sulfur (S_2).

Mulcahy et al. [99] investigated sulfur dioxide afterglow during the reaction between SO_2 and atomic oxygen. They found that SO_2 afterglow starts around 280 nm and diminishes nearly at 500 nm. They credited the occurrence of sulfur dioxide afterglow to the following group of reactions:

$$SO + O \leftrightarrow SO_2^* \quad (2\text{-}47)$$

$$SO_2 + O + O \leftrightarrow O_2 + SO_2^* \quad (2\text{-}48)$$

Reaction (2-47) contributes significantly in SO_2 afterglow in case of high atomic oxygen concentrations. On the other hand, they considered reaction (2-48) to occur on two steps:

$$SO_2 + O + M \leftrightarrow SO_3^* + M \quad (2\text{-}49)$$

$$SO_3^* + O \leftrightarrow {}^1SO_2^* + O_2 \quad (2\text{-}50a)$$

$$SO_3^* + O \leftrightarrow {}^3SO_2^* + O_2 \quad (2\text{-}50b)$$

Singlet and triplet SO_2 afterglow emissions are formed through reactions (2-50a) and (2-50b), respectively. Singlet SO_2 emissions represents the stronger part of the afterglow continuum around 350 nm. However, triplet emissions are responsible for the weaker part of the afterglow around 425 nm.

Halstead et al. [100] examined sulfur dioxide afterglow emanated from reaction between sulfur dioxide and atomic oxygen. They defined the recombination reactions in SO_2 afterglow as follow:

$$SO_2 + O + M \leftrightarrow SO_3^* \quad (2\text{-}51)$$

$$SO + O \leftrightarrow SO_2^* \quad (2\text{-}52)$$

They considered reaction (2-52) to be the dominant reaction that is responsible for SO removal. They also found that SO_2 afterglow intensity at pressures between 0.25 and 0.3 mmHg to be:

$$I = 1.5 \times 10^8 [O] [SO] \text{ cm}^3/\text{mole.s}$$

The presented literature review is a skim through the efforts of pioneers and researchers of sulfur chemistry, generically, and hydrogen sulfide chemistry in specific. We gratefully praise all efforts exerted to clarify issues that could have been obstacles for new researchers unless they were previously addressed. In this dissertation we are building on previous findings about the chemistry of hydrogen sulfide combustion and addressing some areas that are lacking some clarification.

CHAPTER 3: REDUCED MECHANISM FOR HYDROGEN SULFIDE OXIDATION

Computational fluid dynamics (CFD) simulations gained considerable potential in combustion applications lately due to several reasons. Firstly, sound numerical simulations can provide solid platform of information for experimental investigations. Moreover, preparing a running experimental setup equipped with the needed diagnostics can be very expensive and time-consuming. Therefore, CFD simulations might solve a lot of problems that can be encountered in experimental setups. However, CFD simulations of combustion applications are very problematic and challenging because of the high number of species and elementary reactions in reaction mechanisms. This leads to an immense increase in the number of conservation equations and source terms. Consequently, one encounters higher computational cost, code crash, and divergence possibility. However, most of the detailed reaction mechanisms contain several marginal species and elementary reactions that nearly do not affect the chemical kinetics of the process. Therefore, reduction of detailed reaction mechanisms can be very crucial in terms of computational cost savings and code convergence improvement. In this chapter we present systematic procedure of H_2S reaction mechanism reduction. The procedure starts with representation of the detailed reaction mechanism, preliminary reduction procedure, reduction strategy, and comparison and validation. Finally, numerical investigation of the chemical kinetics of H_2S combustion using the reduced mechanism is conducted.

3.1 Detailed Mechanism, Temperature Range, and Major Species

As we discussed in chapter 2, several detailed reaction mechanisms for H_2S combustion have been developed. In this dissertation we have chosen the reaction mechanism developed by Leeds University [37]. This reaction mechanism has been developed, modified, and validated by the research group of Leeds University. It has been reported widely in the literature as one of the most comprehensive reaction mechanisms for H_2S combustion. It consists of 111 revisable elementary reactions which are formed a total of 41 species.

The purpose of having reduced reaction mechanisms is to efficiently simplify and understand combustion processes in practical applications. Accordingly, we have examined the reduced mechanism of H_2S combustion, firstly, under the most favorable reaction conditions of Claus process (prominent application of H_2S combustion). We, then, have broadened the range of temperatures and equivalence ratios for the reduced mechanism validation. Figure 3-1 describes the effect of Claus reactor temperature on S_2 equilibrium mole fraction and conversion efficiency of Claus process.

$$\text{Conversion Efficiency} = \frac{\text{Mass of recovered sulfur}}{\text{Mass of sulfur in inlet } H_2S}$$

One can see that maximum conversion efficiency lies within the temperature range of 1600-1700 K. In this study, we broadened this range of temperatures to extend the range of applicability of our reduced mechanism. The temperature range of our study is 1400-1800 K. On the other hand, the reduced mechanism has been compared with the detailed mechanism under three equivalence ratios, fuel-rich (Claus conditions, Φ=3), stoichiometric conditions (Φ=1), and fuel-lean conditions (Φ=0.5).

It was also crucial to define the major species in the reduced mechanism. The major species are the species we aim to keep their trends and values unaffected in the reduced mechanism except within a predefined error threshold. Generally, the major species would be the reactants and the major products. In this reduction strategy we have defined the major species to be H_2S, O_2 as the reactants, and SO_2, H_2, S_2, and H_2O as the major products.

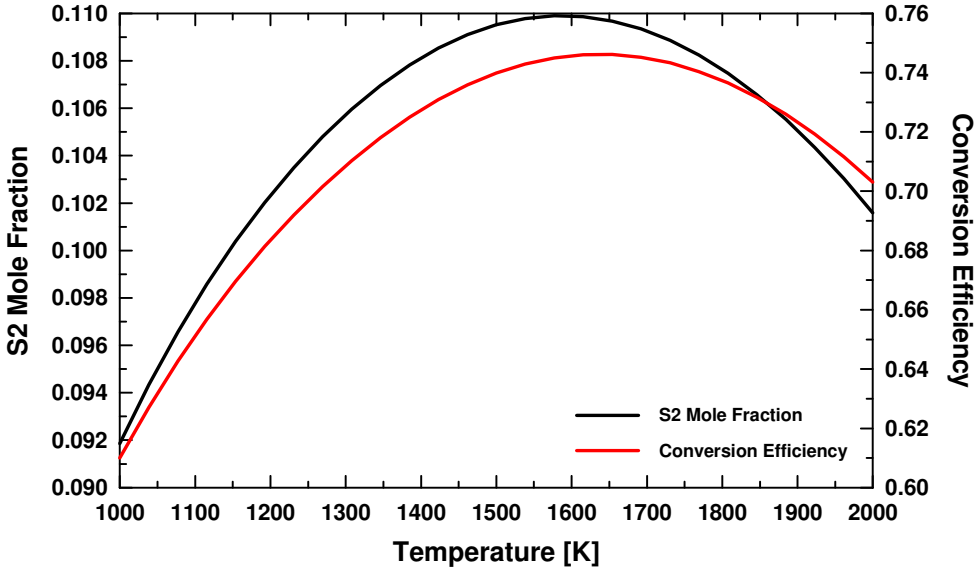

Figure 3-1. Effect of change in reactor temperature on conversion efficiency and S_2 mole fraction in Claus process.

3.2 Reduction Methodology

In this section we introduce a preliminary reduction procedure for the detailed mechanism of Leeds University, the inclusive reduction strategy of the detailed mechanism, and the novel approach we have developed for detailed reaction mechanisms reduction.

3.2.1 Preliminary Reduction Procedure

The reduced mechanism is dedicated primarily to reaction simulations of Claus process, which works at fuel-rich conditions. Although nitrogen is not considered an inert gas within the examined temperature range, the very-rich conditions of the mixture will significantly reduce the

likelihood of its reaction. Moreover, it is not favorable to combust H_2S with air while nitrogen is considered a burden in terms of reducing the overall mixture temperature. On the other hand, methane, in the form of natural gas, is separated from hydrogen sulfide in amine extraction process which always precedes the Claus process. Considering these two facts, reactions that involve carbon or nitrogen are unlikely to occur. Therefore, any reaction or species that contains nitrogen or carbon will be excluded from the detailed reaction mechanism. Implementation of this preliminarily procedure in this study reduced the detailed mechanism down to 86 elementary reactions, and 25 species.

3.2.2 Direct Relation Graph and Error Propagation Methodology

The DRGEP [101-102] is used to form a reduced skeletal mechanism from detailed ones. This methodology depends on the elimination of species that do not have neither qualitative nor quantitative significant effect on the major species. This is being achieved by applying two main approaches on the reaction mechanism. The first approach is the direct relation graph (DRG) while the second approach is the error propagation (EP).

3.2.2.1 Direct Relation Graph (DRG) Approach

The direct relation graph approach is used to provide a relation between major species and all minor species that are directly related, i.e. exist simultaneously, in a group of elementary reactions. It is called direct relation graph because each relation between two species can be represented by a curve on a graph. This relation would be based on the reaction rate analysis. Direct interaction coefficient (r_{AB}) is a parameter that defines the relationship between every major species and all other species. For instance, assume species A and B in a detailed mechanism. The effect of species B on species A, given that they are directly related in one or more elementary reactions, will be determined as follows [101]:

$$r_{AB} = \frac{\left|\sum_{i=1,n_R} \nu_{i,A}\omega_i\delta_B^i\right|}{\max(P_A, C_A)} \quad \text{(Eq.3.1)}$$

where,

$$P_A = \sum_{i=1,n_R} \max(0, \nu_{i,A}\omega_i) \quad \text{(Eq.3.2)}$$

$$C_A = \sum_{i=1,n_R} \max(0, -\nu_{i,A}\omega_i) \quad \text{(Eq.3.3)}$$

$$\omega_i = \omega_{f,i} - \omega_{b,i} \quad \text{(Eq.3.4)}$$

$$\nu_{i,A} = \nu''_{i,A} - \nu'_{i,A} \quad \text{(Eq.3.5)}$$

In these equations ω_i, $\omega_{f,i}$, and $\omega_{b,i}$ are the net, forward, and backward reaction rates respectively. Stoichiometric coefficients of species A in reaction *i* are $\nu''_{i,A}, \nu'_{i,A}$, while δ_B^i equals 1 if reaction *i* contains species B, and zero elsewhere. From (Eq.3.2) and (Eq.3.3) one can notice that the denominator of (Eq.3.1) should be positive. This denominator denotes the total reaction rate of all the elementary reactions that include species A. On the other hand, the numerator of (Eq.3.1) is the reaction rate of only the elementary reactions that include species A and B simultaneously. If the elementary reaction does not include species A, then $\nu_{i,A}$ will be zero. Similarly, if the reaction does not have species B, then δ_B^i will be zero. Therefore, the numerator of (Eq.3.1) will count only for elementary reactions that include both species A and B. The physical meaning of r_{AB} is the error that would reflect on species A if species B is discarded from the detailed mechanism. By defining a reasonable threshold (ε) one can discard any species (B) with r_{AB} less than (ε). In prior research, r_{AB} has been defined with the modulus value in the numerator inside the summation sign [102]. This means that reaction rates of all elementary reactions will be

counted and divided by the denominator. This expression is not perfectly true; assuming two elementary reactions for species A and B with the same reaction rate:

$$A \xrightarrow{k_1} B$$

$$B \xrightarrow{k_2} A$$

Exclusion of species B from the reaction mechanism will not have any effect on species A if the two elementary reactions have the same reaction rate. Therefore, it would be more meaningful to use the modulus sign after summation of reaction rates. It is also worthy to highlight that the definition of (r_{AB}) calculates solely the error associated with discarding species B. In other words, if another species C would be discarded, the total error in A would be summation of r_{AB} and r_{AC}.

Figures 3-2 and 3-3 show examples of the direct interaction coefficient of SO_2 and H_2S respectively with some minor species. In this case, j denotes any minor species. The reaction rates have been calculated using CHEMKIN-PRO software. The inlet conditions are Claus conditions (Φ=3) so that H_2S reacts with O_2 in a continuously stirred tank reactor (CSTR) under steady state conditions.

Implementation of the DRG approach with an error threshold of 0.5% reduced the detailed mechanism down to 37 elementary reactions with only 14 species, see appendix A. The threshold was chosen after trying several values and comparing the gain (number of removed species) to the corresponding error. It was found that increase in threshold value above 0.5% will not provide any additional benefit. The discarded species are SO_3, $HOSO_2$, HOS, HSOH, H_2SO, HOSHO, H_2S_2, H_2SO_4, HSO_2, HOSO, and HO_2.

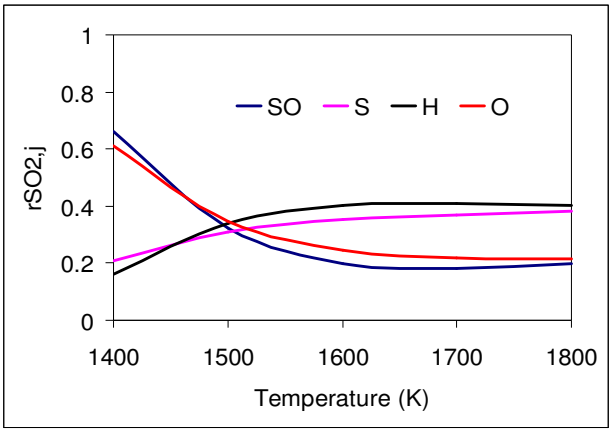

Figure 3-2. Direct interaction coefficient of SO_2 with minor species (SO, S, H, and O) at different reactor temperatures.

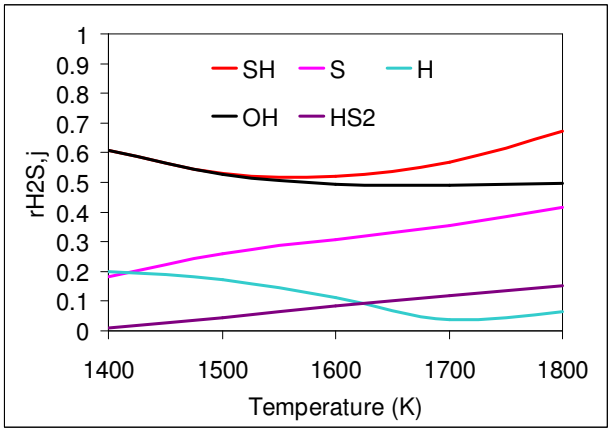

Figure 3-3. Direct interaction coefficient of H_2S with minor species (SH, S, H, OH, and HS_2) at different reactor temperatures.

3.2.2.2 Error Propagation (EP) Approach

The second approach we used to reduce H_2S/O_2 reaction mechanism is the error propagation approach. Although we already discarded the insignificant minor species, it is possible to shrink the number of minor species even further by applying the error propagation approach [101]. The key principle of this approach is that not all the minor species are directly related to the major species, yet this does not mean they do not affect the reaction mechanism. Error propagation approach is used to determine the effect of minor species on a major species that is not directly related to it. Figure

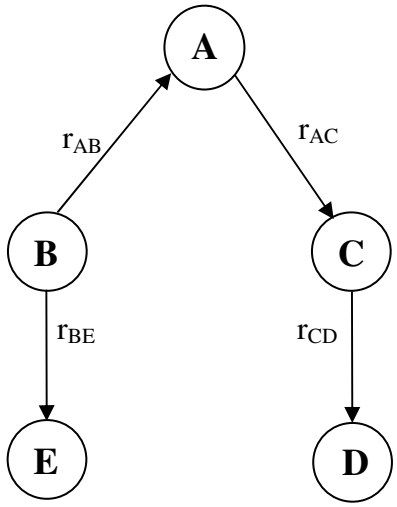

Figure 3-4. Five species reaction mechanism, Species A is major species; species B, C, D, and E are minor species.

3-4 shows the principle of the error propagation approach. Assuming that A is a major species and it is directly related to species B and C and indirectly related to species D and E. One can determine whether species B and C affect species A significantly or not by calculating (r_{AB} and r_{AC}). However, species D and E are not directly related to species A, thus r_{AE} and r_{AD} are zero. However, this does not mean that species E and D are not important. They will affect species B and C by the value of r_{BE} or r_{CD} which, in turn, will affect the major species A. The error associated with the removal of species E or D on species A is quantified as follows:

$$r_{AE} = r_{AB} \text{ x } r_{BE}$$

$$r_{AD} = r_{AC} \text{ x } r_{CD}$$

Exclusion of an indirectly related species may cause, in some cases, higher error than the error associated with the removal of a directly related species. Implementation of this approach might not be useful after using the direct relation graph approach; especially, in case of light fuels reaction mechanisms where elementary reactions are not numerous. In our case, implementation of EP approach reflected significant error on major species, thus it failed to reduce the reaction mechanism any further.

3.2.3 Direct Elementary Reaction Error (DERE) Approach

We have developed a novel approach that allows further reduction to the already reduced reaction mechanism. Direct elementary reaction error approach (DERE) is based on discarding specific elementary reactions that do not have a significant effect on the major species. In other words, it allows the exclusion of elementary reactions while keeping the same number of species. The following equation provides the corresponding error to the removal of elementary reaction *i*:

$$DERE_{A,i} = \sum_{N\ species} \left(\left(\frac{\nu_{i,B}\,\omega_i}{\underbrace{\sum_{i=1,n_s} \left| \nu_{i,B}\,\omega_i \right|}_{P}} r_{jB} \right) r_{Aj} \right)$$

where, $DERE_{A.i}$, direct elementary reaction error, is the error that appears in major species A with the elimination of elementary reaction *i*. On the other hand, *j* represents any species in the reaction mechanism. The number of species in the mechanism is denoted by N; r_{jB} is the direct interaction coefficient between species *j* and B; B is a specie(s) that is included in the discarded elementary reaction *i*. Term P represents the error produced in species B by removing elementary reaction *i* from the reaction mechanism. The multiplication of term P with $r_{jB,}$ represents the error propagated into each species in the mechanism due to elimination of elementary reaction *i*. This error in each species will propagate further to affect the major species A by r_{Aj}. This approach must be repeated for every species B included in elementary reaction *i.* Figures 3-5 and 3-6 depict examples of DERE for two elementary reactions in the 37-reactions mechanism. It is noticeable that these two reactions have negligible effect on O_2 species, i.e., elimination of these two reactions does reflect noticeable error on oxygen mole fraction. On the other hand, reaction $HS_2 + H \leftrightarrow S_2 + H_2$ affects hydrogen mole fraction negatively, i.e., elimination of this elementary reaction reduces H_2 mole fraction based on the reactor temperature. Similarly, discarding reaction $S_2 + O \leftrightarrow SO + S$ will produce error in S_2 mole fraction. However, this error will be an increase in S_2 mole fraction that varies according to the reactor temperature.

In order to optimize the number of discarded species, DERE has been evaluated for all the 37 reactions in the reduced mechanism for every major species over the temperature range of interest. Brute-force algorithm [103] code and JAVA software has been utilized to discard the maximum number of elementary reactions with the least possible error. The code takes input of

DERE values for every major species at each temperature. It, then, calculates the maximum number of DERE values to be eliminated within the assigned error threshold at every temperature for every major species. DERE values eliminated at each temperature and for each species correspond to elementary reactions that can be removed safely from the mechanism. It is to be noted that exclusion of two elementary reactions may produce no error if they affect the major species by the same error magnitude but with different signs. Figure 3-7 shows a simple flow chart of the aforementioned code. Appendix B shows the brute-force code conducted for the purpose of discarding the elementary reactions.

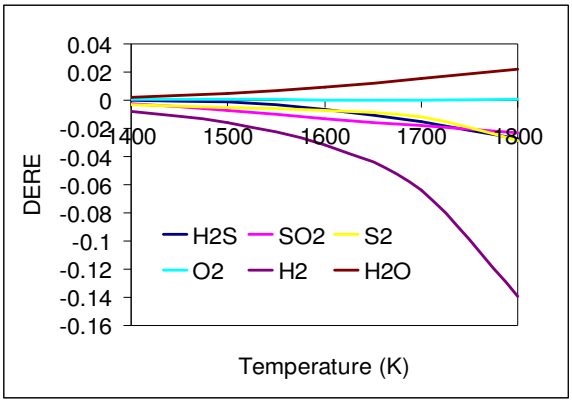

Figure 3-5. DERE of major species for $HS_2 + H \leftrightarrow S_2 + H_2$ reaction.

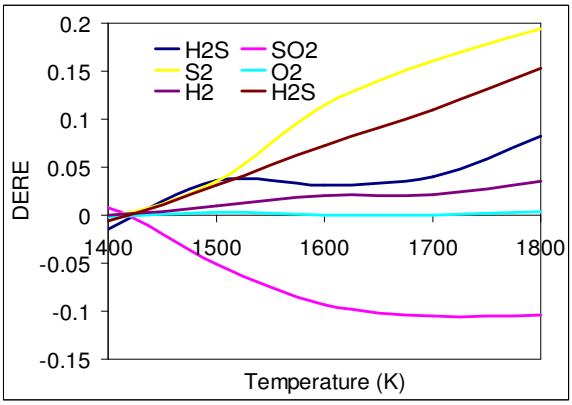

Figure 3-6. DERE of major species for $S_2 + O \leftrightarrow SO + S$ reaction.

Implementation of this novel approach has enabled us to discard 18 elementary reactions from the 37-reactions mechanism with a maximum error of ~15%. Figure 3-8 shows the number of excluded elementary reactions with respect to the associated error. One can see that error increases monotonically up to the exclusion of 18 elementary reactions. However, elimination of one additional reaction results in abrupt increase in the absolute error. Subsequently, it was reasonable to eliminate only 18 elementary reactions of the 37- reactions mechanism. Eliminated reactions are shown in appendix A (italicized reactions). This novel approach allowed us to

reduce the 37-reaction mechanism by more than 48% with absolute maximum error of only 15%. At the present time DRGEP methodology could not reduce the 37-reactions mechanism any further.

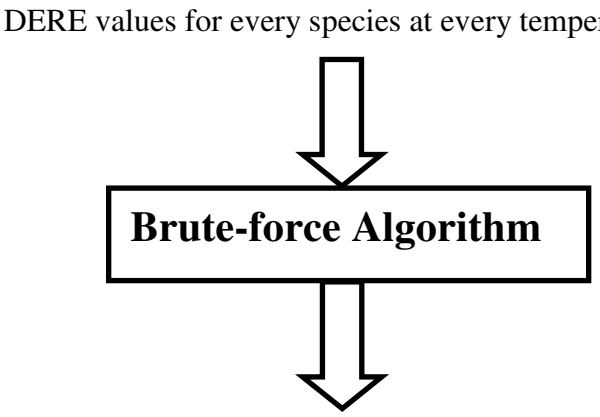

Figure 3-7. Flow chart of the algorithm used for discarding specific elementary reactions.

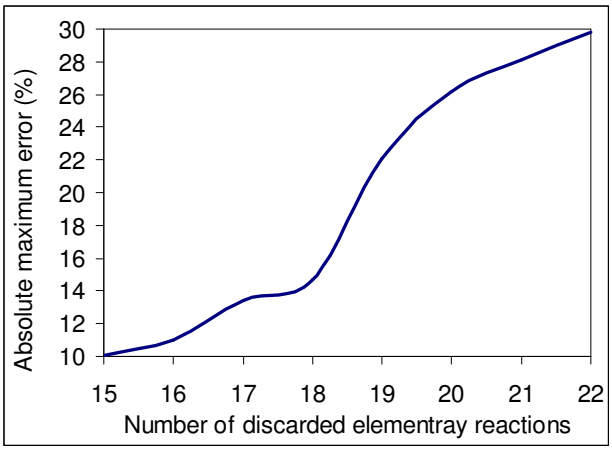

Figure 3-8. Relation between number of discarded elementary reactions and the corresponding error reflected on the reaction mechanism.

3.3 Reduced Mechanism Validation

Validation of the 19-reactions reduced mechanism starts with comparison with the Leeds University detailed mechanism at different conditions. The first comparison is conducted using CHEMKIN-Pro software under Claus conditions. Reactants inlet mole fractions are 0.333 for oxygen and 0.667 hydrogen sulfide which result in an equivalence ratio of 3. The reactor is simulated as plug flow reactor at a speed of 1 cm/s. Reactor is maintained at atmospheric pressure and constant temperature that was varied from 1400K to 1800K in steps of 100K. The comparison is presented at the two temperature extremes in order to ensure that the reduced 19-reactions mechanism can predict the qualitative trend of every major species efficiently over the entire range of temperatures.

Figures 3-9 and 3-10 describe the behavior of major species under Claus conditions at temperature of 1400K using the detailed mechanism and the 19-reactions mechanism, respectively. The comparison showed good qualitative agreement between both mechanisms in terms of reactants decay, products evolution, and ignition delay. However, some quantitative discrepancies were observed in H_2O, H_2, and SO_2 mole fractions. The results revealed that H_2 and SO_2 were over predicted using the 19-reactions mechanism by ~ 12%. On the other hand, H_2O mole fraction was under predicted by ~ 15%, which is the maximum error in the reduced mechanism.

Figures 3-11 and 3-12 show the major species trends under Claus conditions at reactor temperature of 1800 K. The results have been obtained for both detailed reaction mechanism and 19-reactions reduced mechanism. Rate of reactants decay is much faster than what was observed at 1400K because of the reactor high temperature. Improvement in both quantitative and qualitative agreement can be noticed. However, H_2O mole fraction was under predicted by ~ 11.

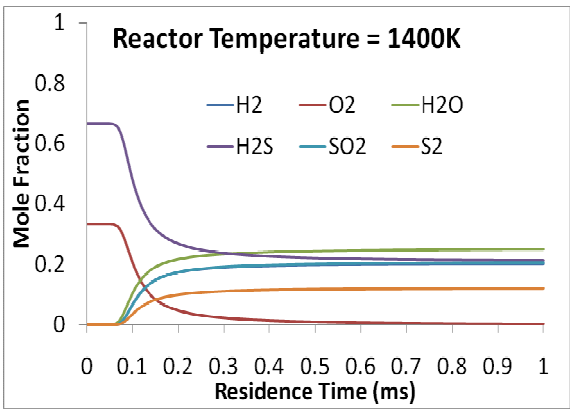

Figure 3-9. Behavior of major species, detailed mechanism, T=1400 K, Φ=3.0.

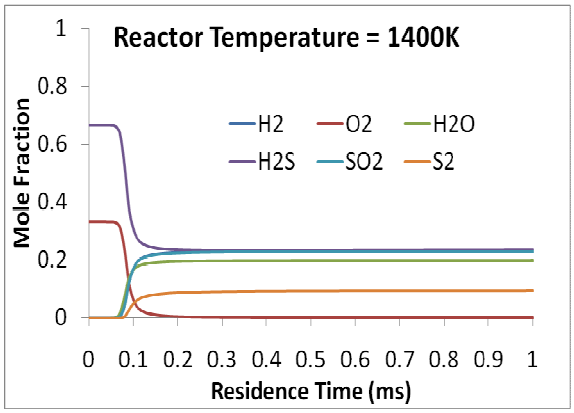

Figure 3-10. Behavior of major species, 19-reactions mechanism, T= 1400 K, Φ=3.0.

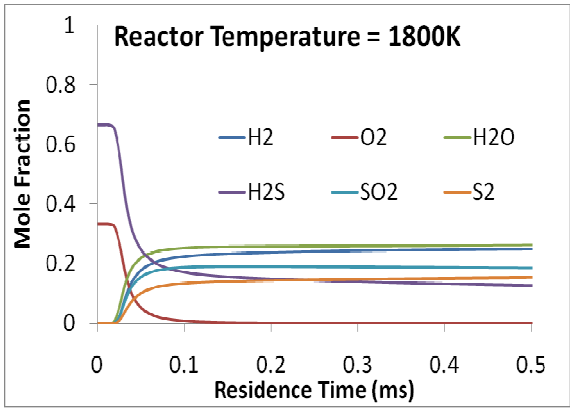

Figure 3-11. Behavior of major species, detailed mechanism, T= 1800 K, Φ=3.0.

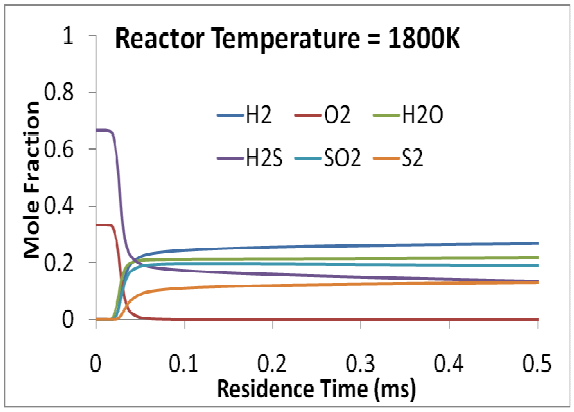

Figure 3-12. Behavior of major species, 19-reactions mechanism, T= 1800 K, Φ=3.0.

The next comparison examines the reduced mechanism fidelity under stoichiometric conditions at the same temperature and pressure conditions. Reactants inlet mole fractions are 0.6 for oxygen and 0.4 hydrogen sulfide which result in an equivalence ratio of 1. The flow speed in the reactor is 1 cm/s flowing in the form of plug flow.

Figures 3-13 and 3-14 depict behavior of major species during the reaction under stoichiometric conditions at reactor temperature of 1400 K. The results have been obtained via both detailed and reduced mechanism conditions. Rate of reactants decomposition is a lot faster

in comparison to Claus process conditions. This is attributed to the availability of higher oxygen amounts which trigger the fast H_2S/O_2 reaction as compared to slow H_2S/SO_2 reaction. In other words, in presence of oxygen, reaction proceeds in the direction of H_2S oxidation to form SO_2. This is a faster reaction as compared to the reaction between SO_2 and H_2S to form S_2. The comparison shows that, the 19-reactions reduced mechanism can qualitatively represent H_2S/O_2 reaction under stoichiometric conditions. Some discrepancies were observed quantitatively in H_2O and H_2 mole (around 15%).

Figures 3-14 and 3-15 describe major species trends under stoichiometric conditions and reactor temperature of 1800 K. Comparison between the two mechanisms showed better agreements from both quantitative and qualitative point of view. Maximum error is found to be in hydrogen mole fraction that was around 12%.

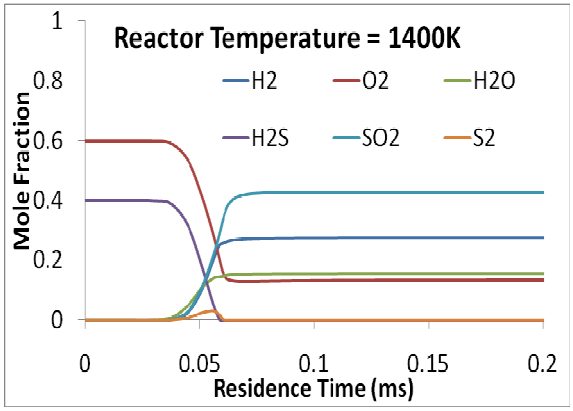

Figure 3-13. Behavior of major species, detailed mechanism, T= 1400 K, Φ=1.0.

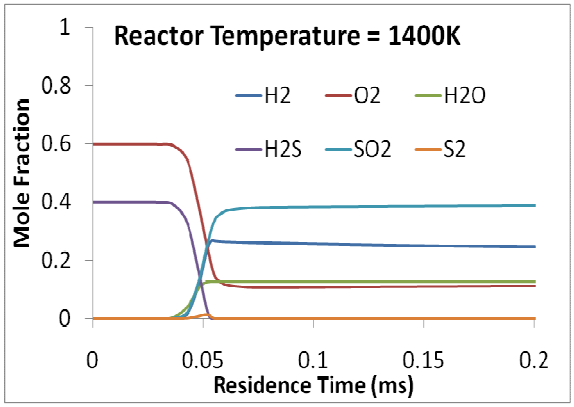

Figure 3-14. Behavior of major species, 19-reactions mechanism, T= 1400 K, Φ=1.0.

Figures 3-17 and 3-18 represent trend of major species under fuel-lean conditions (Φ=0.5) and reactor temperature of 1400 K. The results revealed that S_2 mole fraction is zero throughout the reaction. This is attributed to the presence of strong oxidizing medium which

hinders the formation of S_2. Both reaction mechanisms provide fairly close results from both qualitative and quantitative point of view.

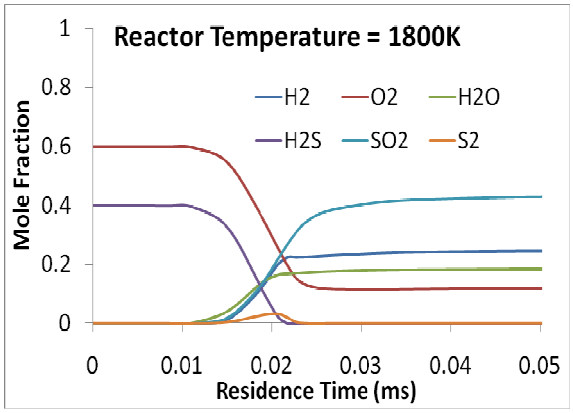

Figure 3-15. Behavior of major species, detailed mechanism, T= 1800 K, Φ=1.0.

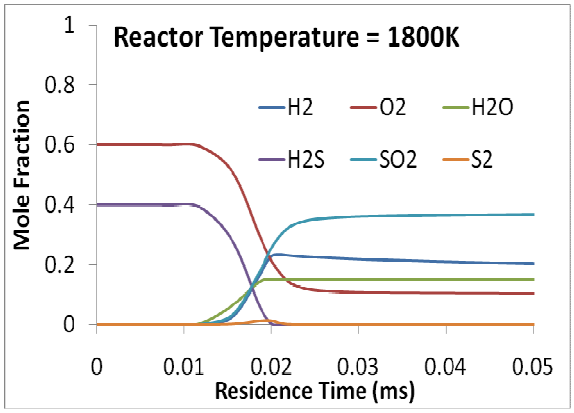

Figure 3-16. Behavior of major species, 19-reactions mechanism, T= 1800 K, Φ=1.0.

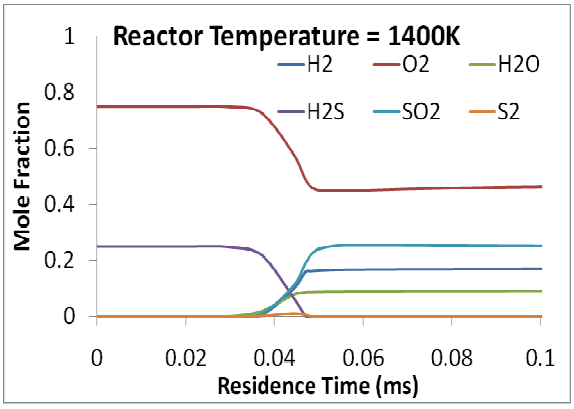

Figure 3-17. Behavior of major species, detailed mechanism, T= 1400 K, Φ=0.5.

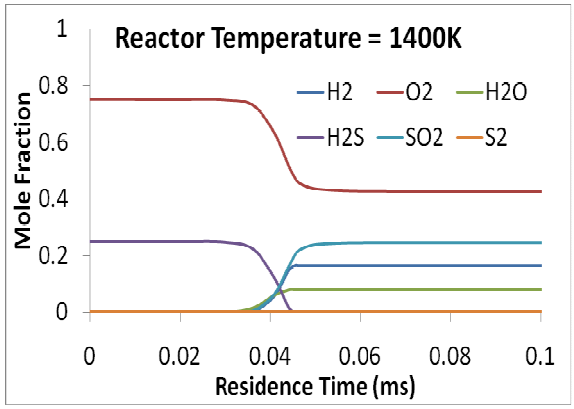

Figure 3-18. Behavior of major species, 19-reactions mechanism, T= 1400 K, Φ=0.5.

Figures 3-19 and 3-20 show behavior of major species formed under fuel-lean conditions and reactor temperature of 1800 K. Similar to previous cases, high reactor temperature triggers reaction to occur a lot faster as compared to the case of 1400K reactor temperature. The comparison provided good qualitative and quantitative agreement.

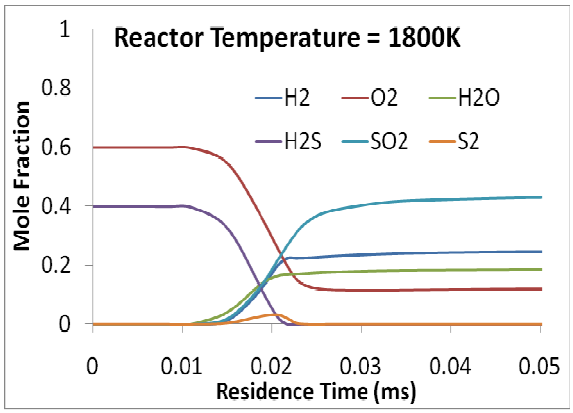

Figure 3-19. Behavior of major species, detailed mechanism, T= 1800 K, Φ=0.5.

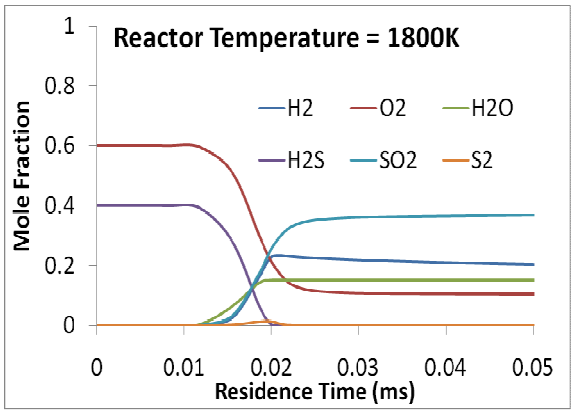

Figure 3-20. Behavior of major species, 19-reactions mechanism, T= 1800 K, Φ=0.5.

The reduced 19-reactions mechanism has also been compared with other reaction mechanisms from the literature. Hydrogen sulfide ignition delay time has been investigated by many researchers numerically and validated experimentally. In this study we compared the ignition delay of H_2S combustion calculated via our reduced mechanism, the experimental results of Bradley et al. [50], and the mechanism introduced by Tsuchiya et al. [29]. Criterion of ignition delay time determination was, the time required to attain a 10% equilibrium value of SO_2 concentration. This criterion is different from the one given by Cerru et al. [38] where the ignition delay was calculated based on the increase in reactor temperature by 600K. Both definitions did not give any major differences in the results. Inlet conditions for the comparison case are:

Inlet pressure: 0.4 atm., inlet stream mole fractions: 0.04 H_2S, 0.06 O_2, and 0.9 argon. Temperature was varied from 1650K to 2500K.

Figure 3-21 provides a comparison between the different mechanisms and the experimental data. The results showed that both mechanisms are in good agreement with the experimental data at low temperatures. The 19-reactions reduced mechanism showed good agreement with the experimental data at high temperatures as well. However, the reaction

mechanism of Tsuchiya et al. [29] showed some discrepancies. It is worthy to mention that the presented data from [29] is based on the reaction between SH, and O_2 to proceed in the direction of SO and OH formation. Any other scenario they have introduced for this reaction will deteriorate the comparison further than what is presented here.

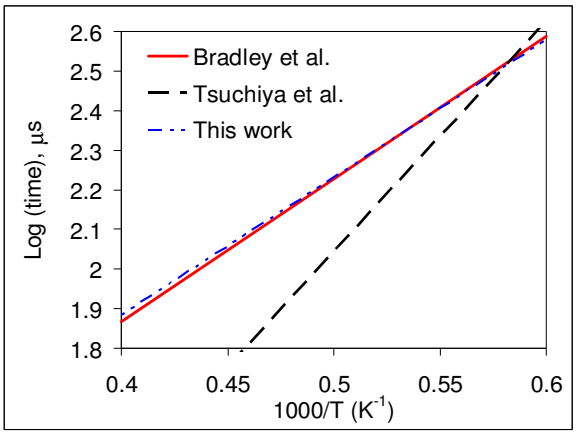

Figure 3-21. Comparison of ignition delays obtained from 19-reactions mechanism, Tsuchiya et al. mechanism [29], and experimental work by Bradley et al. [55].

3.4 Mechanistic Pathways of Claus Reactions

The 19-reactions reduced mechanism has also been used to provide better understanding about the chemical kinetics of H_2S combustion in Claus process. Figures 3-22 and 3-23 describe mechanistic pathways of H_2S combustion under Claus process in a plug flow reactor using the 19-reactions reduced mechanism. Each figure represents reaction pathways at a specific residence time. Figure 3-22 gives the reaction pathways at residence time of 0.0832 ms, while figure 3-23 depicts the mechanistic pathways at residence time of 0.8 ms; inlet flow velocity was 1 m/s. Residence times were chosen to show the difference in mechanistic pathways according to the availability of oxygen in the reaction pool. In other words, oxygen is available at the first residence time to oxidize H_2S, while oxygen is depleted at the reactor section corresponds to residence time of 0.8 ms. Mechanistic pathways presented in figure 3-22 proved that H_2S/O_2

resultant reaction goes in the direction of SO_2 formation. However, reaction pathways of figure 3-23 revealed that several elementary reactions have different trend as compared to the first reactor section. Group of arrows (A) denotes the reactions that have reversed direction as compared to figure 3-22. Group of arrows (B) represent reactions that did not have significant effect on the net reaction at the first section. One can notice that both groups of reactions tend to switch the net reaction into the direction of S_2 formation rather than SO_2. Reactions proceed in the backward direction are:

$$S + H_2 \leftrightarrow SH + H \quad (3\text{-}1)$$

$$S + OH \leftrightarrow H + SO \quad (3\text{-}2)$$

$$SO + OH \leftrightarrow SO_2 + H \quad (3\text{-}3)$$

On the other hand, intermediate species HS_2 appears significant at 0.8 ms residence time while it did not have prominent effect at the first section. This species creates a direct channel between H_2S and S_2. Reactions provide a new channel for S_2 formation are:

$$H_2S + S \leftrightarrow HS_2 + H \quad (3\text{-}4)$$

$$S_2 + H + M \leftrightarrow HS_2 + M \quad (3\text{-}5)$$

Considering the slowness in oxygen-based elementary reactions due to oxygen deletion, we can assure that net reaction will proceed in the direction of S_2 formation. These facts interpret, from the chemical kinetics point of view, the tendency of the resultant reaction to produce S_2 in absence of oxygen.

3.5 Summary

Detailed description of the steps conducted to reduce the detailed reaction mechanism by Leeds University for H_2S oxidation is presented. Direct relation graph and error

propagation methodology (DRGEP) has been implemented. The direction relation graph approach reduced detailed mechanism down to 37 reversible elementary reactions and 14 species. Implementation of the error propagation approach failed to reduce the reaction mechanism any further. A novel error-propagation-based approach was developed in this study so as to allow further reduction of the 37- reactions mechanism. Direct elementary reaction error approach (DERE) was able to reduce the number of elementary reactions down to 19 with a maximum error of 15%. The reduced 19-reactions mechanism has been compared with the detailed reaction mechanism under temperatures ranging from 1400K up to 1800 K. In addition, it has been tested under three equivalence ratios ranging from fuel-rich, stoichiometric, and fuel-lean conditions. The reduced mechanism captured successfully all features provided by the detailed mechanism. Reduced mechanism was also able to track changes occur in the chemical kinetics with change in equivalence ratio and reaction temperature. However, some quantitative discrepancies were observed, especially on H_2O mole fraction, but they were all within the assigned error threshold. Moreover, ignition delay time obtained by the 19-reactions mechanism presented in this work showed good agreement with the experimental data by Bradley et al. [55]. Finally, mechanistic pathways of Claus reactions were presented using the reduced mechanism at two different stages of the reaction. The pathways gave a reasonable elucidation to the behavior of reactions in Claus process, wherein the dominant reactions are different according to the reactants in the reaction pool.

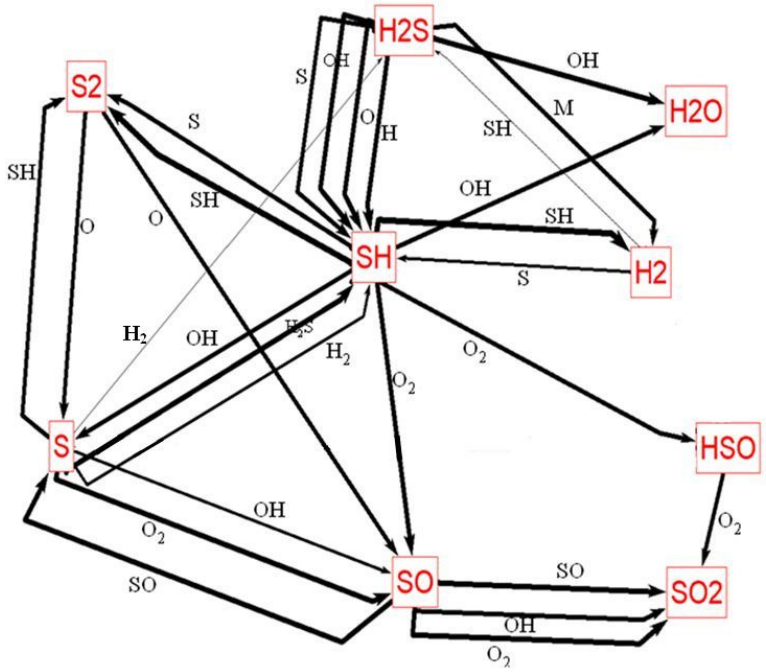

Figure 3-22. Reduced mechanism pathways under Claus conditions, reaction time elapsed is 0.0832 ms.

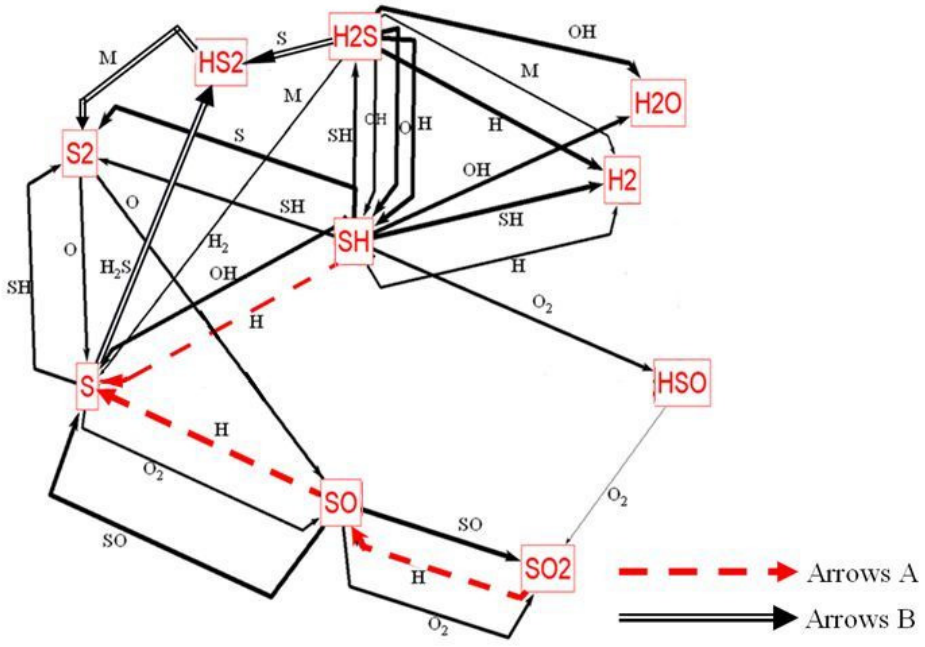

Figure 3-23. Reduced mechanism pathways under Claus conditions, reaction time elapsed is 0.8 ms.

CHAPTER 4: EXPERIMENTAL SETUP AND DIAGNOSTICS

In this chapter we discuss the details of the experimental setup and diagnostics we have used throughout the course of our research. Different burner geometries have been used according to the experimental conditions. Different diagnostics were also used so that we manage to obtain the information required to fulfill our research objectives.

4.1 Experimental Setup

The experimental setup consisted of a burner, reactor, sampling system, and flow rates supply and control system. In this section we will discuss in details each of these three parts.

4.1.1 Burner

Throughout the course of our investigations, we have used two different burners to serve our research goals. Both burners were double concentric tube ones. However, tubes dimensions differed in order to enhance flame stability and avoid flame extinction/blowout. The first burner (burner A), the mostly used, has a bluff body stabilizer at the exit to stabilize the flame immediately downstream of the burner exit. This burner allowed wide range of experimental conditions to be examined (all experimental conditions will be given in chapter 5). Figure 4-1 depicts a schematic diagram of burner A. On the other hand, burner B has been fabricated specifically for experiments of low reactants flow rates; where in burner A could not sustain well-shaped stable flame due to reactants low velocities. Figure 4-2 shows a schematic diagram of burner B.

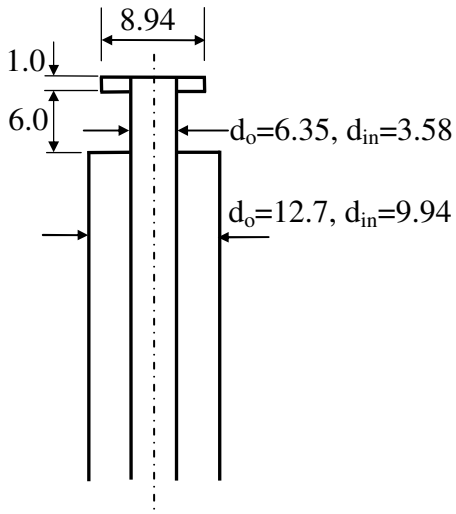

Figure 4-1. Schematic diagram of burner A, all dimensions are in millimeters.

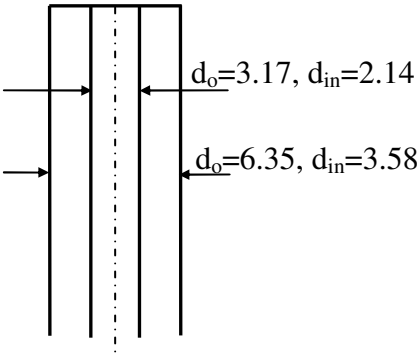

Figure 4-2. Schematic diagram of burner B, all dimensions are in millimeters.

4.1.2 Quartz Tube Reactor

Transparent quartz tube reactor is used for full optical access to the test region for non-intrusive examinations. The reactor is 19 cm in length and 4 cm in diameter. Two steel bases were fabricated with proper dimensions for housing the reactor from both ends of the quartz tube. The bottom steel base has also been used to collect sulfur deposits condensed on reactor walls. Figure 4-3 shows a photo of burner A and quartz reactor assembled in the steel bases.

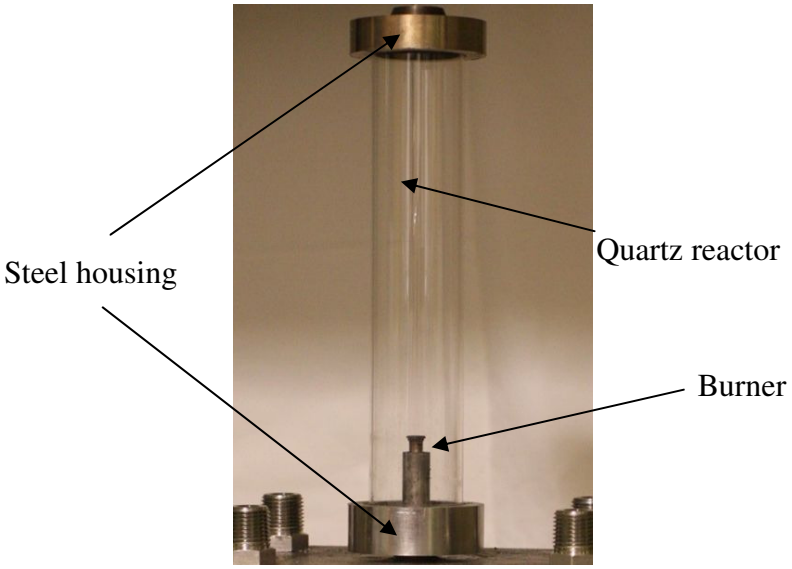

Figure 4-3. Quartz tube reactor and flame burner assembled in steel housing.

4.1.3 Sampling System

Gas sampling from the reactor has been conducted using a quartz tube sampling probe with a fine tip (0.2x0.4 mm in diameter). The fine tip allowed gas sampling with the negligible disturbance to flow field. In addition, sampled gas was accelerated considerably along the fine tip passage of the probe in order to assure instantaneous freeze to chemical reactions. Dimensions of the sampling probe are given in figure 4-4. Sampling

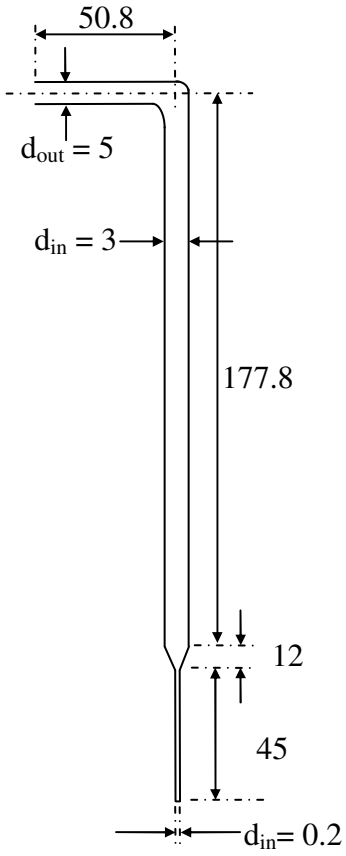

Figure 4-4. Schematic diagram of the sampling probe, dimensions are in millimeter.

probe was mounted on two traverse mechanisms allowing axial, and radial if needed, movement along the reactor. The resolution of traverse mechanisms was (25 microns). Moisture separator has also been installed along the sampling line in order to segregate water in prior to gas analysis. It also has been used as a reservoir in order to have steady flow rate during gas analysis. Finally, a peristaltic pump was used for suction of the sampled gas from the reactor. The pump was able to provide flow rates in the range of 0.3 up to 8 lit/min.

4.1.4 Flow Rates Supply and Control System

Thermal flow meters/controllers were used to deliver the required flow rates of each gas (air, hydrogen sulfide, carbon dioxide…etc). Since a wide range of flow rates have been examined, flow controllers were being changed according to each experiment in order to supply the required flow rates appropriately with the least possible error. For instance, we used five flow controllers with a full scale varies between 20 cm^3/min up to 1000 cm^3/min for H_2S so that it always works within the range of least possible error (±1.5% full scale). It is also important to mention that nitrogen has been used as a reference gas for excess oxygen calculations. In other words, excess oxygen flow rate required for each experiment was calculated with respect to nitrogen flow rate in the reactants corrected by the O_2/N_2 ratio of mole fractions in the combustion products.

4.2 Diagnostics

Several diagnostics have been used throughout this research according to the purpose of each investigation. The major diagnostics we have adopted were gas chromatography, flame spectroscopy, X-Ray powder diffraction, and laser induced breakdown spectroscopy (LIBS). In this section we explain the details of each diagnostics and the purpose it was dedicated for.

4.2.1 Gas Chromatography

Gas chromatograph (GC) was used to obtain analysis of stable combustion products in the reaction pool. The sampled gas was split inside the GC into two streams. First stream was injected into thermal conductivity detector (TCD) which was responsible for the analysis of carbon monoxide, carbon dioxide, oxygen, hydrogen, and nitrogen. Second stream was injected into flame photometric detector (FPD) which was responsible for gas analysis of stable sulfur compounds (hydrogen sulfide, carbonyl sulfide, carbon disulfide, and sulfur dioxide).

4.2.2 Flame Spectroscopy

Non-intrusive gas spectroscopy was conduced to analyze emissions spectra from stable and/or non-stable species in the reaction pool. A spectrometer coupled with an ICCD camera was used for the detection of chemiluminescent signal from the excited species. The spectrometer slit was set at 10 microns. Signal from the flame region was passed to the spectrometer through a fiber optic cable. Two gratings were used for different resolutions of the spectrum. Coarse grating was used to obtain coarse resolution of the spectrum (~270nm) while fine resolution of the spectrum (~70nm) was obtained with the fine grating. A mercury lamp was used for the re/calibration of spectrometer after changing the grating or in case of change in spectrum of interest.

4.2.3 X-Ray Powder Diffraction

X-Ray powder diffraction technique [104] is typically used to provide crystallographic analysis of solid samples. In this research we have used X-Ray powder diffraction during the analysis of the quality of collected sulfur deposits. The goal was to determine the allotrope of

collected sulfur deposits. Samples analysis was demonstrated in The X-Ray Crystallographic Center at The University of Maryland.

4.2.4 Laser Induced Breakdown Spectroscopy (LIBS)

Laser induced breakdown spectroscopy (LIBS) was used to analyze the chemical structure of deposited sulfur. The LIBS setup consisted of seven-channel spectrometer equipped with seven CCD cameras. The spectrometer covered a band of wavelengths extending from 200nm to 970 nm, equally distributed on the seven CCD cameras. A 532nm Nd:YAG laser was used to excite the samples inside LIBS chamber. The LIBS chamber is connected to the seven-channel spectrometer via a fiber optic cable. Figure 4-5 represents a photo of the LIBS setup.

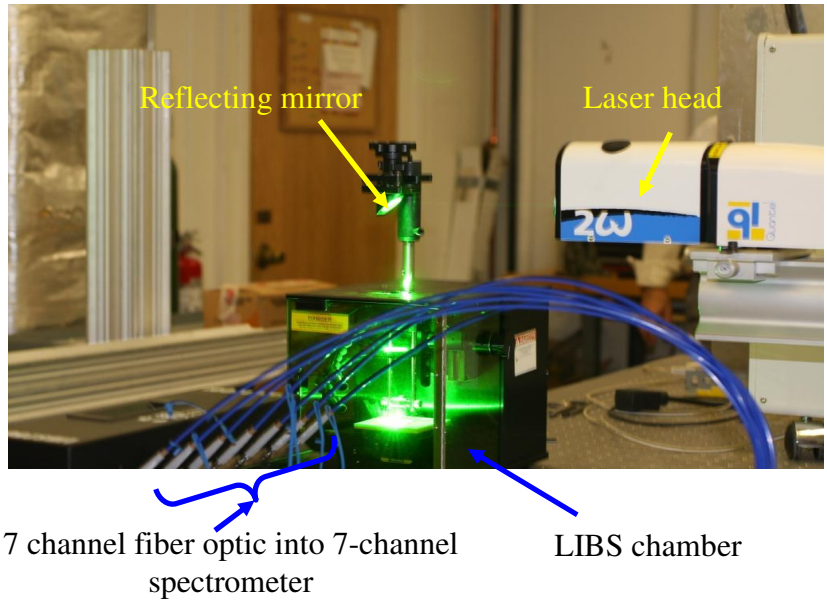

Figure 4-5. Laser induced breakdown spectroscopy (LIBS) setup.

4.3 Experimental Difficulties

The average time of each experimental run was about 5 hours from start to finish. During this period we used to have experimental issues that, sometimes, were forcing us to stop the experiment and start it all over again. Most of the problems were due to sulfur formation and clogging in different places of the experimental setup. Sulfur deposits were forming on the reactor walls, in the sampling probe, and in the sampling line to the GC. Accumulated sulfur in critical spots (hard to be reached and cleaned) used to clog the sampling line after several experimental runs. Figure 4-6 shows some examples of the sulfur deposits formation in the experimental setup. Subsequently, several precautions were being taken in order to lessen the chances of problems caused by sulfur deposits. For instance, after each experiment the sampling line was being blown with a 90 psi air stream, quartz tube reactor walls were being cleaned in a hot water bathe, and the sampling probe was being exposed to a propane torch so that sulfur deposits would melt down.

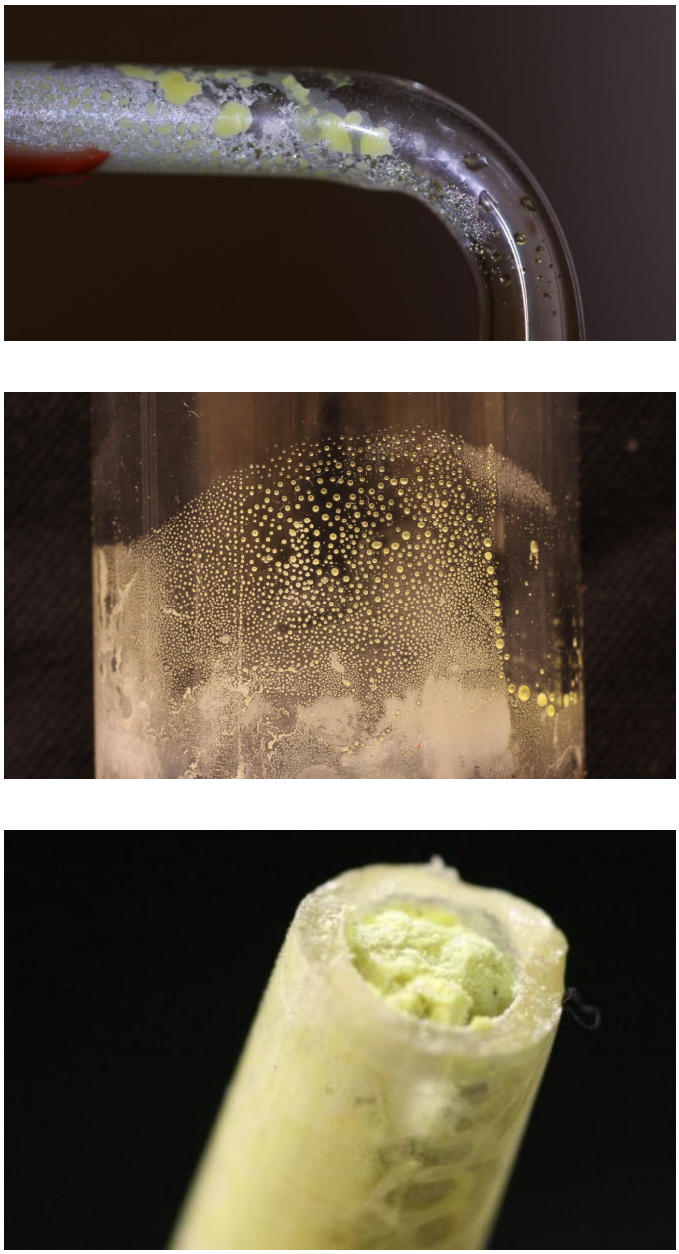

Figure 4-6. Sulfur deposits accumulated in the sampling probe (top), on the reactor walls (middle), and in the sampling line (bottom).

CHAPTER 5: EXPERIMENTAL RESULTS AND DISCUSSION

Experimental investigations discussed in this chapter are divided into four major sections. The first section is dedicated to H_2S combustion in flames (CH_4/air and H_2/air). The second section represents the examination of hydrogen sulfide flame spectroscopy. The third section provides a study on the effect of acid gas composition (H_2S, CO_2, and N_2) on hydrogen sulfide combustion under Claus conditions. The fourth and last section discusses the effect of reactor conditions and acid gas composition on the purity of captured sulfur deposits.

5.1 Hydrogen Sulfide Combustion in Flames

Investigation of hydrogen sulfide combustion has been conducted in CH_4/air flame and H_2/air flame under different equivalence ratios. We have chosen these flames for several reasons; firstly, the chemical kinetics of both flames has been thoroughly investigated and comprehended. Therefore, it will be easier to monitor the changes in chemical kinetics due to H_2S combustion. In addition, H_2S combustion in presence of other flames will help us to understand the conditions under which other sulfur-bearing compounds are formed. Moreover, CH_4/air and H_2/air flames represent completely different flame conditions in terms of intermediate species, flame temperatures, and reaction rates. This will help us to understand more information on H_2S chemical kinetics with respect to different flame conditions. Finally, H_2S combustion in these flames can practically occur in Claus process; for instance, imperfect amine extraction process will results in natural-gas-laden acid gas stream (mainly CH_4). On the other hand, methane combustion can produce hydrogen which will compete in the reaction with hydrogen sulfide.

5.1.1 H_2S Combustion in Methane/Air Flames

Experiments were conducted to investigate H_2S combustion at different equivalence ratios in methane/air flames. Methane/air mixture was burned under slightly fuel-lean conditions with H_2S injected at different flow rates to vary equivalence ratio of H_2S/O_2 mixture. Figure 5-1 describes the configuration of reactants injection into the burner (burner A has been used in these experiments).

Experimental procedure included the following steps. Firstly, methane/air equivalence ratio was adjusted to achieve slightly fuel-lean conditions. Excess oxygen flow was determined using O_2/N_2 mole fraction ratio obtained from GC analysis to combustion products. Hydrogen sulfide gas stream was introduced at the required flow rate to achieve certain H_2S/O_2 equivalence ratio. Three equivalence ratios have been examined representing Claus conditions (Φ=3), stoichiometric conditions (Φ=1), and fuel-lean conditions (Φ=0.5). It is important to mention that the given equivalence ratios are calculated based on hydrogen sulfide/excess oxygen ratio. Gas sampling was carried out at different axial locations and injected directly into the GC. Samples were taken at elevations of (0, 0.635, 1.27, 1.9, 2.54, 3.81, 5.08, 6.35, 7.62, 10.16, 12.7, 15.24, and 17.78 cm) along the longitudinal centerline of the reactor. All experiments were repeated three times in order to check its repeatability. Dimensionless axial distance (W) is used for all represented results. Burner Inner tube (jet) diameter was used to transform the linear distances into dimensionless distances, i.e., W= axial distance/Djet. Table 5-1 describes all experiments flow rates and the corresponding equivalence ratios.

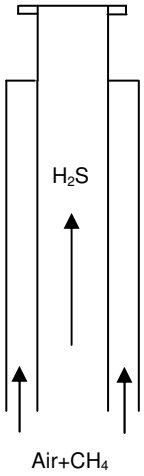

Figure 5-1. Configuration of the reactants injected into the burner.

Table 5-1. Reactants flow rates (CH_4/air/H_2S).

Equivalence Ratio (Φ)	CH_4 (lit/min)	Air (lit/min)	Excess oxygen (cm^3/min)	Hydrogen sulfide (cm^3/min)
3	0.97	9.7	68	137
1	0.97	9.7	68	46
0.5	0.97	9.7	68	23

5.1.1.1 Temperature Measurements

Temperature measurements were carried out along the reactor centerline using a K-type thermocouple (thermocouple bead diameter was 0.8 mm). Temperature distribution in the reactor was measured by traversing the thermocouple axially upward. Figure 5-2 shows temperature distribution along the longitudinal centerline of the reactor for CH_4/air flame, both without and with H_2S addition at Claus conditions. Only temperature distribution at Claus condition is discussed because it represents the highest concentration of H_2S; also to avoid figure complexity. Temperature was found to decrease with hydrogen sulfide injection immediately upon entry into the reactor because of relatively cold flow of H_2S (injected at room temperature). However,

further downstream, temperature increased to slightly surpass temperature of methane/air flame, but the eventual temperatures were almost the same.

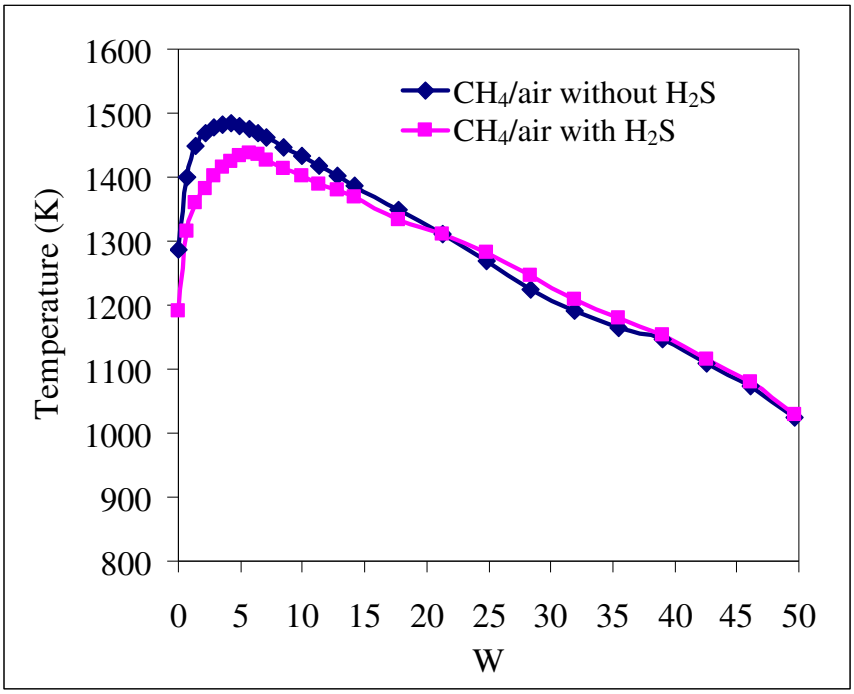

Figure 5-2. Temperature distribution along reactor centerline for CH_4/air flame without/with H_2S addition under Claus conditions.

5.1.1.2 Combustion Products Analysis

Mole fraction of hydrogen sulfide for different H_2S/O_2 equivalence ratios, ranging from fuel-lean, stoichiometric to fuel-rich conditions are shown in Figures 5-3, 5-4, and 5-5, respectively. The results were repeated at least three times for data repeatability. Good repeatability of the experiments was obtained; however, small discrepancy in H_2S mole fraction was observed at small axial distances downstream of the burner exit. This can be credited to the error in reactants flow controllers (±1.5% full scale). The mole fraction of hydrogen sulfide decayed along centerline of the reactor for all cases. However, under Claus conditions (at Φ =3.0) hydrogen sulfide does not decay to zero because of the depletion of oxidizer. Decay of H_2S

can be divided into two major zones. In the primary zone H_2S thermal and chemical decomposition occurs, while in the secondary zone hydrogen sulfide oxidation takes place. The main elementary reactions that can elucidate the primary zone of H_2S reaction are described in our reduced mechanism for H_2S/O_2 reaction [105-106] as well as in the detailed mechanism of Leeds University [37]:

$$H_2S + M \leftrightarrow S + H_2 + M \quad (5\text{-}1)$$

$$H_2S + H \leftrightarrow HS + H_2 \quad (5\text{-}2)$$

$$H_2S + S \leftrightarrow 2HS \quad (5\text{-}3)$$

$$HS + S \leftrightarrow S_2 + H \quad (5\text{-}4)$$

$$HS + H \leftrightarrow S + H_2 \quad (5\text{-}5)$$

Reactions (5-1), (5-2), and (5-3) describe the initial decomposition of H_2S. Reaction rate of the initiation step (5-1) is negligible as compared to propagation steps given in reactions (5-2) and (5-3). This group of elementary reactions provides both thermal and chemical decomposition of hydrogen sulfide and the onset of hydrogen formation, if any will be formed.

The secondary zone where combustion of hydrogen sulfide takes place can be described by the following group of elementary reactions:

$$H_2S + O \leftrightarrow SH + OH \quad (5\text{-}6)$$

$$H_2S + OH \leftrightarrow SH + H_2O \quad (5\text{-}7)$$

Mole fraction of sulfur dioxide at fuel lean, stoichiometric and fuel rich equivalence ratios of H_2S/O_2 is shown in figures 5-6, 5-7, and 5-8, respectively. At fuel-lean and stoichiometric conditions (figures 5-6 and 5-7) SO_2 mole fraction increases monotonically to reach an asymptotic value. This can be explained by the oxidation of hydrogen sulfide to form SO_2. However, at Claus conditions (figure 5-8), sulfur dioxide mole fraction increases to a

maximum then decreases to reach an asymptotic value. The following group of elementary reactions [105-106] describes the formation of SO_2:

$$S + OH \leftrightarrow SO + H \quad (5\text{-}8)$$

$$SH + O_2 \leftrightarrow HSO + O \quad (5\text{-}9)$$

$$SH + O_2 \leftrightarrow SO + OH \quad (5\text{-}10)$$

$$HSO + H \leftrightarrow S + H_2O \quad (5\text{-}11)$$

$$S + O_2 \leftrightarrow SO + O \quad (5\text{-}12)$$

$$HSO + H \leftrightarrow SO + H_2 \quad (5\text{-}13)$$

$$SO + OH \leftrightarrow SO_2 + H \quad (5\text{-}14)$$

$$SO + SO \leftrightarrow SO_2 + O \quad (5\text{-}15)$$

$$SO + O_2 \leftrightarrow SO_2 + O \quad (5\text{-}16)$$

$$HSO + O_2 \leftrightarrow SO_2 + OH \quad (5\text{-}17)$$

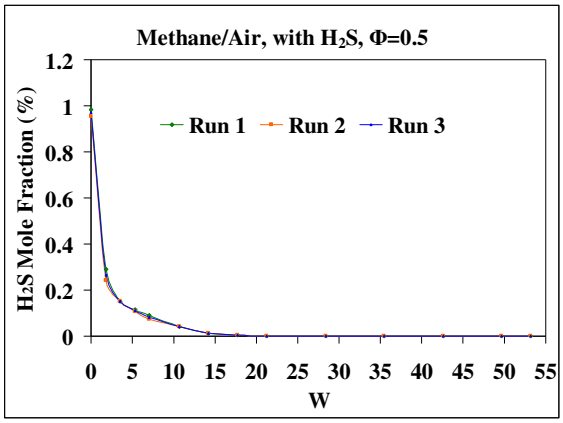

Figure 5-3. H_2S mole fraction. Flame conditions: methane/air with H_2S, Φ =0.5.

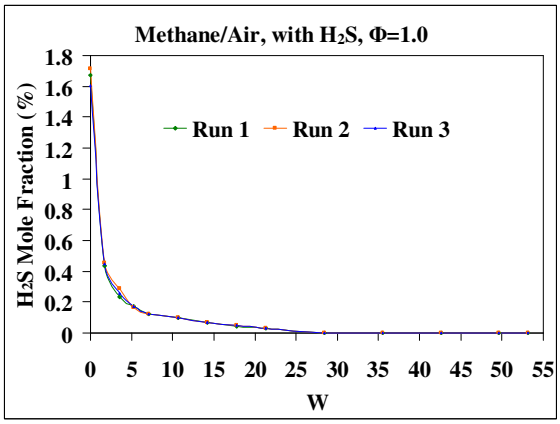

Figure 5-4. H_2S mole fraction. Flame conditions: methane/air with H_2S, Φ =1.0.

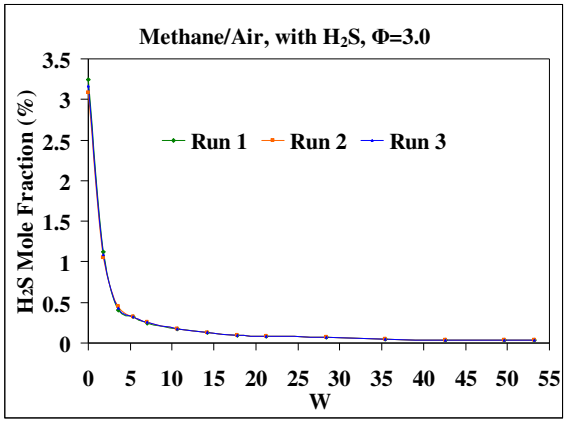

Figure 5-5. H_2S mole fraction. Flame conditions: methane/air with H_2S, Φ =3.0.

Formation of SO_2 from H_2S oxidation passes through multiple stages. The first stage is the oxidation of H_2S to form intermediate species (S, SO, SH, and HSO). This stage is represented by reactions (5-6) through reaction (5-13). The second stage is the recombination of intermediate species to form sulfur dioxide which is represented by reactions (5-14) through (5-17). It was found that the formation of sulfur dioxide strongly depends on the presence of oxygen in the reaction pool. The above mechanism in its entirety elucidates H_2S/O_2 reaction until it reaches the end product (SO_2) provided that enough oxygen is present in the reaction pool (fuel-lean or stoichiometric conditions). On the other hand, in absence of oxygen in the reaction pool several elementary reactions were found to contribute to the formation of other products (through reaction propagation in the reverse direction). Reactions (5-8), (5-13), and (5-14) contribute in the backward direction with the depletion of oxygen in the reaction pool. These reactions in their reverse direction hinder the formation of sulfur dioxide and create a strong channel for the formation of sulfur, S_2, through the following reactions:

$$SH + S \leftrightarrow S_2 + H \quad (5\text{-}18)$$

$$SO + S \leftrightarrow S_2 + O \quad (5\text{-}19)$$

$$H_2S + S \leftrightarrow HS_2 + H \quad (5\text{-}20)$$

$$HS_2 + M \leftrightarrow S_2 + H \qquad (5\text{-}21)$$

The previous mechanism interprets the tendency for H_2S to form sulfur dioxide in presence of oxygen. This is indeed the case for fuel-lean conditions (Φ =0.5) and stoichiometric conditions (Φ =1.0). However, under Claus conditions H_2S is combusted to form SO_2 in the first phase of reaction. With the depletion of oxygen in the reaction pool, the resultant reaction starts to shift to its direction towards elemental sulfur formation. This phase of elemental sulfur formation was found to be very slow as compared to the phase of sulfur dioxide formation.

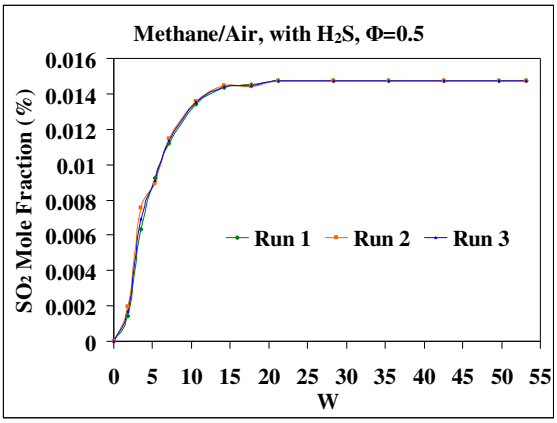

Figure 5-6. SO_2 mole fraction. Flame conditions: methane/air with H_2S, Φ =0.5.

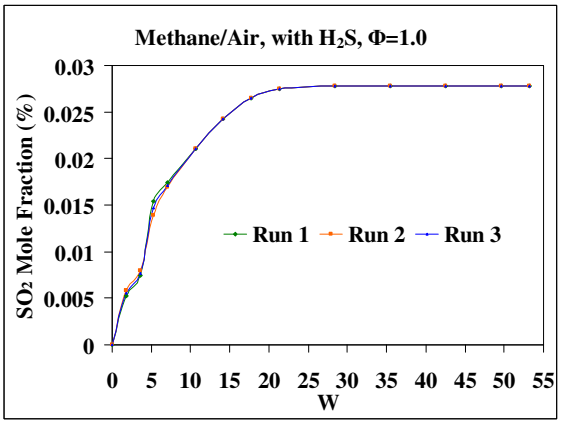

Figure 5-7. SO_2 mole fraction. Flame conditions: methane/air with H_2S, Φ =1.0.

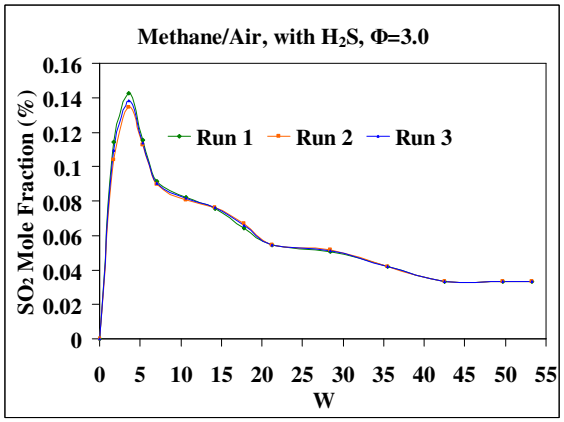

Figure 5-8. SO_2 mole fraction. Flame conditions: methane/air with H_2S, Φ =3.0.

Hydrogen mole fractions at different equivalence ratios, both without and with H_2S addition into CH_4/air flame, is shown in figures 5-9, 5-10, 5-11, and 5-12. In case of methane/air combustion, hydrogen mole fraction decreases along the reactor centerline and reaches to zero at the reactor exit. In contrast, with H_2S addition, hydrogen reaction is divided into two zones. In the primary zone, hydrogen increases due to the presence of H_2S which is an oxidation inhibitor for H_2. Sulfur dioxide poses also a significant role on H_2 oxidation inhibition by enhancing atomic hydrogen recombination [31-32], reactions (5-22) and (5-23):

$$H + SO_2 + M \leftrightarrow HOSO + M \quad (5\text{-}22)$$

$$HOSO + H \leftrightarrow SO_2 + H_2 \quad (5\text{-}23)$$

In the secondary zone, H_2 decays, to reach an asymptotic value, but not necessarily diminishes. Both the maximum and asymptotic value of H_2 mole fraction increases with the increase in H_2S addition into the reacting mixture.

Under fuel-lean and stoichiometric conditions, H_2 oxidation occurs in the secondary zone due to the presence of O and OH radicals [25] through reactions (5-24) and (5-25) wherein the competition of H_2S and H_2 oxidation occurs. These results are also highlighted by several other investigators [25,69] in the literature who have stated that in presence of oxidizer, H_2S prevents primarily the oxidation of hydrogen. However, further downstream oxidation competition between H_2S and H_2 starts in the secondary reaction zone of the reaction.

$$H_2 + O \leftrightarrow H_2O \quad (5\text{-}24)$$

$$H_2 + OH \leftrightarrow H_2O + H \quad (5\text{-}25)$$

Although oxygen is totally consumed in the first reaction stage under Claus condition (Φ =3.0) H_2 mole fraction decreases further downstream. This is attributed to the above mentioned

explanation that direction of several elementary reactions is reversed. Reactions (7) and (15) provide an important role in hydrogen consumption in absence of oxygen.

$$H_2 + S \leftrightarrow SH + H \qquad (-5\text{-}5)$$

$$H_2 + SO \leftrightarrow HSO + H \qquad (-5\text{-}13)$$

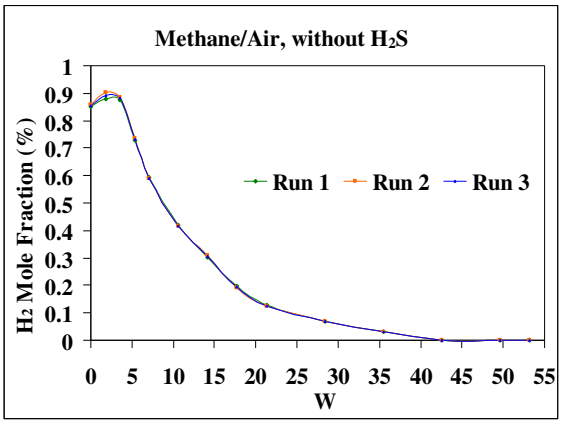

Figure 5-9. H_2 mole fraction. Flame conditions: methane/air without H_2S.

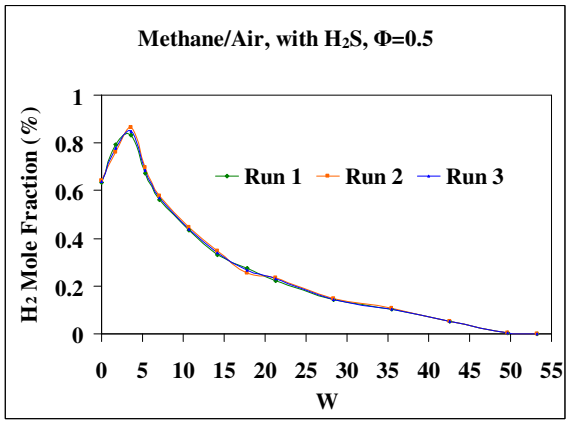

Figure 5-10. H_2 mole fraction. Flame conditions: methane/air with H_2S, Φ =0.5.

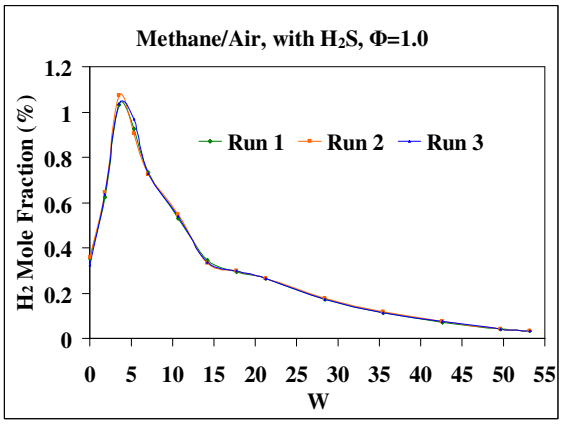

Figure 5-11. H_2 mole fraction. Flame conditions: methane/air with H_2S, Φ =1.0.

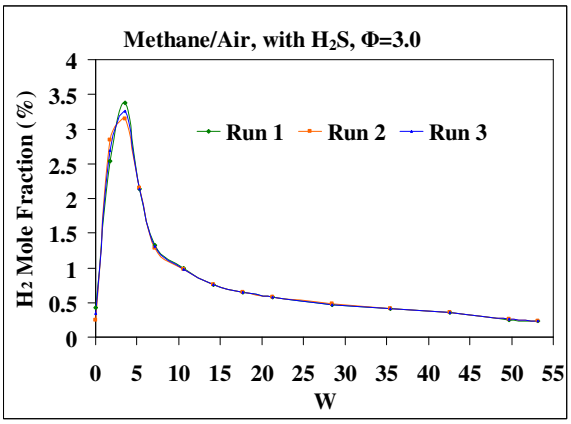

Figure 5-12. H_2 mole fraction. Flame conditions: methane/air with H_2S, Φ =3.0.

Carbon monoxide mole fractions, both without and with H_2S addition, at different equivalence ratios are shown in figures 5-13, 5-14, 5-15, and 5-16. For methane/air combustion, carbon monoxide decreases along the centerline of the reactor and reaches to zero at the reactor

exit. However, with H_2S addition, CO mole fraction increases to reach a peak, then decays to an asymptotic value, but never diminishes. This is attributed to H_2S addition which causes depletion of the oxidizing medium. On the other hand, hydrogen sulfide introduction into the reaction zone dilutes the concentrations near the burner tip which contributes to the decrease of CO mole fraction near the burner exit. Oxidation of carbon monoxide did not cause any significant impact on carbon dioxide so that the average CO_2 mole fraction showed negligible change under all examined conditions.

At Claus conditions, formation of hydrocarbons was observed from the gas chromatography data. In contrast, no hydrocarbons were detected at fuel-lean or stoichiometric conditions. Figure 5-17 shows the presence of increased averaged amounts of series of hydrocarbons formed during the methane/air reaction with the injection of H_2S under Claus conditions. The peak of these compounds occurs at the same residence time in the reactor (at about 15 cm downstream from the burner exit, W=42). The amounts of ethylene and propane were significant at this location as compared to acetylene and ethane. The formation of higher hydrocarbons is attributed to the presence of a coupling catalyst in the reaction [107]. Sulfur dioxide provides this role in our case, where it enhances the dimerization of CH_3 radical formed during CH_4 reaction to form ethane. Dehydrogenation of ethane can form ethylene which reacts with CH_3 to form propylene and propane. Several of these compounds (acetylene, ethane, ethylene and propane) have been detected here with the addition of H_2S in the reactor. This is significant as it offers means to provide potential for a value added products, besides sulfur recovery, from the Claus reaction.

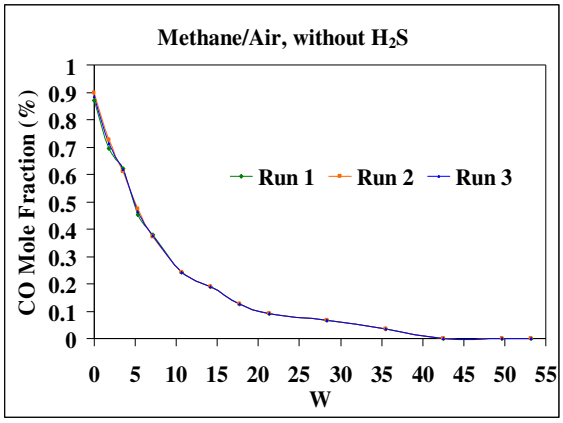

Figure 5-13. CO mole fraction. Flame conditions: methane/air without H_2S.

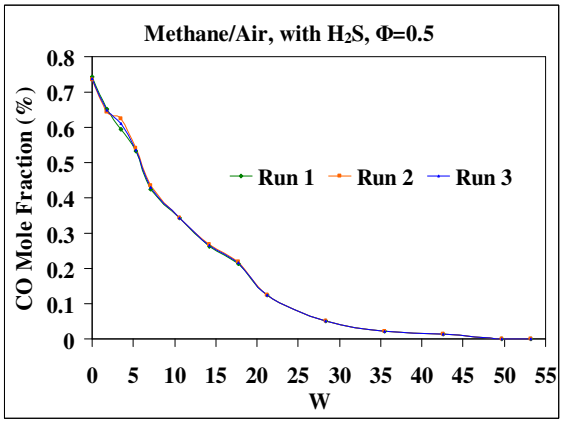

Figure 5-14. CO mole fraction. Flame conditions: methane/air with H_2S, Φ =0.5.

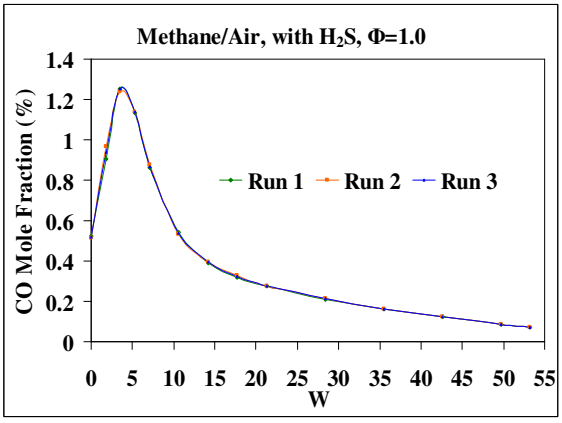

Figure 5-15. CO mole fraction. Flame conditions: methane/air with H_2S, Φ =1.0.

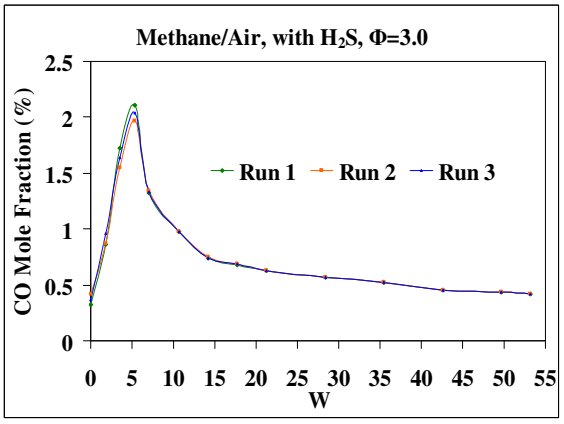

Figure 5-16. CO mole fraction. Flame conditions: methane/air with H_2S, Φ =3.0.

5.1.1.3 Summary

Effect of H_2S/O_2 equivalence ratio in methane air flames has been examined. Methane was combusted under slightly fuel-lean conditions and hydrogen sulfide was introduced accordingly to achieve the desired equivalence ratio of the H_2S/O_2. Three equivalence ratios were examined that extended from fuel-lean (Φ=0.5), stoichiometric (Φ=1.0), to fuel-rich (Claus condition, Φ =3.0). Experiments were repeated at least three times for every condition in order to

assure data repeatability. The results showed good repeatability at all locations with only small discrepancies observed in the behavior of combustion products at small axial distances (close to the burner exit). Analysis of combustion products revealed that H_2S reaction starts with thermal and chemical decomposition. The presence of H_2S prevents hydrogen (formed from CH_4/air combustion) oxidation in the primary reaction zone. However, in the secondary reaction zone oxidation competition occurs between H_2 and H_2S. In presence of oxygen, H_2S oxidation causes primarily the formation of sulfur dioxide. However, under Claus conditions, and with the depletion of oxygen, direction of H_2S net reaction shifts towards the direction of sulfur formation. This is justified from the chemical kinetics point of view as several elementary reactions contribute in their reverse (backward) direction. This proved the numerical simulations findings presented in chapter 4. Higher hydrocarbons were formed in trace amounts under Claus conditions. This is attributed to SO_2 role as a coupling catalyst which enhances the dimerization of CH_3 radical to form higher series of hydrocarbons, such as, acetylene, ethylene, ethane, and propane.

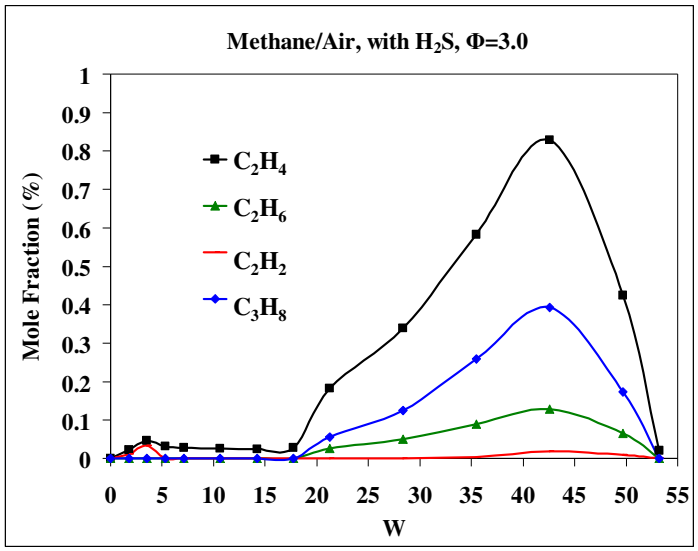

Figure 5-17. Average mole fraction of higher hydrocarbons with H_2S addition to methane/air flame under Claus conditions at Φ =3.0.

5.1.2 H_2S Premixed Combustion in CH_4/Air Flames

Experiments were conducted to investigate hydrogen sulfide combustion in methane/air flame under premixed conditions at difference equivalence ratios. Experimental procedures are similar to what have been discussed in section (5.1.1). However, configuration of reactants injected into the reactor has changed in order to have premixed CH_4/H_2S/air mixture. Figure 5-18 depicts configuration of reactants injection into the burner, burner A. According to figure 5-18 reactants are expected to expand radially outward into the reactor, thus measurements (gas sampling and temperature) were conducted axially along three radial locations of the reactor. Flame photos showed acceptable flame symmetry; hence all measurements were carried out on only one half section of the reactor (left half). Dimensionless axial (W) and radial (R) distances are used to show the trends of temperature measurements and combustion products evolution. Inner jet diameter was used to transform the linear distances to dimensionless parameters, i.e., W= axial distance/Djet, and R= radial distance/Djet. Table 5-2 describes reactants flow rates with respect to the investigated equivalence ratios. It is important to highlight that axial scanning of the entire reactor at three radial locations used to take, from start to finish, about 6 hours. Subsequently, it was impossible to perform more than one experiment daily. This justifies the slight change in methane flow rate at different equivalence ratios.

5.1.2.1 Reactor Temperature Distribution

Reactor mean temperatures were measured using a K-type thermocouple radially and axially using computer controlled traverse mechanisms. Figure 5-19 shows the temperature contours of CH_4/air flame for the left side of the reactor under Claus conditions. Under fuel-lean and stoichiometric conditions wherein H_2S flow rate is minimal, temperature distribution did not reflect considerable change as compared to CH_4/air flame. A direct comparison between CH_4/air

flame temperatures without/with H_2S revealed that temperatures did not change considerably away from the flame zone. However, H_2S addition increased temperature around the flame zone with maximum increase in temperature of ~50 °C at W= 2.83 and R=0.

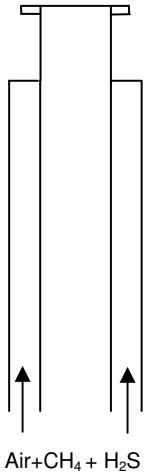

Figure 5-18. Configuration of the reactants (premixed CH_4/H_2S/air) injected into the burner.

Table 5-2. Reactants flow rates (premixed CH_4/air/H_2S).

Equivalence ratio (Φ)	Air flow rate (lit/min)	CH_4 flow rate (lit/min)	Excess oxygen (cm^3/min)	H_2S flow rate (cm^3/min)
Φ=3.0	9.7	0.99	55	110
Φ=1.0	9.7	0.97	90	60
Φ=0.5	9.7	0.95	144	48

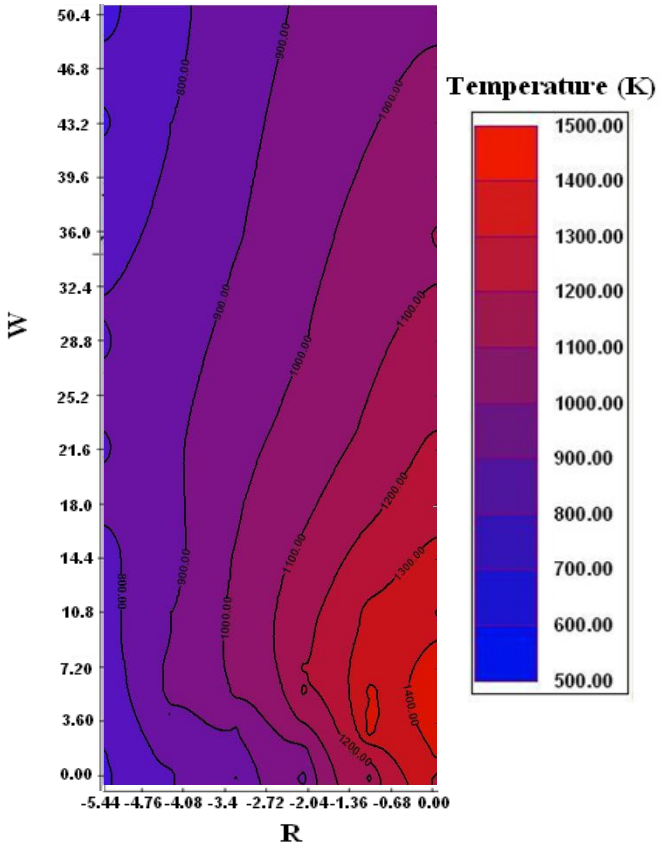

Figure 5-19. Spatial temperature distribution of the reactor under Claus conditions.

5.1.2.2 Hydrogen Sulfide Combustion Analysis

Figures 5-20, 5-21, and 5-22 describe the distribution of hydrogen mole fraction at different equivalence ratios along the reactor at three radial locations. Constant decrease in H_2 mole fraction was observed at any equivalence ratio along the reactor centerline. Presence of H_2 at the reactor centerline is attributed to the flow recirculation as a direct result of the presence of a bluff body, which acts as a flow obstruction object. The constant decrease in H_2 mole fraction is due to either oxidation or reaction with sulfur intermediate species, such as S and SO [108]. However, radially outwards, hydrogen mole fraction tends to peak, at any equivalence ratio, to a maximum then a monotonic decrease is observed. The peak of H_2 mole fraction is attributed to fact that the burner configuration dictates reactants and products to spread radially outward; in addition, the presence of H_2S which considered an inhibitor to hydrogen oxidation [108]. Further

downstream hydrogen oxidation starts to be more competitive with hydrogen sulfide reaction. Consequently, H_2S inhibition to hydrogen oxidation justifies the increase of H_2 mole fraction upstream. Further downstream, hydrogen decreases due to the oxidation competition between H_2 and H_2S. On the other hand, at Φ=1.0 and Φ=0.5, one can notice that H_2 peak at R= 1.77 exceeds the corresponding value of H_2 mole fraction at R=0.0. This is attributed to the availability of higher amounts of oxygen at R=1.77. This is translated to higher oxidation rates of hydrogen. This leads to lower amounts of hydrogen present in the flow recirculation zone downstream of the bluff body. In general, increase in equivalence ratio leads to an increase in H_2 magnitudes. This is attributed to the increase in the fuel-richness and the higher availability of H_2S acting as an oxidation inhibitor for H_2.

Figures 5-23, 5-24, and 5-25 depict carbon monoxide mole fraction at different equivalence ratios along the reactor at three radial locations. Similar to the behavior of hydrogen, carbon monoxide decreases monotonically along the centerline of the reactor. However, radially outward, carbon monoxide peaks up to a maximum and then it decreases. All three CO mole fraction values are almost equal at the reactor exit. Near to the burner exit, CO mole fraction at R=1.77 is higher as compared to the values at R=0.0 and R=3.54. This is attributed to the presence of bluff body which imposes the flow to spread radially outwards close to R=1.77, where higher reaction rates are observed. Nevertheless, CO oxidation to CO_2 occurs so that small percentage of CO is presented at R=0.0 and R=3.54.

The mole fraction distribution of hydrogen sulfide at different equivalence ratios at three different radial locations in the reactor is shown in figures 5-26, 5-27, and 5-28. At all equivalence ratios, H_2S peaks to a maximum at R= 1.77 and then decreases in a consistent fashion. This is attributed to the fact that at R=1.77 the sampling probe is in the vicinity of

injected reactants pathlines. Under Claus conditions, considerable amount of H_2S is observed at R=3.54. This is attributed to the lack of oxygen (mixture is fuel-rich) which prevents the rapid combustion of H_2S. Hydrogen sulfide around the centerline is always negligible since most of H_2S is combusted in the recirculation region downstream of the bluff body.

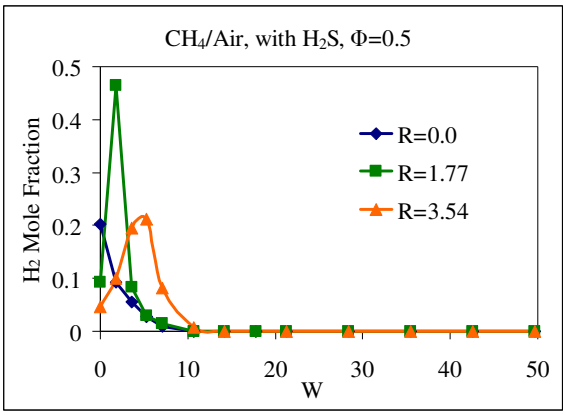

Figure 5-20. H_2 mole fraction. Flame conditions: methane/air with H_2S, Φ =0.5.

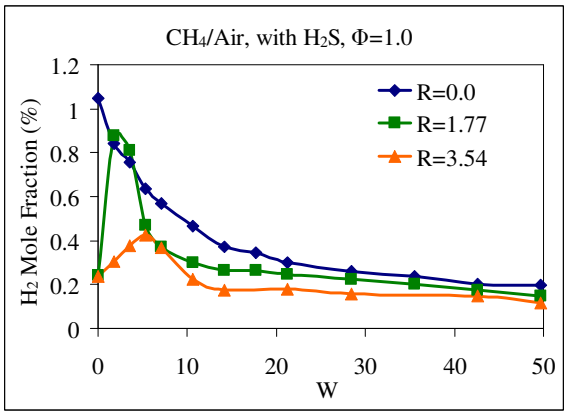

Figure 5-21. H_2 mole fraction. Flame conditions: methane/air with H_2S, Φ =1.0.

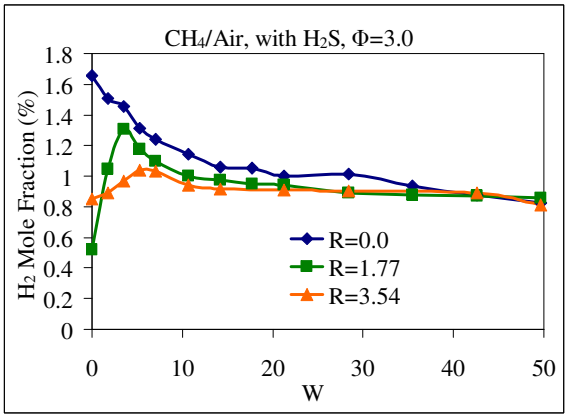

Figure 5-22. H_2 mole fraction. Flame conditions: methane/air with H_2S, Φ =3.0.

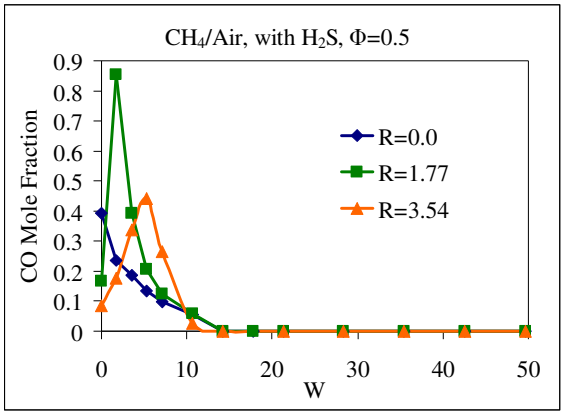

Figure 5-23. CO mole fraction. Flame conditions: methane/air with H_2S, Φ =0.5.

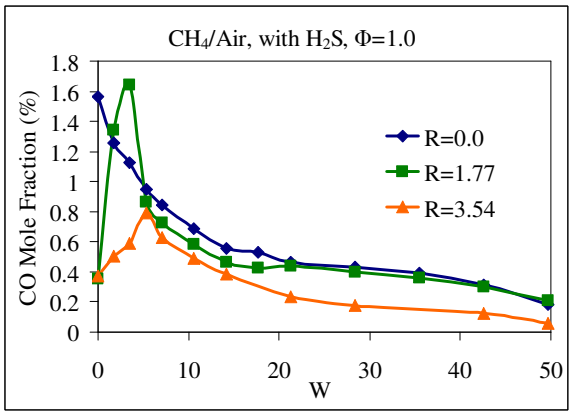

Figure 5-24. CO mole fraction. Flame conditions: methane/air with H_2S, Φ =1.0.

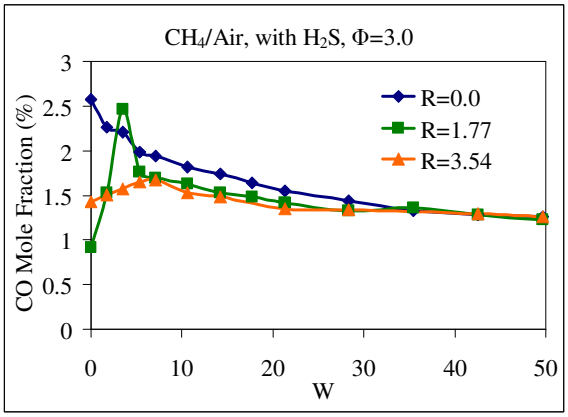

Figure 5-25. CO mole fraction. Flame conditions: methane/air with H_2S, Φ =3.0.

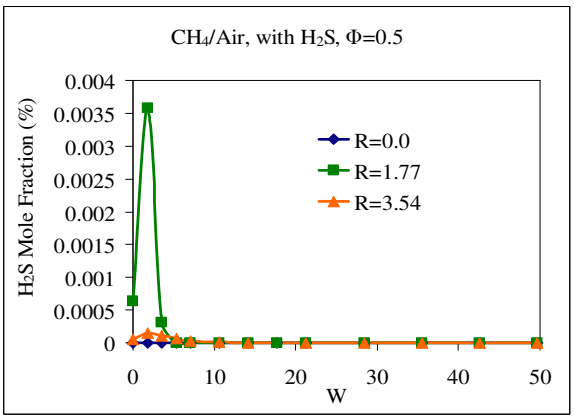

Figure 5-26. H_2S mole fraction. Flame conditions: methane/air with H_2S, Φ =0.5.

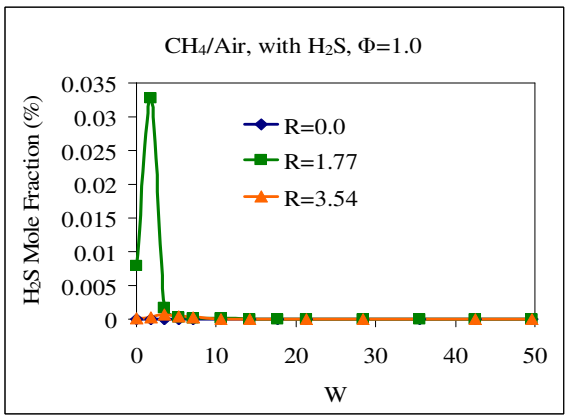

Figure 5-27. H_2S mole fraction. Flame conditions: methane/air with H_2S, Φ =1.0.

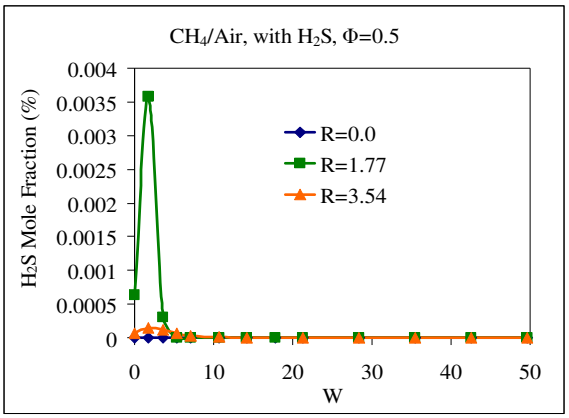

Figure 5-28. H_2S mole fraction. Flame conditions: methane/air with H_2S, Φ =3.0.

Figures 5-29, 5-30, and 5-31 present the behavior of sulfur dioxide mole fraction at different equivalence ratios along the reactor at three radial locations. At any equivalence ratio, SO_2 mole increases monotonically until it researches somewhat asymptotic value. These results differ from what we presented in section (5.1.1) where H_2S was injected into the central tube. According to what we concluded in section (5.1.1) and since all reactants are premixed, probability of H_2S oxidation is high as it competes with methane. This justifies the strong presence of SO_2 just downstream of the burner tip where H_2S has swiftly transformed into SO_2 at any equivalence ratio. Under all conditions SO_2 mole fraction does not change significantly in the radial direction at the reactor exit.

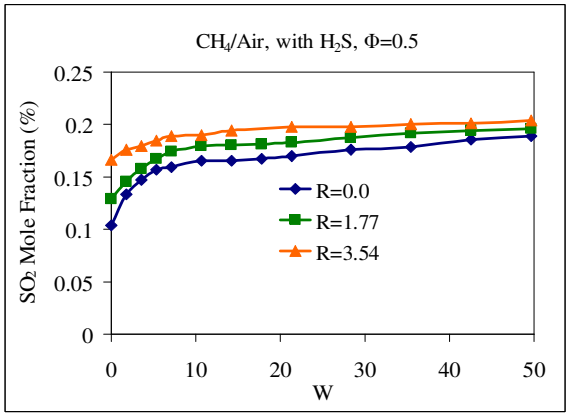

Figure 5-29. SO_2 mole fraction. Flame conditions: methane/air with H_2S, Φ =0.5.

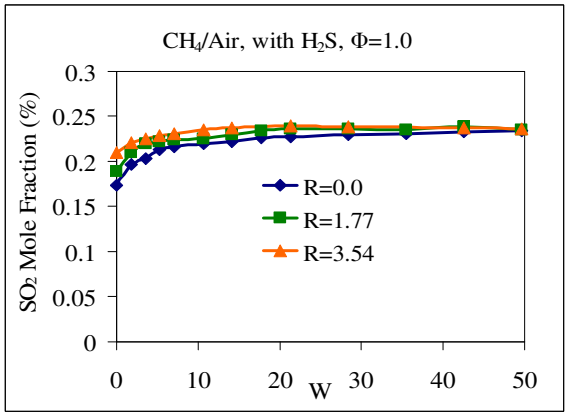

Figure 5-30. SO_2 mole fraction. Flame conditions: methane/air with H_2S, Φ =1.0.

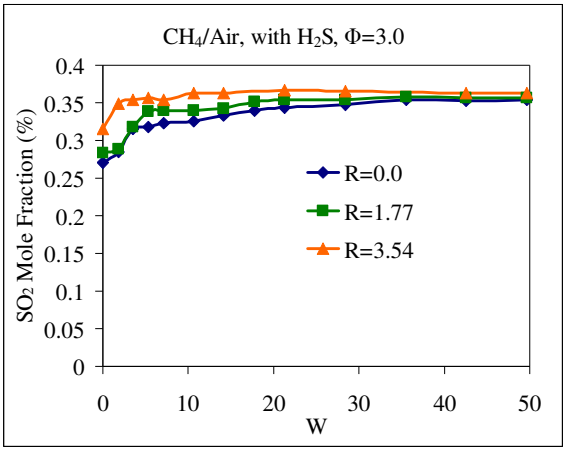

Figure 5-31. SO_2 mole fraction. Flame conditions: methane/air with H_2S, Φ =3.0.

Figures 5-32 and 5-33 show the distribution of carbon disulfide mole fraction at Φ=3.0 and Φ =1.0, while it was not observed under lean conditions (Φ=0.5). The formation of carbon disulfide is attributed primarily to the reaction of CH_4 and H_2S byproducts. Reactions (5-26) through (5-29) describe the possible channels for CS_2 formation [109, 110]:

$$CH_4 + 2\ S_2 \leftrightarrow CS_2 + 2\ H_2S \quad (5\text{-}26)$$

$$CH_4 + 2\ S \leftrightarrow CS_2 + 2\ H_2 \quad (5\text{-}27)$$

$$CH + 2\ H_2S \leftrightarrow CS_2 + 2.5\ H_2 \quad (5\text{-}28)$$

Under Claus and stoichiometric conditions, it is more common for these reactions to take place. However, under lean conditions, oxidation of H_2S and CH_4 to form SO_2 and CO_2, respectively, is more dominant. Under Claus conditions, CS_2 mole fraction is almost one order of magnitude higher than CS_2 value under stoichiometric conditions. This is mainly emanated from the rarity of CH and S radicals where the availability of more oxygen will transform these radicals into SO and OH. The latter radicals will dictate the reaction to form other end-products, such as, SO_2, H_2O, and CO_2.

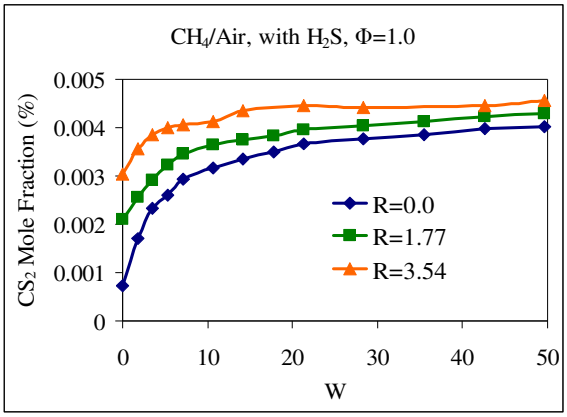

Figure 5-32. CS_2 mole fraction. Flame conditions: methane/air with H_2S, Φ =1.0.

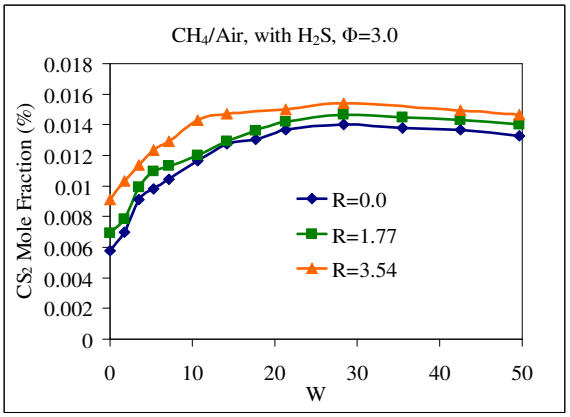

Figure 5-33. CS_2 mole fraction. Flame conditions: methane/air with H_2S, Φ =3.0.

Figures 5-34 and 5-35 depict the formation of hydrocarbons (ethane and ethylene) in the reaction pool at R=1.77 and R=3.54 under Claus conditions. The formation of hydrocarbons is attributed to CH_3 dimerization to form C_2H_6. On the other hand, ethane dehydrogenation forms ethylene. The dimerization of alkyl groups emanates from the presence of SO_2 which acts as a coupling catalyst. In section (5.1.1), we discussed the formation of hydrocarbons around the centerline of the reaction zone wherein H_2S was injected into the central tube. The absence of hydrocarbons around the centerline, in this study, justifies and validates the hypothesis of SO_2 effect as a coupling catalyst for CH_3. Higher hydrocarbons were not observed under stoichiometric and lean conditions. This is attributed to the relatively low SO_2 concentrations which reduce the chances of CH_3 dimerization. In addition, the higher availability of oxygen enhances the chance of hydrocarbons oxidation. It is noticeable that C_2H_4 and C_2H_6 abruptly decompose downstream to form lower hydrocarbons that contribute in CO, CO_2, and CS_2 formation.

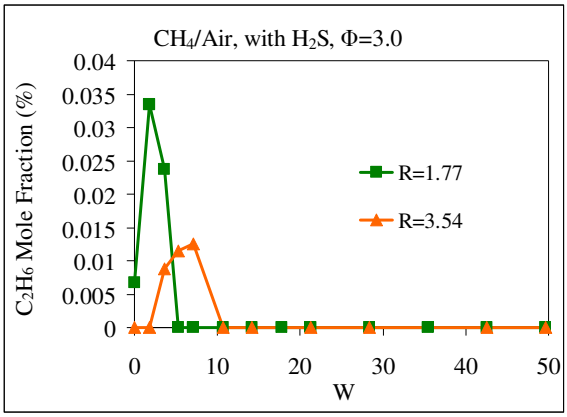

Figure 5-34. Ethane mole fraction. Flame conditions: methane/air with H_2S, Φ =3.0.

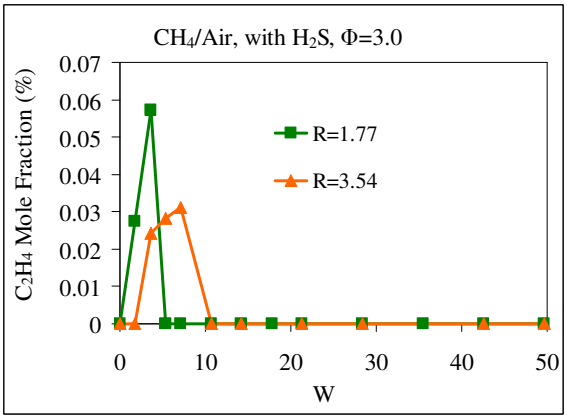

Figure 5-35. Ethylene mole fraction. Flame conditions: methane/air with H_2S, Φ =3.0.

5.1.2.3 Summary

Combustion of premixed mixture of CH_4/air/H_2S mixtures has been investigated at different equivalence ratios ranging from fuel-lean, stoichiometric to fuel-rich conditions. Gas sampling was carried out axially at three different radial locations (R=0.0, R=1.77, and R=3.54, where R is a dimensionless radial distance). The results showed that H_2 and CO mole fractions exist with higher concentrations away from the reactor centerline. Hydrogen sulfide mole fraction showed its maximum values at R=1.77 at any equivalence ratio. On the other hand, SO_2 showed a consistent (almost-constant) trend for all the equivalence ratios examined. The fact that reactants were premixed prior to combustion substantiated oxidation competition between H_2S and CH_4, thus reaction of H_2S formed SO_2 rather than S_2. Carbon disulfide was formed under stoichiometric and Claus conditions only. It was found that carbon disulfide is formed due to the presence of methane which reacts with sulfur compounds to form CS_2. Finally, hydrocarbons (ethane and ethylene) were observed under Claus conditions at R=1.77, and R=3.54. Comparison between the study conducted in section (5.1.1) and the current study solidified the fact that

hydrocarbons formation is attributed to role of SO_2 as a coupling catalyst to the alkyl group (CH_3).

5.1.3 Acid Gas (H_2S and CO_2) Combustion in H_2/Air Flames

In this section, examination of acid gas (H_2S+CO_2) combustion in H_2/air flames was conducted under the same equivalence ratios and in the same experimental setup presented previously. Several reasons encouraged us to examine the effect of CO_2 on the combustion process. Firstly, carbon dioxide is the most important contaminant that can exist in acid gas along with H_2S. Secondly, the absence of any carbonaceous compounds in the main flame (H_2/air) allowed us to accurately understand CO_2 effect on H_2S combustion. Thirdly, one of our major goals is to understand the reactor conditions and chemically kinetics under which other sulfurous compounds are formed during H_2S combustion. Accordingly, baseline case was investigated first (H_2/air flame), while effect of acid gas was examined in two stages. The first stage represents acid gas of 100% hydrogen sulfide and the second stage represents (50% H_2S and 50%CO_2) acid gas stream. Same experimental procedures of sections (5.1.1 and 5.1.2) were followed here. Figure 5-36 depicts the configuration of reactants injection into the reactor. On the other hand, table 5-3 shows the experimental conditions of all experiments presented in this section.

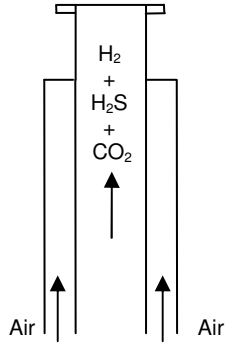

Figure 5-36. Configuration of the reactants (H_2/air/H_2S/CO_2) injected into the burner.

Table 5-3. Reactants flow rates (H_2/air/H_2S/CO_2).

Flow Rate (lit/min)		H_2	Air	Excess oxygen	H_2S	CO_2
Baseline case (without acid gas addition)		2	5.6	0.165	0	0
100% H_2S acid gas	Φ=3.0 (Claus)	2	5.6	0.165	0.33	0
	Φ=1.0 (Stoich.)	2	5.6	0.165	0.11	0
	Φ=0.5 (lean)	2	5.6	0.165	0.055	0
50% H_2S and 50% CO_2 acid gas	Φ=3.0 (Claus)	2	5.6	0.165	0.33	0.33
	Φ=1.0 (Stoich.)	2	5.6	0.165	0.11	0.11
	Φ=0.5 (lean)	2	5.6	0.165	0.055	0.055

5.1.3.1 Temperature Measurements

Mean temperature of the reactor was measured along the reactor centerline using K-type thermocouple. Figure 5-37 shows temperature profile for hydrogen/air flame both without and with the addition of 100% H_2S acid gas. In case of H_2/air flame, temperature near the burner exit was found to be considerably lower than the main flame region. This is attributed to the fact that hydrogen is injected into the central tube at room temperature. On the other hand, temperature increases downstream of the burner exit wherein hydrogen mixes with oxygen and starts to burn. Decrease in temperature beyond W~12 is attributed to the heat loss to reactor walls. In case of 100% H_2S acid gas addition, slight reduction in reactor temperature close to the burner exit was observed. In addition, slight increase in temperature was observed around W~10 due to H_2S combustion. However, addition of hydrogen sulfide proved, in general, to have marginal effect on temperature profiles. Figure 5-37 shows only temperature profile in case of 100% H_2S acid

gas addition at Φ=3.0 where the highest effect of H_2S can be observed. Addition of CO_2 in the acid gas (not shown to avoid complexity and clarity in the figure) had shallower effect on temperature profile as compared to the 100% H_2S case.

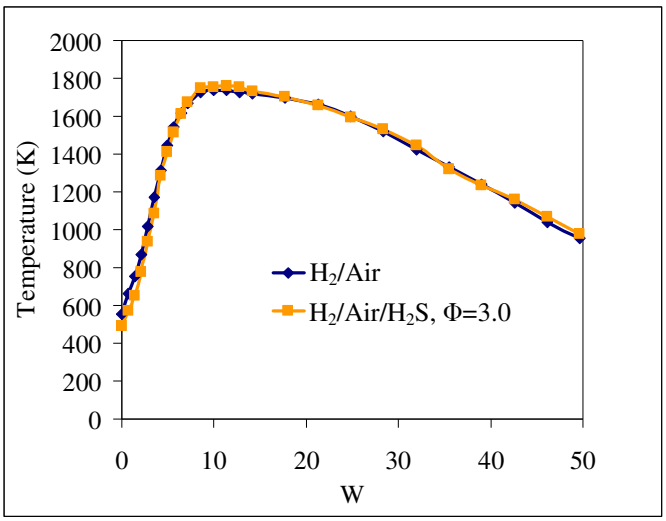

Figure 5-37. Temperature distribution along the reactor centerline for H_2/air flame without/with the addition of 100% H_2S acid gas at Φ=3.0.

5.1.3.2 Hydrogen/Air Flame

Figure 5-38 shows hydrogen distribution along the reactor centerline in hydrogen/air flame under slightly fuel-lean conditions. Consistent decay of hydrogen mole fraction can be observed along the reactor centerline until it completely diminishes. This is attributed to the availability of oxygen to achieve complete combustion. Hydrogen mole fraction can be observed to be nearly 100% close to the burner exit where the sampling probe is located very close to the burner tip. This causes most of the sampled gas to be unburned hydrogen.

5.1.3.3 Addition of 100% H_2S Acid Gas

Addition of H_2S-laden acid gas caused combustion products to contain several sulfurous compounds. Figure 5-39 shows hydrogen sulfide mole fraction along the reactor centerline at different equivalence ratios. Results showed that decay rate of H_2S increases with the decrease of

equivalence ratio. This is attributed to the increase in oxygen amounts in the reaction pool, thus increase in H_2S oxidation rates occurs. It also was found that, H_2S mole fraction decrease nearly to zero regardless of the equivalence ratio. The group of elementary reactions describes H_2S oxidation was discussed in section (5.1.1).

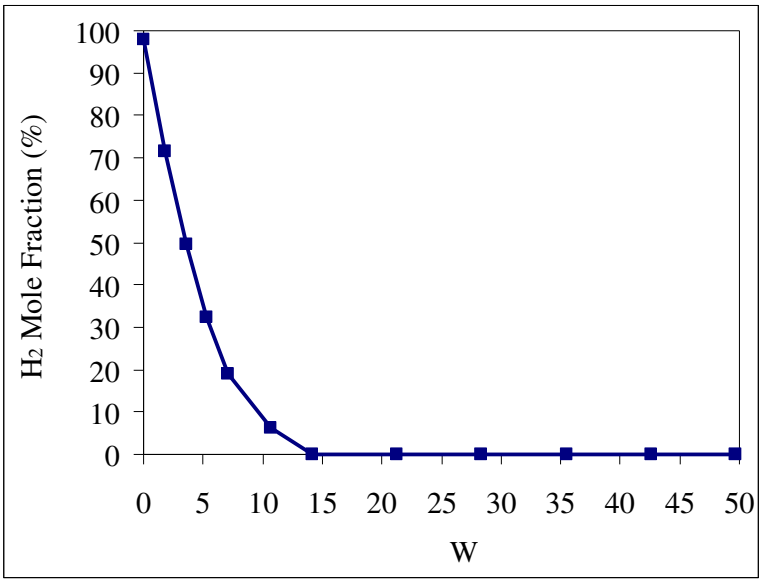

Figure 5-38. Hydrogen mole fraction. Flame conditions: Hydrogen/air, Φ =0.86.

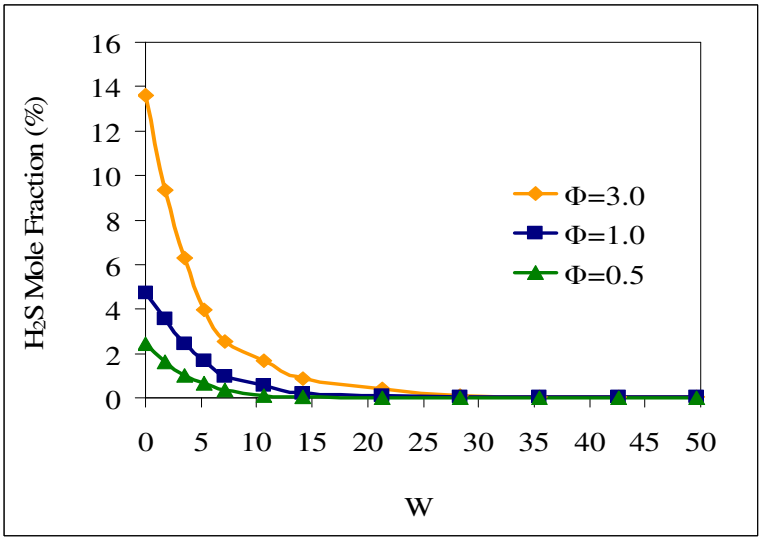

Figure 5-39. H_2S mole fraction. Flame conditions: Hydrogen/air with 100% H_2S acid gas.

On the other hand, figure 5-40 describes sulfur dioxide formation along the reactor centerline at each equivalence ratio examined. The results revealed that SO_2 increases monotonically until it reaches to an asymptotic value. Change in equivalence ratio affects the rate of increase in sulfur dioxide and the magnitude of asymptotic value. Increase in equivalence ratio increases the asymptotic value of SO_2 because of the higher amounts of H_2S introduced into the reaction pool. On the contrary, increase in equivalence ratio decreases the rate of SO_2 production due to the presence of fuel-rich mixture which lowers down the rate of H_2S oxidation. Reaction between H_2S and SO_2 to form sulfur did not occur (even under Claus conditions, Φ=3.0). This is attributed to the tendency of H_2S to form SO_2 in presence of oxygen.

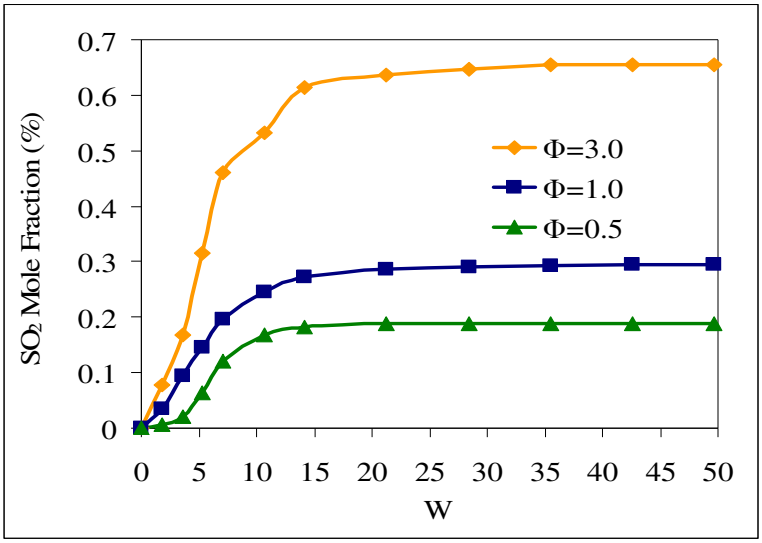

Figure 5-40. SO_2 mole fraction. Flame conditions: Hydrogen/air with 100% H_2S acid gas.

Figure 5-41 depicts hydrogen mole fraction under the investigated conditions. Hydrogen decreases near the burner tip, W=0.0, with the increase in equivalence ratio. This is attributed to addition of higher amounts of H_2S to achieve the targeted equivalence ratio. However, rate of hydrogen oxidation is a lot higher in case of fuel-lean conditions as compared to Claus conditions. This is because of the availability of higher amounts of oxygen. It is also worthy mentioning that, H_2 mole fraction does not reach to zero under Claus conditions. This can be

emanated from two reasons; firstly, the fuel-rich mixture makes it difficult for all reactants to be completely oxidized. Secondly, hydrogen sulfide is considered an inhibitor for hydrogen oxidation. Subsequently, under fuel-rich conditions hydrogen mole fraction does not diminish. This also interprets the disappearance of H_2S downstream regardless of the equivalence ratio.

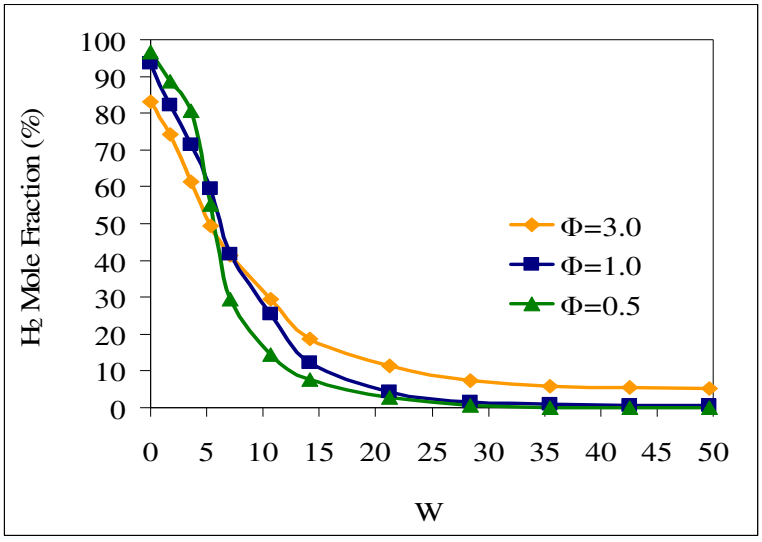

Figure 5-41. H_2 fraction. Flame conditions: Hydrogen/air with 100% H_2S acid gas.

5.1.3.4 Addition of 50% H_2S/50% CO_2 Acid Gas

Figures 5-42, 5-43 and 5-44 present the mole fractions of hydrogen sulfide, sulfur dioxide, and hydrogen, respectively, along the centerline of reactor at different equivalence ratios. Same trends in section (5.1.3.3) were observed in this section. However, rate of decay in case of hydrogen sulfide and hydrogen were faster in this section as compared to section (5.1.3.3). Also rate of sulfur dioxide production was slightly faster in this section as compared to section (5.1.3.3). The faster rate of products decay/production is emanated from the presence of carbon dioxide which acts as oxygen provider into the reaction pool.

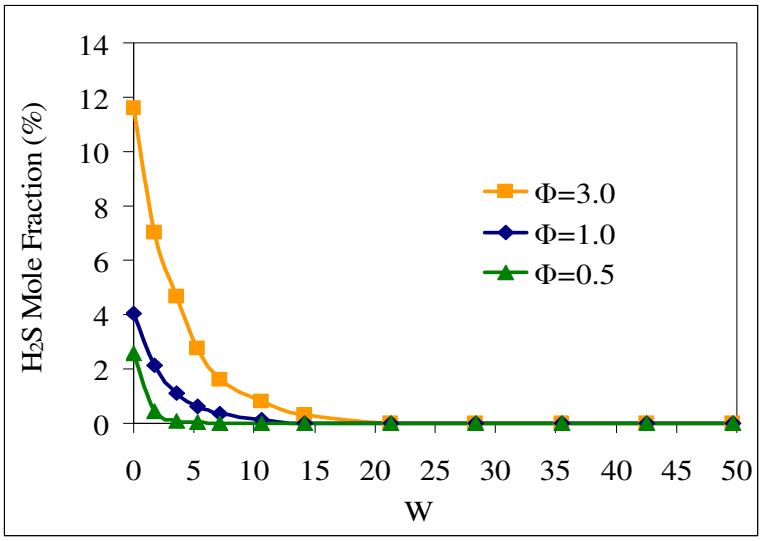

Figure 5-42. H_2S mole fraction. Flame conditions: Hydrogen/air with 50% H_2S and 50% CO_2 acid gas.

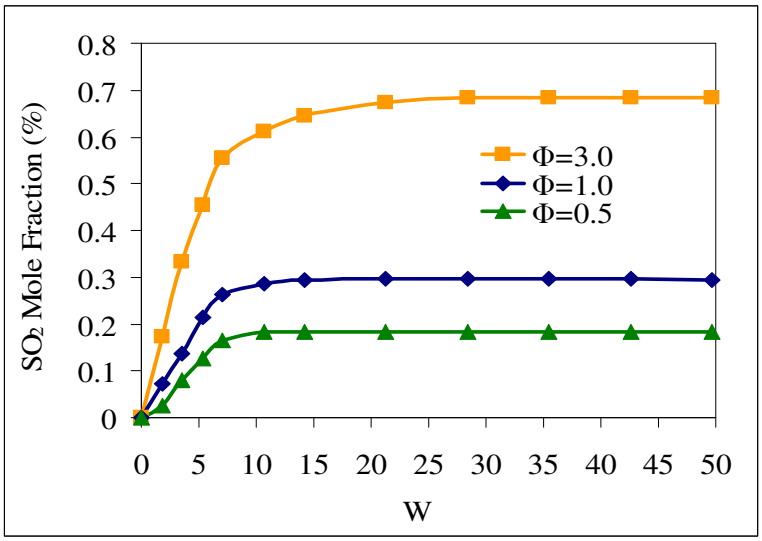

Figure 5-43. SO_2 mole fraction. Flame conditions: Hydrogen/air with 50% H_2S and 50% CO_2 acid gas.

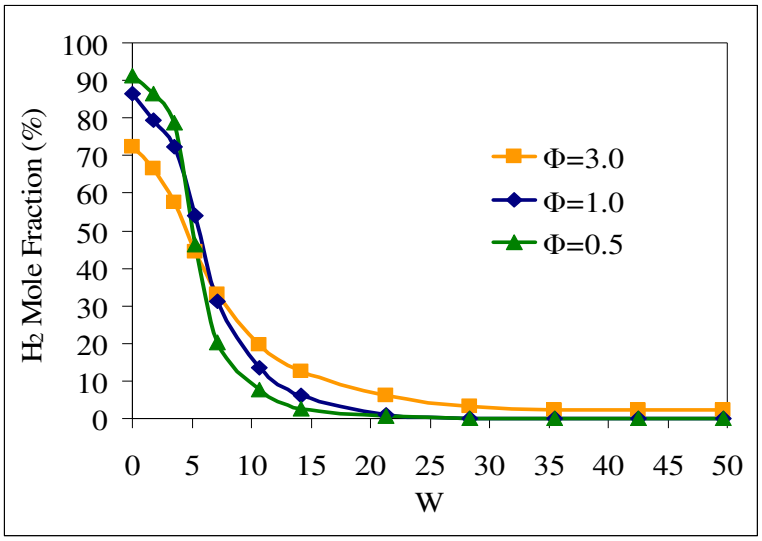

Figure 5-44. H_2 mole fraction. Flame conditions: Hydrogen/air with 50% H_2S and 50% CO_2 acid gas.

Figure 5-45 shows mole fraction of carbon monoxide along the reactor centerline. Presence of carbon dioxide is evident from the oxygen-providing role of carbon dioxide. Carbon monoxide increases at higher equivalence ratios because of the higher amounts of CO_2 addition. Formation of carbon monoxide can occur through CO_2 thermal or chemical decomposition, reactions 5-29 and 5-30 respectively.

$$CO_2 + M \leftrightarrow CO + O + M \quad (5\text{-}29)$$

$$CO_2 + H \leftrightarrow CO + OH \quad (5\text{-}30)$$

Reaction 5-29 is considered to be more dominant reaction. This is emanated from the fact that reactor temperature is relatively low to substantiate CO_2 thermal decomposition [111]. In addition, presence of atomic hydrogen is expected to be significant in H_2/air combustion which will enhance the formation of carbon monoxide thorough reaction 5-30. On the other hand, carbon monoxide mole fraction decreases downstream until it reaches to near zero value in case of fuel-lean and stoichiometric conditions. This is attributed to, firstly, the dilution effect caused by the inward radial diffusion of air injected into the reactor from the burner annulus. Secondly,

reaction with sulfur dioxide and oxygen takes place to recombine carbon dioxide (reactions 5-31 and 5-32). Effect of CO_2 on H_2S combustion will be addressed with more details in section (5.3).

$$SO_2 + CO \leftrightarrow CO_2 + SO \quad (5\text{-}31)$$

$$CO + O_2 \leftrightarrow CO_2 + O \quad (5\text{-}32)$$

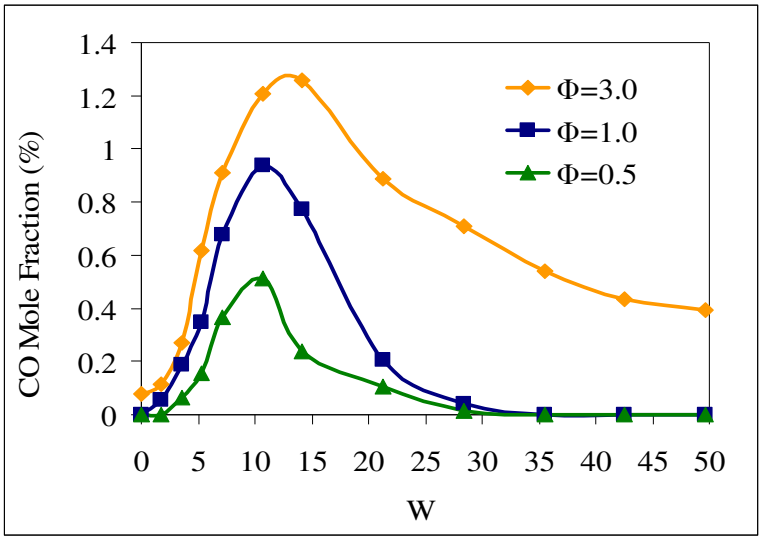

Figure 5-45. Carbon monoxide mole fraction. Flame conditions: Hydrogen/air with 50% H_2S and 50% CO_2 acid gas.

Figure 5-46 represents behavior of carbon disulfide mole fraction under the examined conditions. Reactions 5-33 through 5-38 describe the formation of carbon disulfide [112-114]. This group of reactions reveals that formation of carbon disulfide depends significantly on the presence of carbon monoxide in the reaction pool.

$$CO + S \leftrightarrow CS + O \quad (5\text{-}33)$$

$$CO + SO \leftrightarrow CS + O_2 \quad (5\text{-}34)$$

$$CO + S_2 \leftrightarrow CS_2 + O \quad (5\text{-}35)$$

$$CS + SO \leftrightarrow CS_2 + O \quad (5\text{-}36)$$

$$CS + S_2 \leftrightarrow CS_2 + S \quad (5\text{-}37)$$

$$CS + SO_2 \leftrightarrow CS_2 + O_2 \quad (5\text{-}38)$$

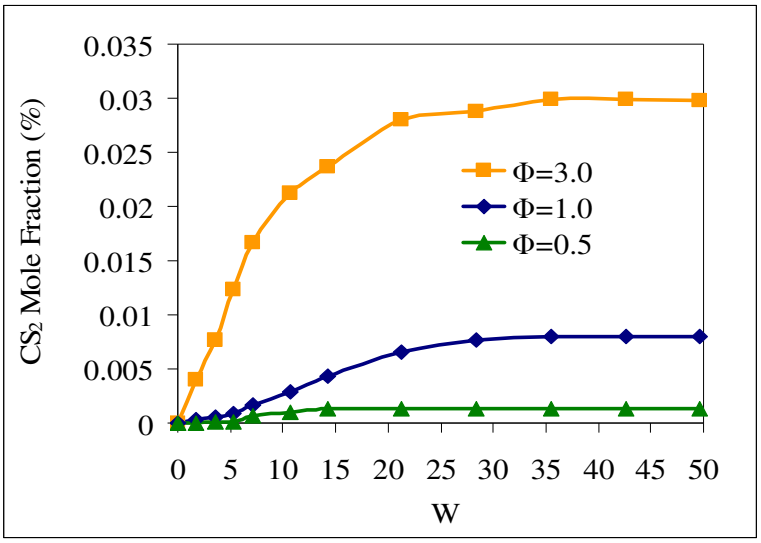

Figure 5-46. Carbon disulfide mole fraction. Flame conditions: Hydrogen/air with 50% H_2S and 50% CO_2 acid gas.

Figure 5-47 shows the distribution of carbonyl sulfide mole fraction along reactor centerline at different equivalence ratios. Carbonyl sulfide was not formed under lean conditions. This is attributed to the lack of CO and CS_2 which are the key species contribute in COS formation. On the other hand, absence COS upstream near the burner exit is attributed to the lack of high temperatures required for COS formation [113]. Reactions 5-39 through 5-41 show the possible channels for COS formation [112-114].

$$CO + SO \leftrightarrow COS + O \quad (5\text{-}39)$$

$$CS + O_2 \leftrightarrow COS + O \quad (5\text{-}40)$$

$$CS_2 + O \leftrightarrow COS + S \quad (5\text{-}41)$$

In the investigations we presented previously sections (5.1.1 and 5.1.2) we did not notice any signature of COS formation. This is attributed to the lack of the required high temperatures for COS formation (highest temperature in this study is ~ 200K higher than reactor temperatures in sections 5.1.1 and 5.1.2). All three investigations in section (5.1) proved that H_2S combustion

can produce sulfurous compounds other than sulfur dioxide such as CS_2 and COS (at high temperatures).

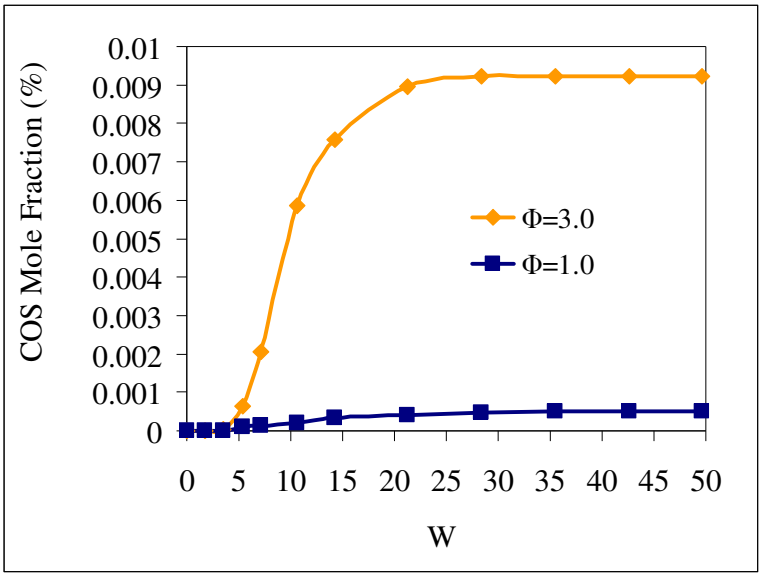

Figure 5-47. Carbonyl sulfide mole fraction. Flame conditions: Hydrogen/air with 50% H_2S and 50% CO_2 acid gas.

5.1.3.5 Summary

Acid gas (H_2S and CO_2) combustion was examined in hydrogen/air flames at different equivalence ratios. Acid gases of 100% H_2S composition and 50% H_2S/50% CO_2 composition were examined. Three equivalence ratios were studied ranging from Claus conditions (Φ=3.0), stoichiometric conditions (Φ=1.0), to fuel-lean conditions (Φ=0.5). Addition of 100% H_2S acid gas deteriorates hydrogen rate of oxidation while sulfur dioxide showed monotonic increase until it reached asymptotic value. Decrease in equivalence ratio increased the rates of production of SO_2 and decay of H_2 and H_2S. Same trends were observed for H_2S, SO_2, and H_2 with the addition of 50% H_2S/50% CO_2 acid gas. However, the rates of decay and production of all products were faster compared to the 100% H_2S acid gas case due to the presence of CO_2. .Presence of carbon monoxide was a distinct mark on the oxidizing role of CO_2 in the reaction. Presence of carbon

monoxide also triggered the formation of other sulfurous-carbonaceous compounds, such as COS and CS_2.

5.2 Hydrogen Sulfide Flame Spectroscopy

Flame spectroscopy has always been used to identify stable or intermediate species in flames non-intrusively. Several intermediate species have been identified successfully in different flames such as OH*, C_2*, and CH* via flame spectroscopy techniques; this actually contributed remarkably to the understanding of chemistry of these flames. In section (5.1) we have investigated H_2S combustion under different flame conditions and determined the conditions under which other hazardous sulfur compounds can be formed. In this section, we examined H_2S flame emissions in order to identify the species (stable or intermediate) that are responsible for the detected emissions. This enriched the understanding we have already gained in section (5.1) to H_2S combustion chemistry.

Experimental setup components have been illustrated in chapter 4. Burner A has been used along with the computer controlled traversing mechanisms. A spectrometer coupled with an ICCD camera was used for the detection of chemiluminescent signals from the excited species, see section (4.2.2).

5.2.1 H_2S/O_2 Flame Spectroscopy

Emissions of H_2S/O_2 flame combusted under lean conditions were identified first in this investigation. Figure 5-48 shows the configuration of reactants injected into the burner (burner A); reactants flow rates were as follows:

H_2S flow rate: 0.3 lit/min and oxygen flow rate: 0.9 lit/min (Φ= 0.5)

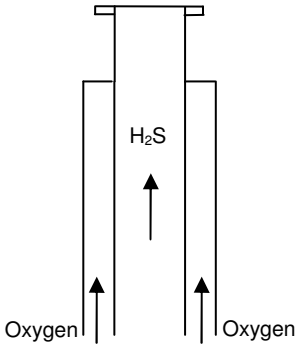

Figure 5-48. Configuration of the reactants (H_2S/O_2) injected into the burner.

Figure 5-49 shows the emissions spectrum obtained from H_2S/O_2 flame using the coarse grating (covers ~ 270nm). A high-intensity continuum was obtained along the range of the presented spectrum. This continuum is attributed to SO_2* afterglow which is a strong chemiluminescent continuum band reported in the literature to be between 250-500 nm [97-99,69]. The presence of SO_2 afterglow proved to mask any other flame emissions, if they exist.

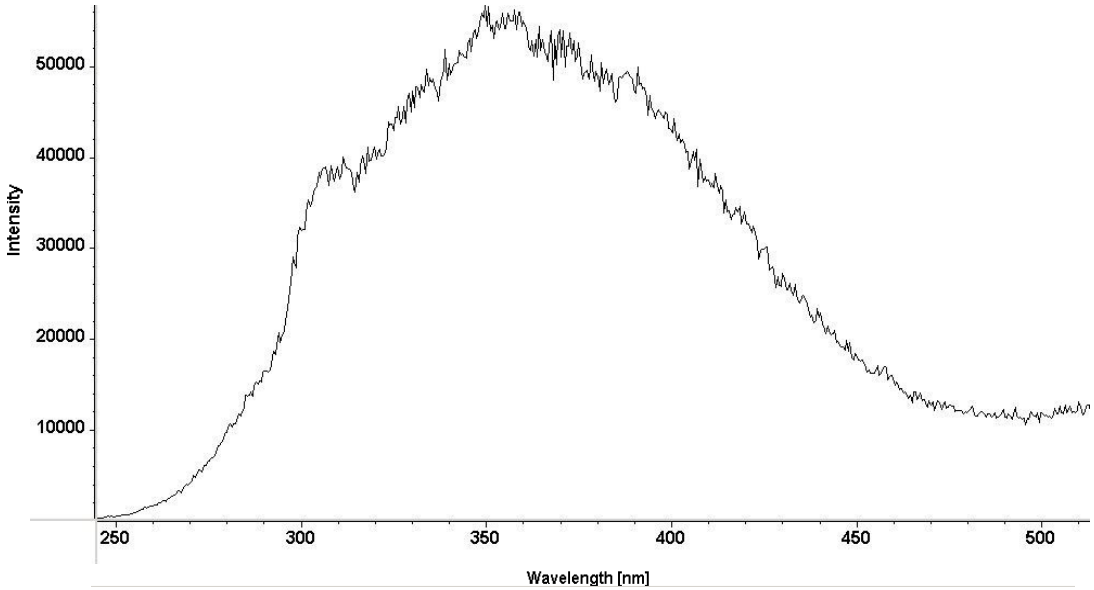

Figure 5-49. SO_2* afterglow emitted from H_2S/O_2 flame.

Because of the wide variation in peaks intensity which hindered showing all the spectrum details in one figure, we have used the fine grating (covers ~70 nm) to break it down into smaller spectra as shown in figures 5-50, 5-51, 5-52, and 5-53. The spectra showed groups of distinct

peaks superimposed on the continuum band between 280-310nm, and 370-480nm. The first group of peaks is attributed to the absorption bands of SO_2 [98,115] (in the range of 280-315nm). Although SO is considered an important intermediate species for SO_2 production, the presence of distinct SO* peaks is uncertain because they are masked by the strong continuum of SO_2 afterglow, if indeed they exist. The peaks observed beyond 370 nm have been suggested by several investigators to be attributed to SO* [116], SO_2* [99,117], or SO_3* [97,69]. However, the presence of SO_2* afterglow makes it very difficult to pinpoint the peaks and the wavelengths they are emitted at. The dominance of SO_2* afterglow continuum has been a problem that we encountered in all the flames we have investigated (CH_4/air/H_2S, C_3H_8/air/H_2S…etc). It also has been an established fact in the literature that it is hard to identify emissions of any species in presence of SO_2* afterglow.

Mulcahy et al. [99] suggested that the afterglow continuum is formed by excited singlet and triplet states of SO_2*. He suggested that the singlet emission of SO_2* is in the region around 350nm while the triplet emission is around 425nm. This agrees with our findings presented here where the continuum peaks at ~365 because of singlet SO_2* emission and the continuum beyond 400nm is much weaker which is attributed to triplet emission of SO_2*. The group of chemiluminescent reactions responsible for this continuum is as follows [16,99,100]:

$$SO + O \leftrightarrow SO_2^* \qquad (5\text{-}42)$$

$$SO_2 + O + O \leftrightarrow O_2 + SO_2^* \qquad (5\text{-}43)$$

Reaction (5-42) contributes significantly in SO_2 afterglow in case of high atomic oxygen concentrations (which is the case in our study, Φ=0.5) and it was found to produce triplet SO_2 emission [100]. Reaction (5-43) is assumed to occur in two steps [99] as follows:

$$SO_2 + O + M \leftrightarrow SO_3^* + M \qquad (5\text{-}44)$$

$$SO_3^* + O \leftrightarrow {}^1SO_2^* + O_2 \quad (5\text{-}45a)$$

$$SO_3^* + O \leftrightarrow {}^3SO_2^* + O_2 \quad (5\text{-}45b)$$

In case of oxygen depletion chemiluminescent reactions will not progress to reaction 5-45.

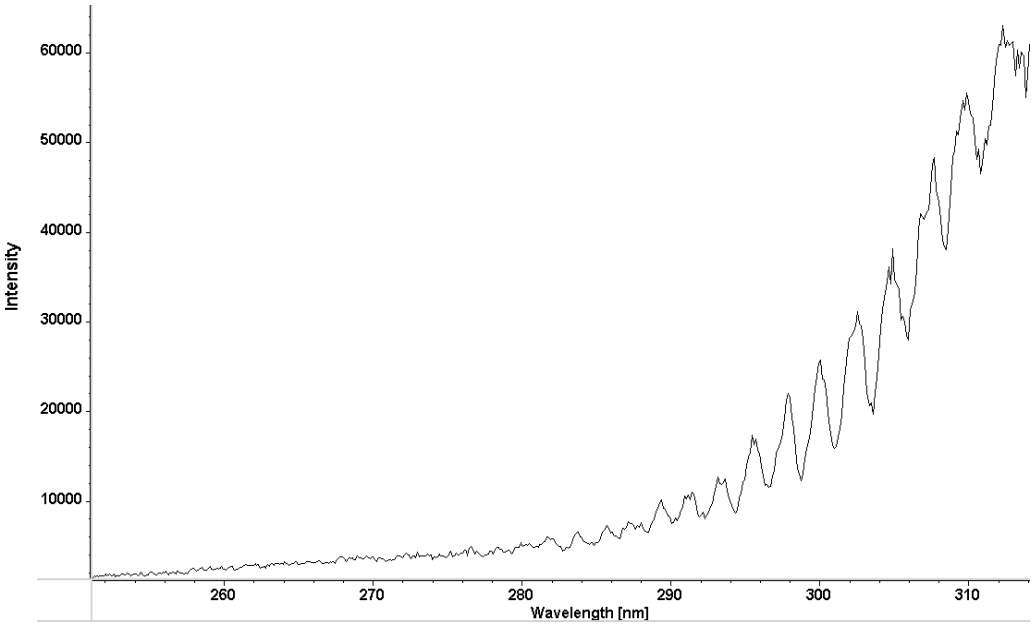

Figure 5-50. Emission spectrum of H_2S/O_2 flame (250-314nm).

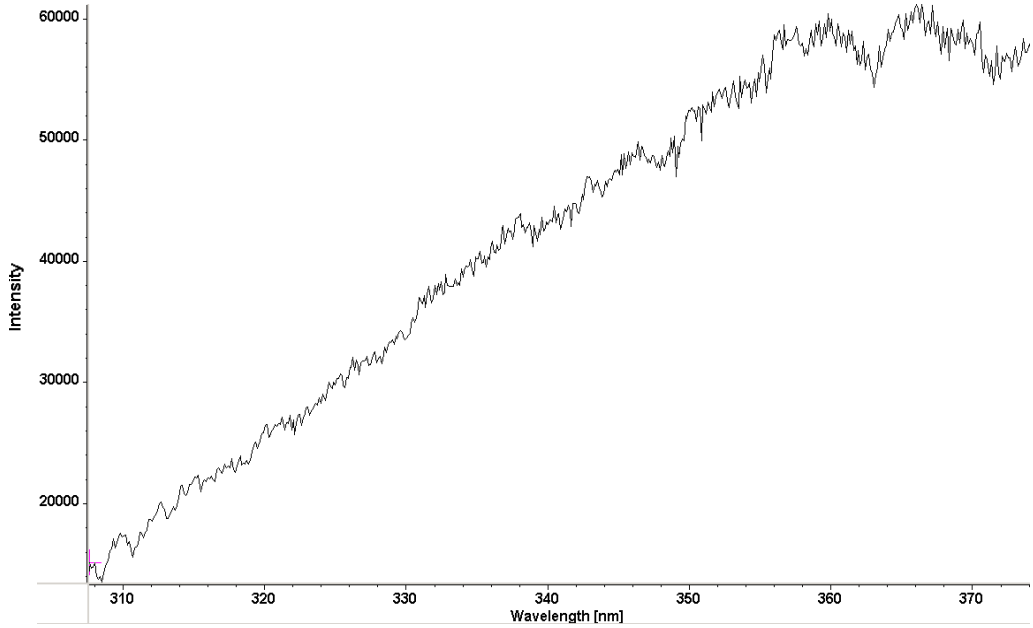

Figure 5-51. Emission spectrum of H_2S/O_2 flame (308-374nm).

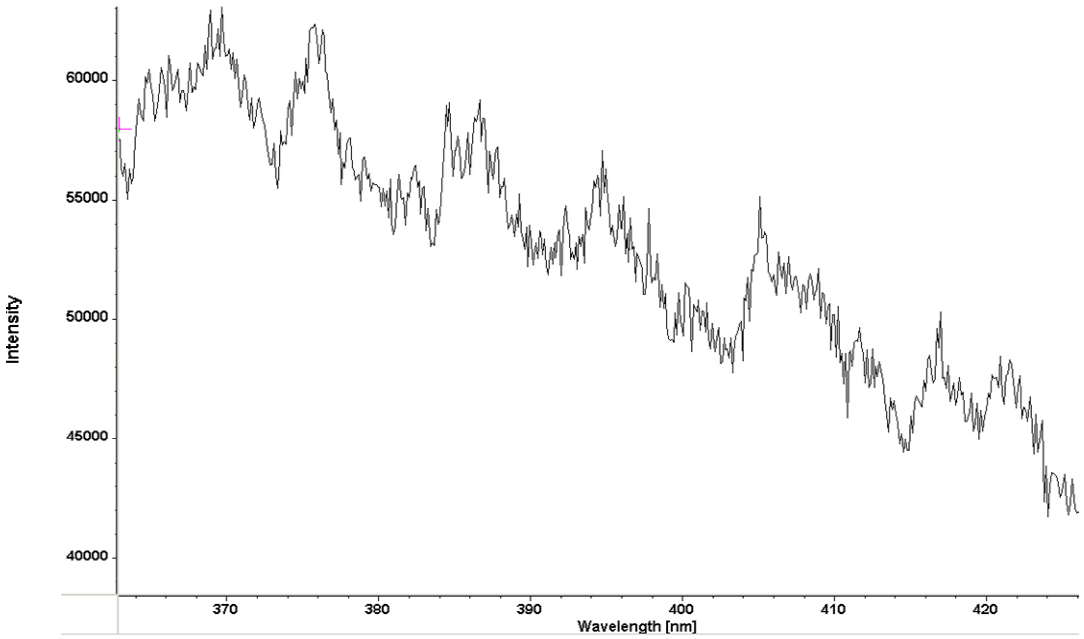

Figure 5-52. Emission spectrum of H_2S/O_2 flame (362-426nm).

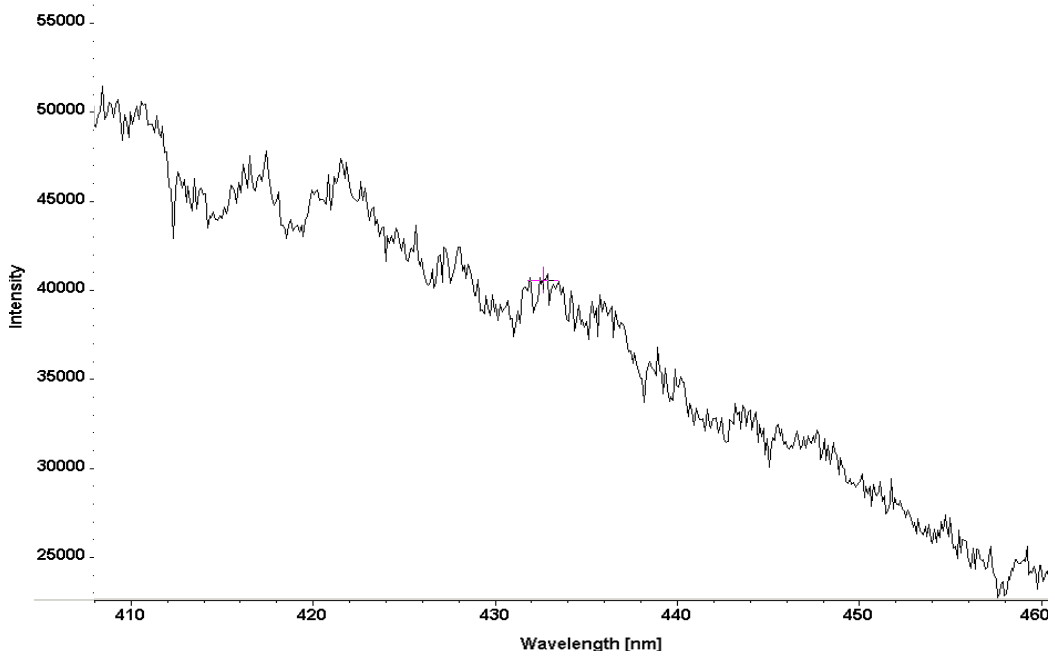

Figure 5-53. Emission spectrum of H_2S/O_2 flame (408-460nm).

5.2.2 H_2/Air/H_2S Flame Spectroscopy

Neutralization of SO_2 afterglow continuum is crucial in order to detect sulfurous compounds bands from H_2S flames. In this section we investigate H_2/air flame emissions without/with the injection of trace amounts of H_2S. We have used trace amounts of H_2S in order to avoid the high concentration of SO_2, if formed. In addition, the mixture was adjusted to be nearly stoichiometric to avoid the availability of higher amounts of atomic oxygen, thus effect of reaction (5-45) will be minimal. Figure 5-54 shows the configuration of reactants injection into the reactor. Reactants flow rates were as follows:

Hydrogen flow rate: 3 lit/min, air flow rate: 7.2 lit/min, H_2S flow rate: 4 cm^3/min.

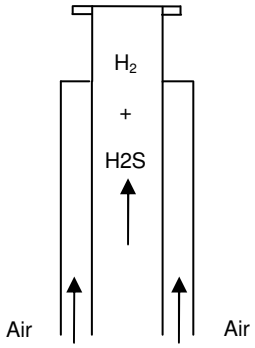

Figure 5-54. Configuration of the reactants (H_2S/O_2) injected into the burner.

Figures 5-55 and 5-56 present the spectrum of hydrogen/air flame, without H_2S addition, using both coarse and fine gratings, respectively. Figure 5-55 shows a wide spectrum of hydrogen/air flame between 230nm and 500nm. The spectrum shows one global peak at 309.13nm which is attributed to OH* radical. Figure 5-56 elaborates the global peak of OH* using the fine grating between 250nm and 315n where three major peaks of OH* radical were observed. The first peak is at 306.13nm, the second peak (strongest amongst the OH*peaks) is at 309.09 nm, and the third major peak is at 312.9nm. These results agree with the general findings reported in the literature on the OH* by several investigators [85,118]. However, the exact wave

length of the strongest peak of OH* is still controversial. For example, Smith et al. [119] reported that strongest OH* peak at 306 nm, Walsh et al. [120] stated that OH* to peak at 307.8 nm, Harber et al. [121] mentioned that reported OH* maximum peak at 308 nm, and Gaydon [85] reported that OH* to peak at 310 nm. This clearly shows that there are wide variations in the observed OH* peak wavelength value. Our results support the close proximity of the observed OH* peak by Gaydon [85].

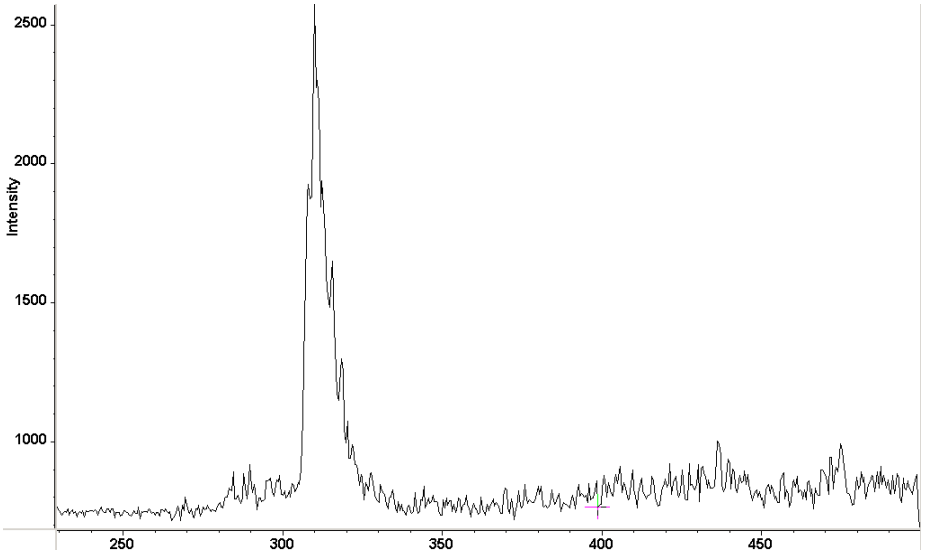

Figure 5-55. Emission spectrum of hydrogen/air flame (230nm-500nm).

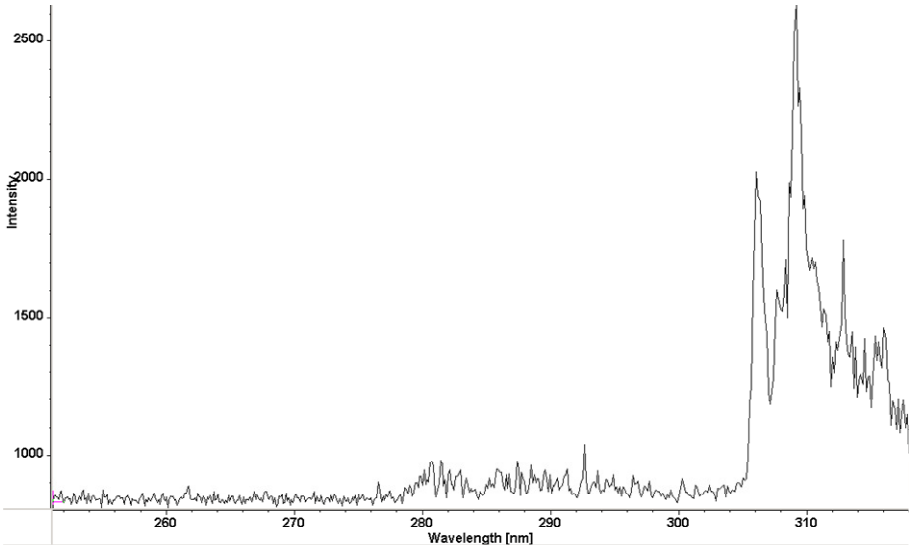

Figure 5-56. Emission spectrum of hydrogen/air flame (250nm-318nm).

Hydrogen/air flame has a very faint color (almost colorless), see figure 5-57a. However, with the addition of only a trace amount of H_2S a strong bluish inner cone was formed at the flame base, see figures 5-57b and 5-57c. Increased amounts of H_2S to the H_2/air flame resulted in bluish white color flame, see figure 5-57d where SO_2* afterglow starts to dominate. In this section we examined the characteristics of blue cone formed with addition of trace amount of H_2S into H_2/air flame. In order to provide an understanding for the distinct change associated with the addition of trace mount of H_2S, flame spectroscopy was used at various locations in the formed blue cone. Figure 5-57d defines the blue cone in dimensionless axial and radial distances (W and R).

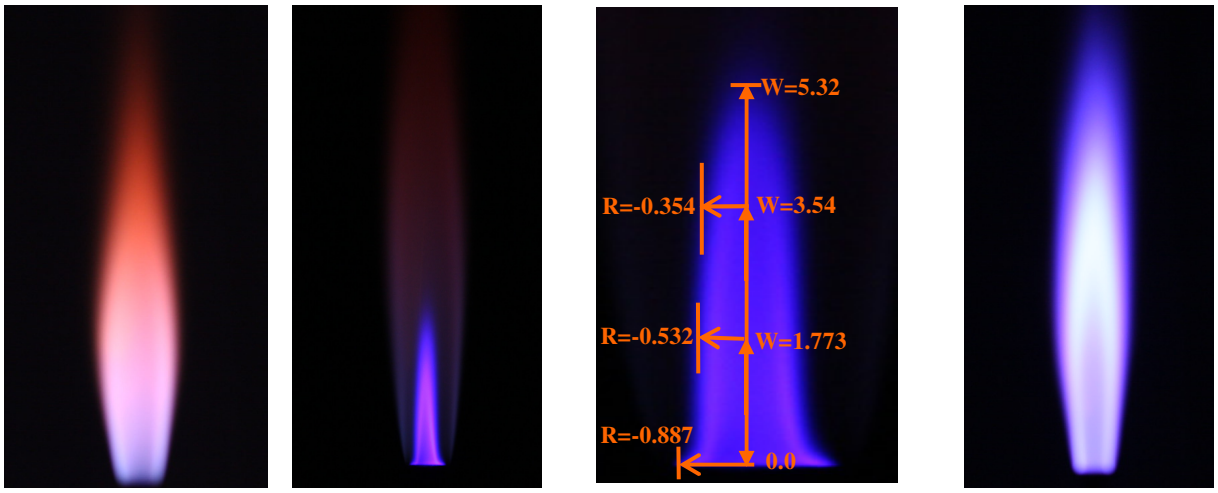

(a) (b) (c) (d)

Figure 5-57. Flame photograph with (a) Hydrogen/air flame, (b) Hydrogen/air flame with trace amount of H_2S addition, (c) blue cone defined in dimensionless axial and radial distances, (d) Hydrogen/air flame with increased amounts of H_2S addition.

Figure 5-58 shows the spectrum of the blue cone obtained on longitudinal axis of the flame at W=1.773 (where, W and R are the dimensionless distances defined previously) using a coarse grating in the spectrometer. Spectrum clearly shows the absence of SO_2* afterglow while

a strong series of peaks were observed within 320-470 nm. It is noticeable that, blue cone emissions possess a lot higher intensity as compared to the previously-observed OH* peaks. Moreover, emission spectrum of the inner blue cone did not change within its core. However, the spectrum of the inner blue cone starts to fade near its tip (at W=5.32) and OH* peak starts to dominant the spectrum at immediately downstream of the blue cone tip. Figure 5-59 shows the spectrum at the tip of the blue cone where OH* peak becomes dominant and the blue cone bands diminish. This conjectures that hydrogen sulfide combustion has almost completed and this point.

Spectrum of the blue cone has been examined in further details using the fine grating in order to provide improved spectrum resolution. The fine grating in the spectrometer helped us to judicially identify the wavelength of each peak, and to assist in better understanding of the various chemical species responsible for the emission spectrum. Figures 5-60, 5-61, and 5-62 present in details the spectrum of the inner blue cone formed in H_2/air flame with the injection of trace amount of H_2S. No significant bands were observed below 306nm while OH* peaks were identified ~ 308 nm. As we mentioned in section (5.2.2), several researchers credited the peaks observed beyond 320nm to be attributed to SO* [116], SO_2* [99,117], or SO_3* [97,69]. The spectrum of SO* was found to be extended from 244.2nm to 394.1nm with more than 40 peaks distributed along this band of wavelengths. However, these bands are not likely to be occurring under one experimental condition and they are more common in rich flames. In the current study, it is unlikely to have all these bands since the concentration of sulfur species is very small. However, some of the observed peaks match up with SO* peaks in the literature [97], which are the relatively weak bands within 320-350nm. On the other hand, peaks at 324.03 nm and 328.62 nm are most likely attributed to SH absorption bands [86]. The likelihood of SO_2* to be the

cause of bands beyond 350nm is very minimal. This is because, the reported spectra of SO_2* in the literature showed distinct peaks superimposed on the continuum of SO_2* afterglow [98,99,69,117]. With the absence of the afterglow continuum presence of SO_2* can be confidently denied. Accordingly, the explanation of SO_3* responsible for the peaks beyond 350nm is the most acceptable one he findings by Gaydon et al. [97,122] and Dooley et al. [123] suggested that the peaks beyond 350nm are attributed to the presence of SO_3*. Sulfur trioxide can be formed in the reaction zone due to the reaction between sulfur dioxide and atomic oxygen or hydroxyl group as follows [97,122,123]:

$$SO_2 + O \leftrightarrow SO_3^* \quad (5\text{-}46)$$

$$SO_2 + OH \leftrightarrow SO_3^* \quad (5\text{-}47)$$

Reactions (5-46) and (5-47) create a strong channel for the formation of SO_3* which is responsible for the continuous band of peaks beyond 340nm. On the other hand, several peaks beyond 400 nm were found to match up with Balmer [94,95] bands peaks obtained from H*. Since presence of atomic hydrogen is surely significant in H_2/air/H_2S flame, we can not neglect the possibility of having contribution from Balmer bands in the blue cone. However, differentiation between SO_3* and H* is still controversial. Table 5-4 shows the wavelength of all peaks observed in the spectrum of the inner blue cone in the flame.

Table 5-4. Blue cone emissions peaks.

Wavelength (nm)	Species	Wavelength (nm)	Species	Wavelength (nm)	Species
309.09	OH*	346.59	SO* band	408.43	SO_3 and H* bands
322.21	SO*	347.83		415.86	
324.03	SH (absorption band)	349.85		425.71	
326.62	SO*	355.24	SO_3 and H* bands	430.0	
328.62	SH (absorption band)	358.77		439.6	
333.92	SO* band	364.75		443.7	
336.99		368.42		449.09	
338.97		373.42		453.8	
341.61		383.16		458.8	
343.15		393.71		465.2	
344.7		404.57			

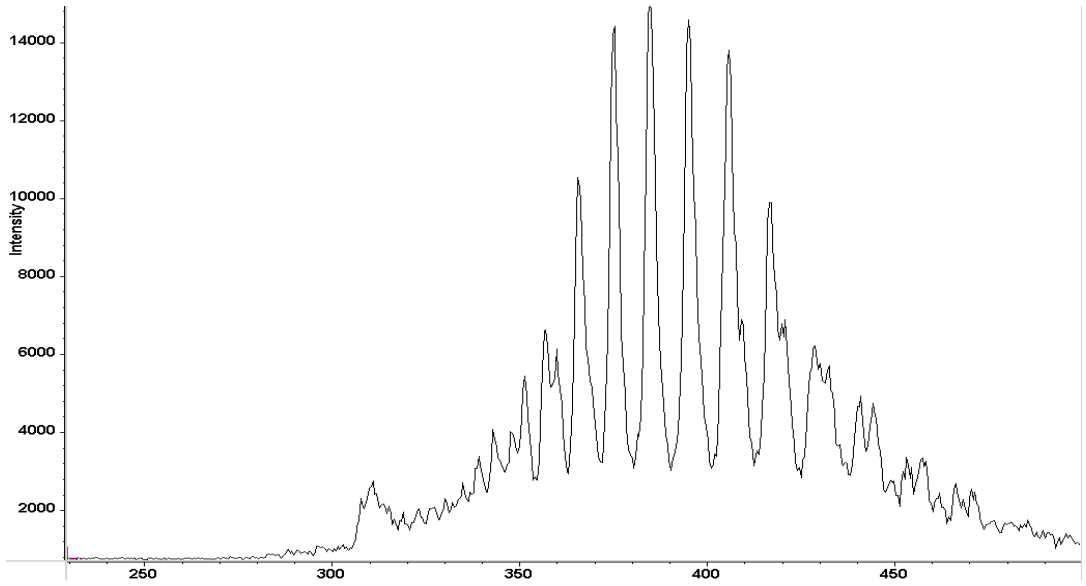

Figure 5-58. Emission spectrum of hydrogen/air flame, with trace amounts of H_2S addition in the range 230nm-500nm.

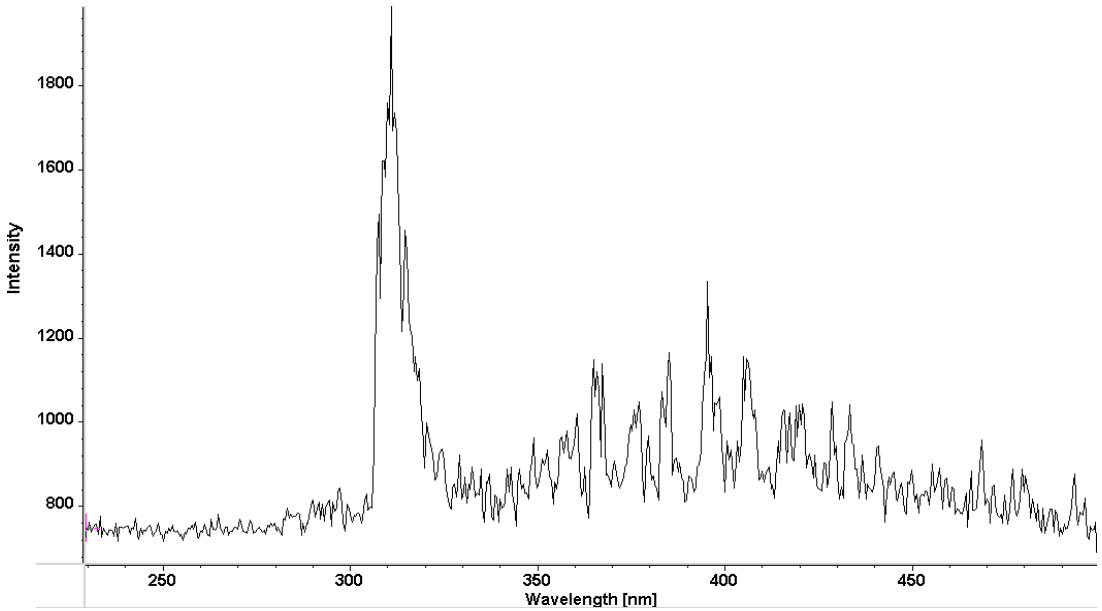

Figure 5-59. Emission spectrum of hydrogen/air flame with the addition of H_2S at the tip of the inner cone (230nm-500nm).

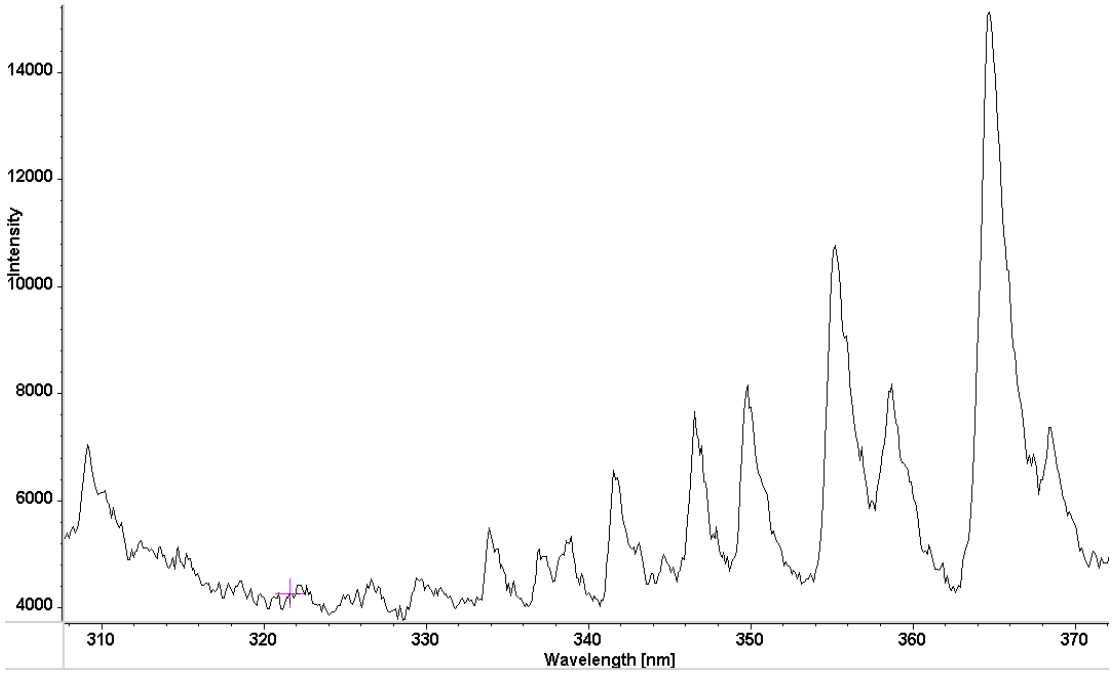

Figure 5-60. Emission spectrum of hydrogen/air flame with addition of trace amount of H_2S (308-372nm).

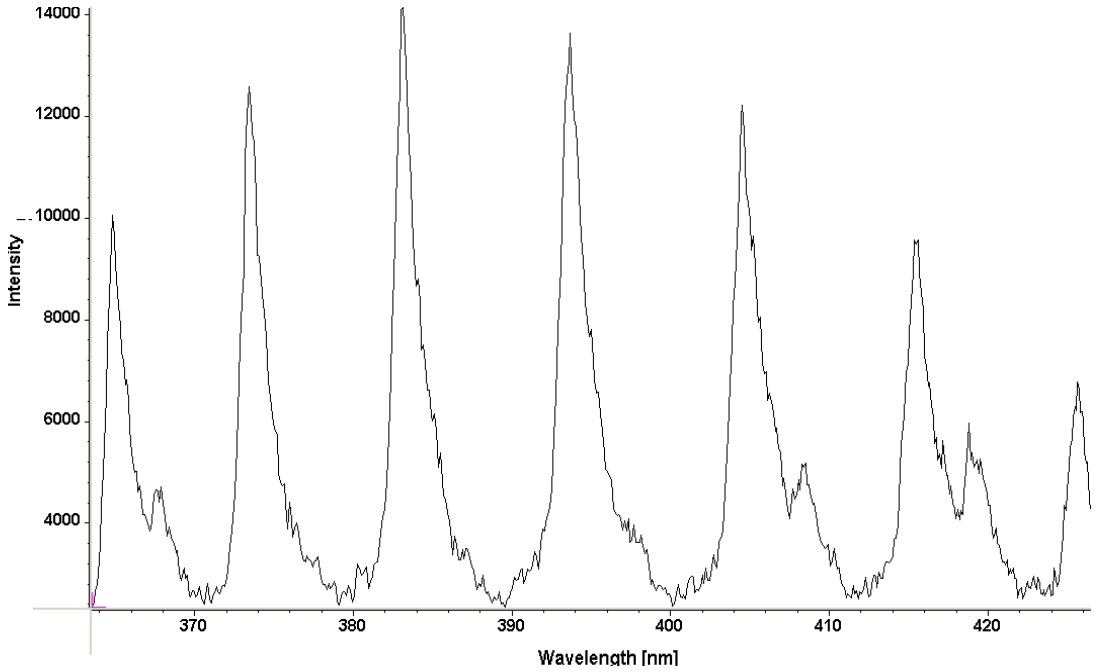

Figure 5-61. Emission spectrum of hydrogen/air flame with addition of trace amount of H_2S (364-426nm).

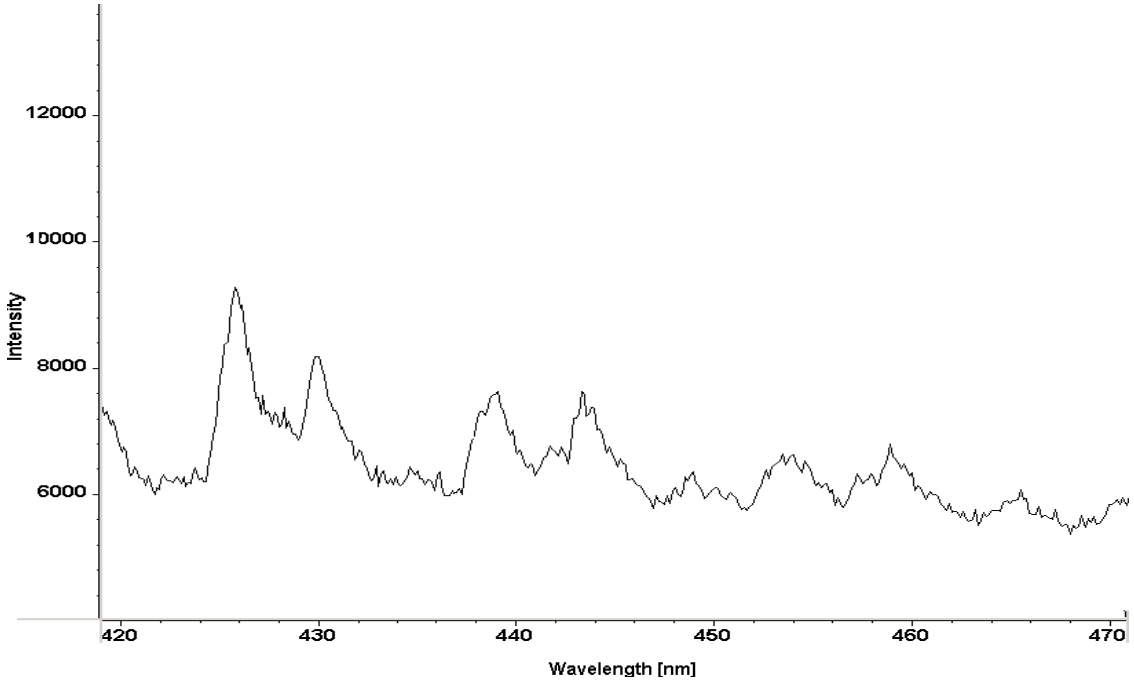

Figure 5-62. Emission spectrum of hydrogen/air flame with addition of trace amount of H_2S (420-470nm).

5.2.3 Summary

Spectra of excited species of hydrogen sulfide flames have been examined. The spectra of H_2S/O_2 flame under lean conditions (Φ=0.5) showed strong absorption bands of SO_2* within 280-310nm. Strong continuum was observed between 280-460nm wherein group of peaks were found to be superimposed beyond 370 nm. The continuum is attributed to singlet and triplet SO_2* afterglow. Singlet excited SO_2* afterglow is around 365nm region while the triplet excited SO_2* afterglow is beyond 400nm. In order to avoid the presence of SO_2* afterglow trace amounts of H_2S were injected into H_2/air flame. Without the addition of H_2S, hydrogen/air flame showed one distinct global peak of OH* at 309.13nm. However, higher resolution of the spectrum showed that OH* is responsible for three major peaks at 306.13, 309.09, and 312.9nm. Addition of a trace amount of H_2S into H_2/air flame caused the formation of a strong bluish inner cone located near to the flame base. The spectrum of the blue cone showed very strong group of peaks within 320-470nm. The group of peaks formed inside the blue cone was grouped into three major bands. The first band is caused by SO* within 320-350nm, the second band is attributed to SO_3*, and the third band is due to H*. The distinction of SO_3* band and H* band is still controversial. Absorption bands of SH were observed at 324.03nm and 328.62nm.

5.3 Effect of Acid Gas Composition on H_2S Treatment

As we discussed in chapter 1, acid has stream is likely to contain contaminants other than hydrogen sulfide such as carbon dioxide and nitrogen. In this section, we investigated experimentally the effect of carbon dioxide and nitrogen on H_2S reaction under Claus conditions. Firstly, experiments were conducted to examine the combustion of H_2S/O_2 mixture and the evolution of the stable end-products. Secondly, effect of CO_2 or N_2 addition into H_2S stream in

the reaction pool was demonstrated. Burner B has been used during this investigation because of the relatively low flow rates of the reactants. Figure 5-63 shows the configurations of reactants injected into the reactor burner. Flow rates of hydrogen sulfide and oxygen were kept constant during all the experiments. However, carbon dioxide and nitrogen flow rates were adjusted with respect to their targeted concentrations in the acid gas stream. Maximum concentration of carbon dioxide or nitrogen examined in the acid gas stream during the experiments was 30%, in increments of 10%. Table 5-5 shows the flow rates of oxygen, hydrogen sulfide, carbon dioxide, and nitrogen for each tested conditions reported here.

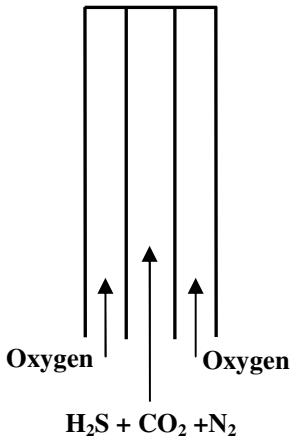

Figure 5-63. Configuration of the reactants (H_2S /O_2/CO_2/N_2) injected into the burner.

5.3.1 Temperature Measurements

Axial temperature distribution within the flame zone was measured using a K-type thermocouple. Figure 5-64 shows temperature distribution along the reactor centerline for H_2S/O_2 flame both without and with the addition of carbon dioxide. Figure 5-65 shows measured temperature distribution along the centerline of the reactor both without and with the addition of nitrogen. Both cases represent 30% concentration of CO_2 or N_2 so that the highest effect of acid gas contaminant on temperature distribution is obtained. It is worthy mentioning

that dimensionless distance (W= axial distance/D_{jet}) is calculated based on D_{jet} of burner B. Temperature measurements at the burner exit (W=0) were not attainable due to flame extinction problems cause by the thermocouple tip. Addition of nitrogen or carbon dioxide caused flame temperature to decrease immediately upon injection. This is attributed to injection of relatively cold flow of carbon dioxide or nitrogen into the reaction zone. Despite CO_2 heat capacity is higher than nitrogen within the reactor temperature range; temperature drop is higher in case of nitrogen addition as compared to CO_2 addition. This is attributed to the fact that nitrogen behaves as an inert gas within the reaction zone which only dilutes the reactants. However, carbon dioxide acts as an oxidizer (discussed further in the next section). This supports the increase in reactor temperature at downstream locations with CO_2 addition where H_2S oxidation rate is higher.

Table 5-5. Reactants flow rates (H_2S /O_2/CO_2/N_2).

	H_2S (cm^3/min)	CO_2/N_2 (cm^3/min)	O_2 (cm^3/min)
Acid gas composition (100% H_2S, 0% CO_2/N_2)	105	0	52.5
Acid gas composition (90% H_2S, 10% CO_2/N_2)	105	11.6	52.5
Acid gas composition 80% H_2S, 20% CO_2/N_2)	105	26.25	52.5
Acid gas composition (70% H_2S, 30% CO_2/N_2)	105	45	52.5

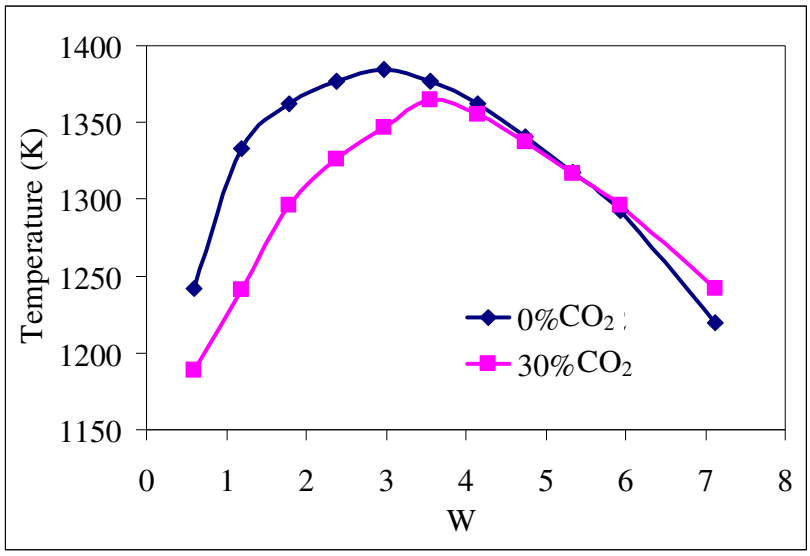

Figure 5-64. Effect of CO_2 addition on temperature distribution along centerline of the reactor.

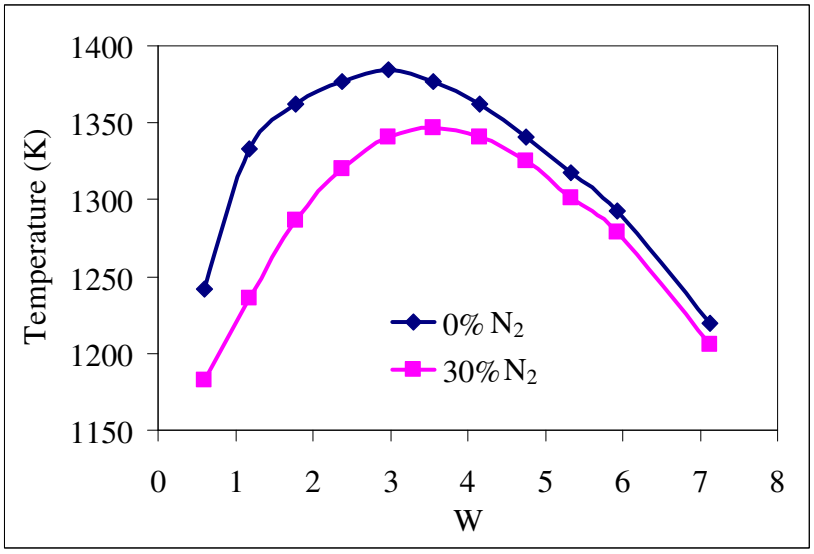

Figure 5-65. Effect of N_2 addition on temperature distribution along centerline of the reactor.

5.3.2 Combustion of CO_2-Laden Acid Gas

Effect of carbon dioxide addition was examined under different concentrations in the acid gas stream. Baseline case was demonstrated first wherein acid gas (100% H_2S) reacts with oxygen. Carbon dioxide concentration in the acid gas stream was varied between 0% and 30% in increments of 10%. Figure 5-66 shows the behavior of both H_2S and SO_2 along centerline of the

reactor obtained from combustion of 100% H_2S acid gas with oxygen. The results showed that H_2S decays monotonically to an asymptotic value while SO_2 increases until it reaches a peak, and then it decreases monotonically. The increase in SO_2 mole fraction is attributed to H_2S reaction with oxygen. However, the decrease in SO_2 is attributed to reaction of SO_2 and H_2S to form sulfur. Conversion efficiency of sulfur was evaluated and found to be 46%.

$$\text{Conversion Efficiency} = \frac{\text{Mass of recovered sulfur}}{\text{Mass of sulfur in inlet } H_2S}$$

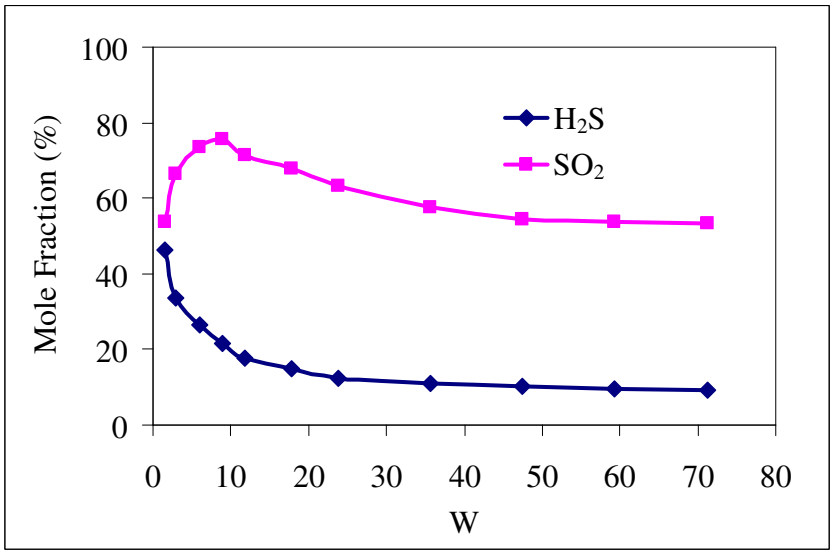

Figure 5-66. H_2S and SO_2 mole fraction along the reactor (100% H_2S acid gas).

Figure 5-67 presents H_2S and SO_2 mole fractions along the reactor centerline for acid gas composition of 90% H_2S and 10% CO_2. Hydrogen sulfide decays to a lower asymptotic value as compared to the 100% H_2S acid gas case. Sulfur dioxide increases until it reaches a peak, but decreases with a lower rate as compared to 100% H_2S case. This is attributed to increase in the oxidation medium due to the presence of CO_2. Carbon dioxide acts as an oxidizer which reacts with higher amounts of H_2S to form SO_2. In presence of oxygen H_2S tends to react with oxygen to form SO_2 rather than reacting with SO_2 to form sulfur, see section (5.1). Sulfur conversion efficiency was evaluated to be 31.5%. Figure 5-68 shows mole fraction of carbon monoxide

along the reactor centerline. Since reactor temperature is not high enough trigger CO_2 dissociation [111,124], presence of carbon monoxide is attributed to the reaction of CO_2 with H (reaction 5-48) [125]. Carbon monoxide decay to zero is attributed to its reaction with SO_2 to form sulfur monoxide and carbon dioxide (reaction 5-49).

$$H + CO_2 \leftrightarrow CO + OH \quad (5\text{-}48)$$

$$SO_2 + CO \leftrightarrow SO + CO_2 \quad (5\text{-}49)$$

Both radicals formed from reactions 5-48 and 5-49 contribute to the formation of sulfur dioxide at the expense of sulfur formation. In other words, formed sulfur monoxide and hydroxyl radicals dictates the formation of sulfur dioxide through reactions 5-7, 5-8, 5-15, and 5-16, see section (5.1.1.2). Subsequently, addition of carbon dioxide results in higher oxidation rates of H_2S to form sulfur dioxide. This weakens the net reaction between hydrogen sulfide and sulfur dioxide to form sulfur. Sulfur conversion efficiency was evaluated to be 31.5%.

Figure 5-69 presents H_2S and SO_2 mole fractions along the centerline of the reactor from the combustion of 80% H_2S and 20% CO_2 acid gas stream with oxygen. Hydrogen sulfide decreases until it reaches an asymptotic value. The asymptotic H_2S mole fraction is less than the previous two cases of 0% CO_2 or 10% CO_2. This supports the aforementioned hypothesis that CO_2 liberates oxygen which reacts with H_2S to form SO_2. Consequently, reaction between H_2S and SO_2 is dwindled according to the behavior of SO_2 mole fraction. Figure 5-70 shows carbon monoxide mole fraction along centerline of the reactor. Similar to the previous case reactions 5-48 and 5-49 dominate the behavior of CO along the reactor. Sulfur conversion efficiency was evaluated to be 16.8%.

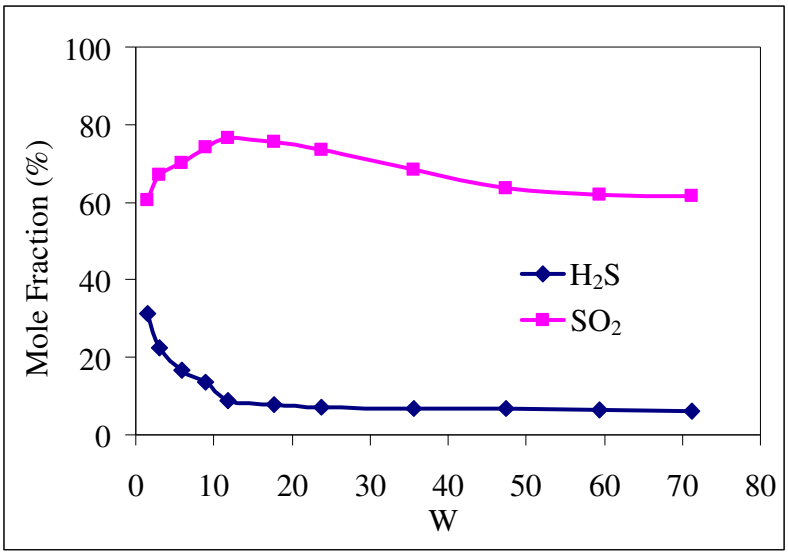

Figure 5-67. H_2S and SO_2 mole fraction along the reactor (90% H_2S, 10% CO_2 acid gas).

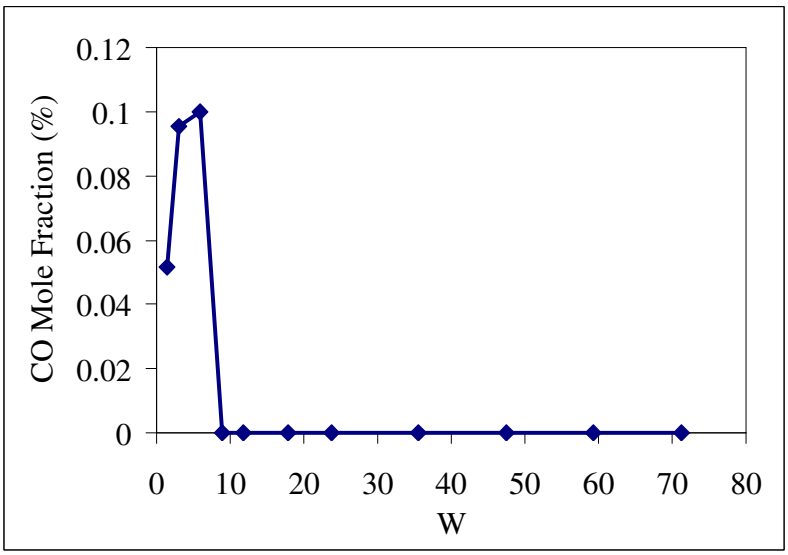

Figure 5-68. CO mole fraction along the reactor (90% H_2S, 10% CO_2 acid gas).

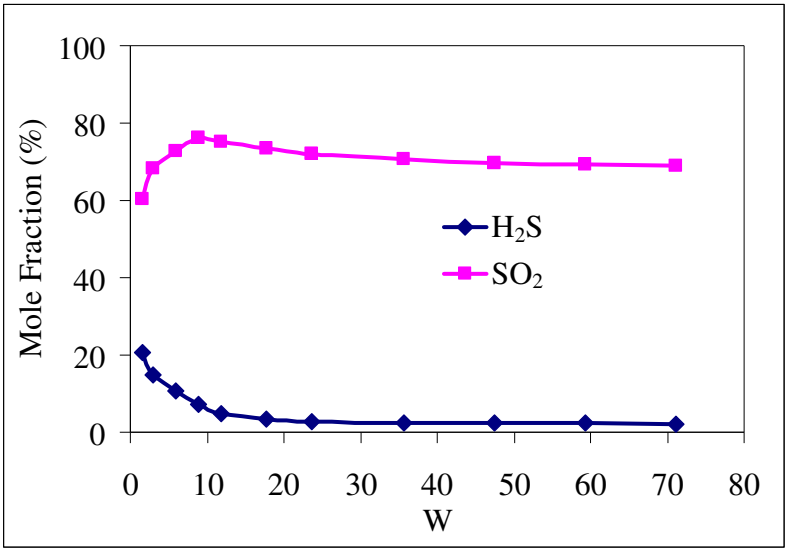

Figure 5-69. H_2S and SO_2 mole fraction along the reactor (80% H_2S, 20% CO_2 acid gas).

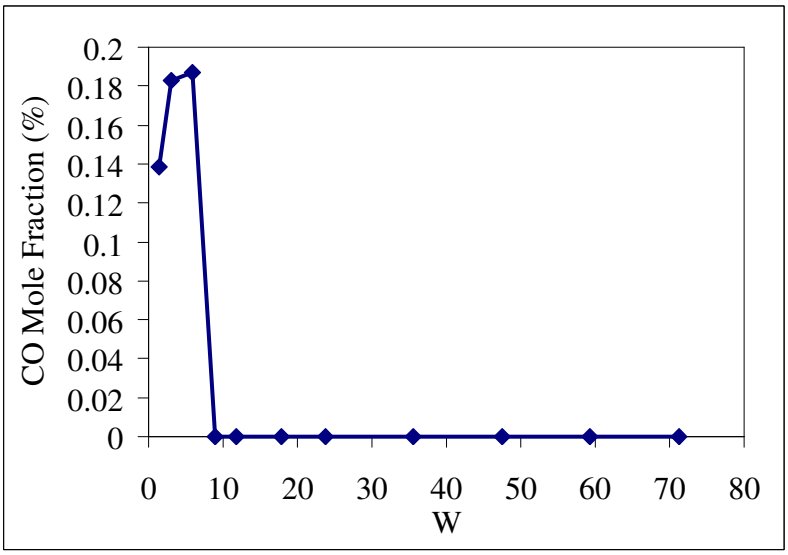

Figure 5-70. CO mole fraction along the reactor (80% H_2S, 20% CO_2 acid gas).

Figure 5-71 shows H_2S and SO_2 mole fractions for the combustion of acid gas composed of 70% H_2S and 30% CO_2. Similar to the previous case, H_2S decreased to an asymptotic value and SO_2 reached a peak and then slightly decreases. Figure 5-72 shows CO mole fraction where higher amounts of CO can be observed as compared to the previous cases. Sulfur conversion

efficiency with 30% CO_2 addition was evaluated to be only 3.5%. It is clear that sulfur conversion efficiency decreases significantly with the presence of CO_2 in the acid gas stream.

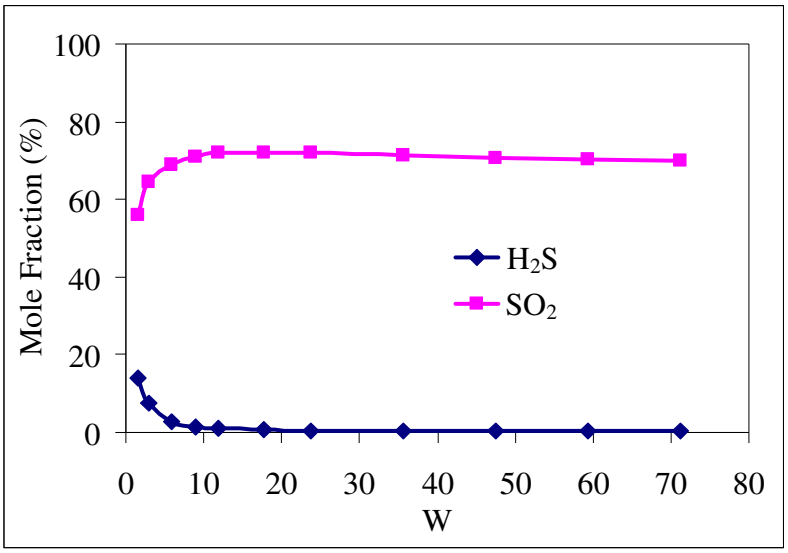

Figure 5-71. H_2S and SO_2 mole fraction along the reactor (70% H_2S, 30% CO_2 acid gas).

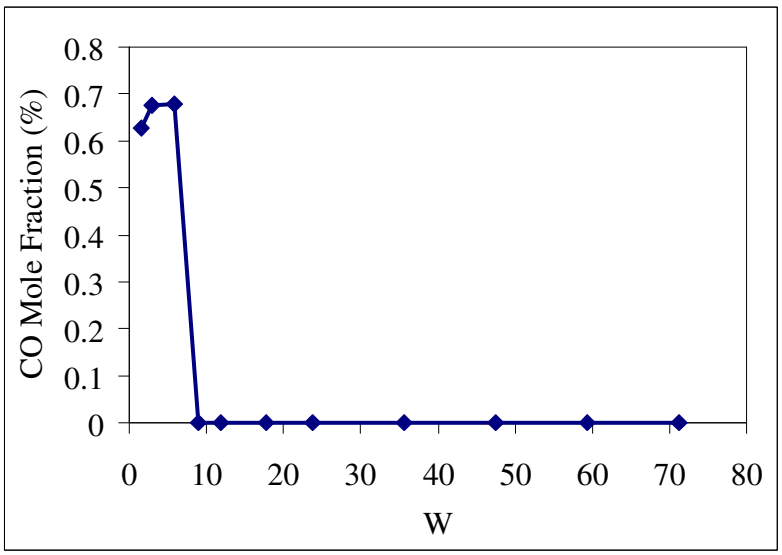

Figure 5-72. CO mole fraction along the reactor (70% H_2S, 30% CO_2 acid gas).

It is also worthy mentioning that for all cases presented previously hydrogen mole fraction was observed at the first measured data point (W= 1.48) with very marginal values

(concentration was 10^{-4} order of magnitude), and then it was oxidized to zero at the second measured data point.

5.3.3 Combustion of N_2-Laden Acid Gas

Acid gas stream with different nitrogen concentrations was examined in order to identify the effect of nitrogen on H_2S chemical reaction chemical reaction. Same baseline case was used (100% H_2S acid gas). Figures 5-73, 5-74, and 5-75 show the mole fraction of H_2S and SO_2 with the input acid gas stream contains 10% N_2, 20% N_2, and 30% N_2, respectively. Results revealed that behavior of SO_2 and H_2S did not change significantly with the increase of nitrogen in the acid gas. However, rates of evolution and decomposition were found to be slightly slower. This is attributed to that nitrogen acts as an inert gas in the reaction which can be considered a diluent of the mixture. In addition, temperature measurements showed that combustor temperature range is not high enough to trigger nitrogen reactions. Moreover, the richness of mixture (Φ=3) deteriorates the likelihood of nitrogen to react. Subsequently, nitrogen poses negligible effect on the trends of both H_2S and SO_2 under any concentration.

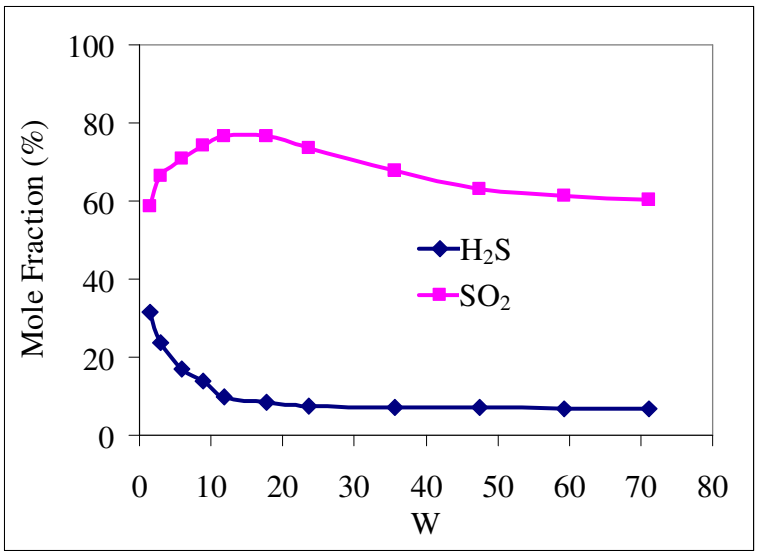

Figure 5-73. H_2S and SO_2 mole fraction along the reactor (90% H_2S, 10% N_2 acid gas).

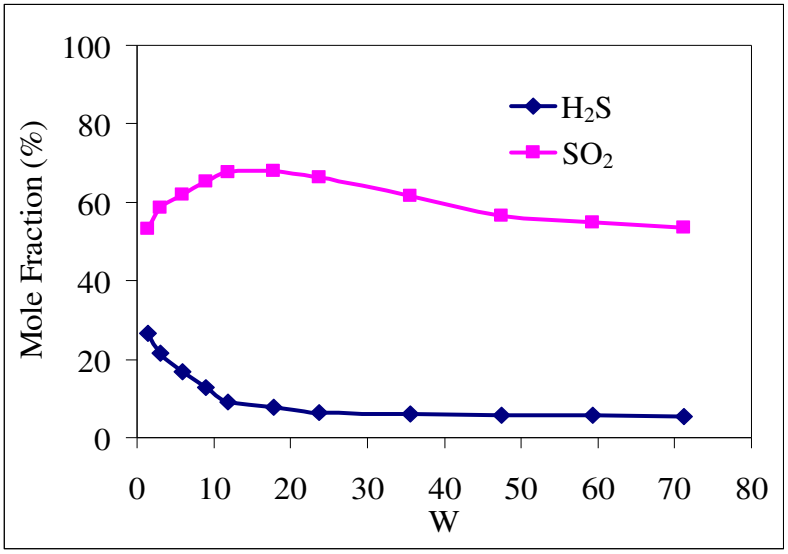

Figure 5-74. H_2S and SO_2 mole fraction along the reactor (80% H_2S, 20% N_2 acid gas).

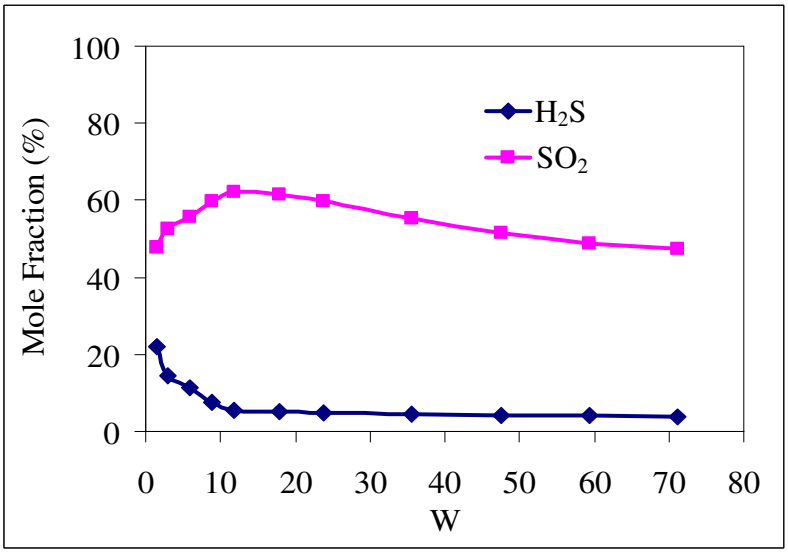

Figure 5-75. H_2S and SO_2 mole fraction along the reactor (70% H_2S, 30% N_2 acid gas).

5.3.4 Summary

Effect of the presence of nitrogen and carbon dioxide in acid gas on H_2S combustion was investigated. Concentration of nitrogen or carbon dioxide was varied up to 30% in the acid gas stream in increments of 10%, while effect of each gas was examined solely. All cases were compared with the baseline case of 100% H_2S acid gas stream. It was found that N_2 and CO_2

pose significantly different effects on the fate of product species. Temperature measurements showed that injection of CO_2 or N_2 decreases the flame temperature immediately upon injection. However, injection of CO_2 resulted in temperature increase further downstream in the reactor. Increase in CO_2 in acid gas increased SO_2 mole fraction in the products, but it decreased H_2S asymptotic value after combustion. Furthermore, the presence of CO_2 decreased the amount of sulfur captured during reaction. On the other hand, presence of nitrogen in the acid gas stream did not affect reaction chemistry drastically. However, slight slowness in the rate of H_2S decay and SO_2 evolution was observed. In all cases, hydrogen mole fraction was not detected except for the first measured data point at (W= 1.48) with a negligible magnitude.

5.4 Effect of Reaction Parameters on the Quality (Purity) of Captured Sulfur in Claus Process

Elemental sulfur is being used in several applications such as phosphate fertilizers and sulfurous acids [126]. It is expected that consumption rate of phosphate fertilizers will grow during 2011-2016 by 2.7-2.9%, thus higher amounts of sulfur will be required. On the other hand, accumulated sulfur collected from oil and gas refinery processes through Claus process is considered a major source for pure elemental sulfur. In this section, we examined the quality of sulfur collected with respect to reactor conditions (gas stream composition, equivalence ratio, and hydrocarbon fuels). Laser induced breakdown spectroscopy (LIBS) was used for most of this study to analyze the chemical structure of deposited sulfur. The LIBS setup has been described in details previously, see section (4.2.4). Since LIBS gives only the elemental analysis of the sample, X-Ray powder diffraction technique has been used primarily to determine the allotrope

of collected sulfur, see section (4.2.3). Burner A has been used in this investigation while the steel housing was used to collect sulfur droplets as show in figure 5-76.

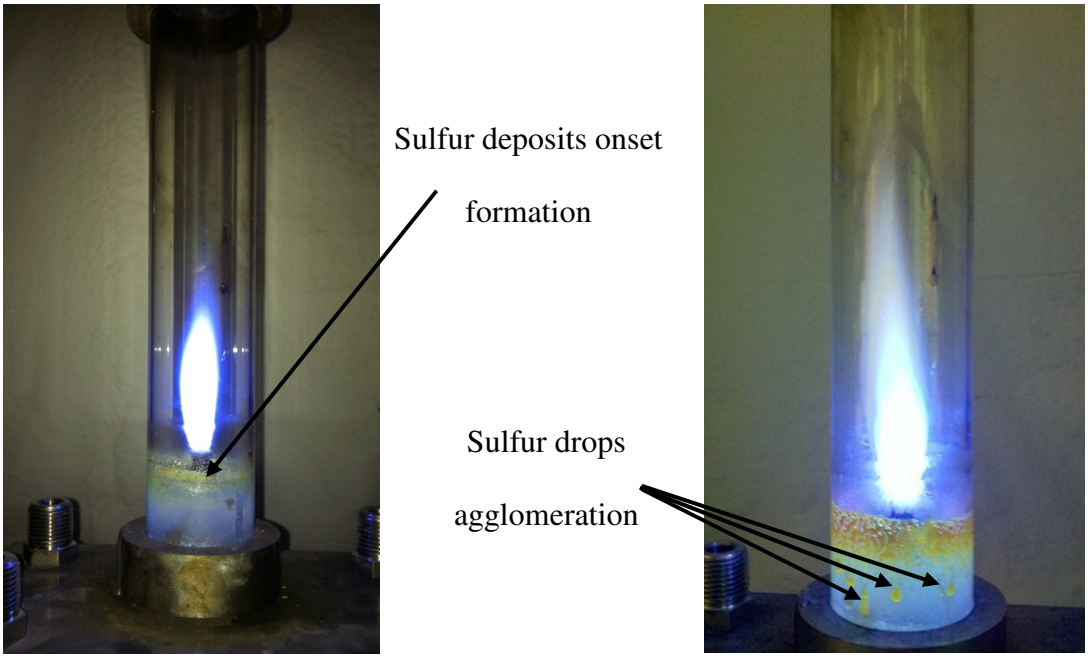

Figure 5-76. The onset of sulfur formation, agglomeration and precipitation in reactor housing.

Selected experimental conditions have been examined in this study. Firstly, we investigated the effect of reactants equivalence ratio on the quality of collected sulfur deposits. Two equivalence ratios examined here (stoichiometric and Claus conditions). The rate of sulfur production under fuel-lean conditions was very slow; thus it is not included in this study. Secondly, effect of other contaminant (carbon dioxide) likely to accompany hydrogen sulfide in the acid gas stream is examined. Finally, effect of hydrogen sulfide combustion in presence of hydrocarbon fuels (methane and propane) on the quality of captured sulfur is tested. Table 5-6 shows the test matrix used for this investigation.

5.4.1 Effect of Equivalence Ratio

Sulfur deposits were collected inside the reactor housing under both stoichiometric and Claus conditions. X-Ray diffractogram of captured samples revealed that sulfur deposits were all

of cyclo-S_8 (α-sulfur) allotrope with orthorhombic crystal structure. Formation of S_8 is attributed to the molecular growth of sulfur in its gas phase starting with S and S_2 [114]. Change in reactants equivalence ratio showed insignificant effect on the crystal structure of the captured sulfur. Diffractogram of collected sulfur deposits under Claus and stoichiometric conditions is presented in figure 5-77. These results are also compared with the typical diffractogram of cyclo-S_8 (α-sulfur) available in the literature [127] and showed good agreement.

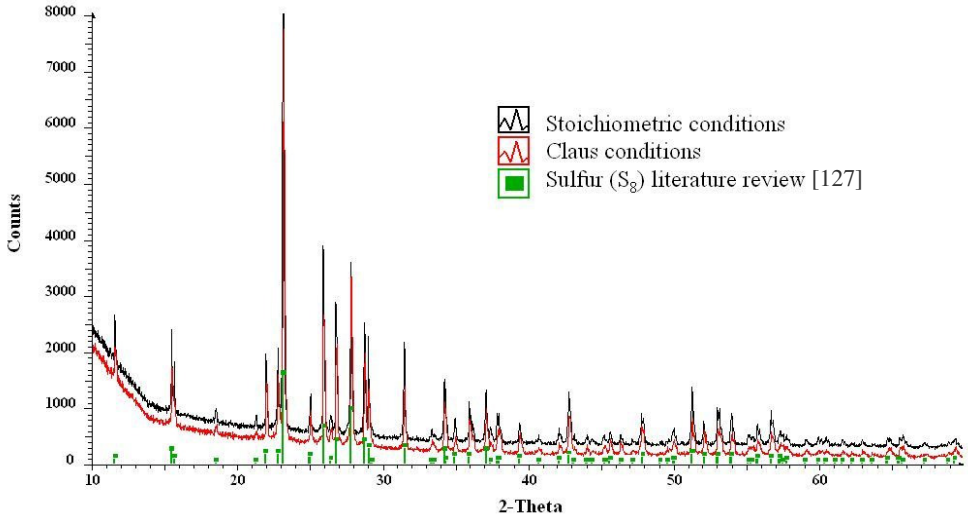

Figure 5-77. Diffractograms of different sulfur samples.

Table 5-6. Reactants flow rates for H_2S/O_2, $H_2S/O_2/CO_2$, $H_2S/O_2/CH_4$, and $H_2S/O_2/C_3H_8$.

Investigation	Case #	Reactants	Reactants flow rates, respectively, lit/min
Effect of equivalence ratio	1	H_2S/O_2 (stoichiometric)	0.7/1.05
	2	H_2S/O_2 (Claus)	0.7/0.35
Effect of acid gas contaminants	3	$H_2S/O_2/CO_2$	0.7/0.35/0.3
Effect of hydrocarbon fuels	4	$H_2S/O_2/CH_4$	0.7/1.35/0.5
	5	$H_2S/O_2/C_3H_8$	0.7/2.85/0.5

After the determination of sulfur allotrope, LIBS experiments were conducted to investigate the quality of sulfur samples. The objective was to identify elemental analysis of sulfur deposits as affected by different experimental conditions. Figures 5-78 and 5-79 show the spectra of sulfur samples collected from cases 1 and 2. Emission spectra depict the presence of sulfur peaks within 547 to 564 nm. These results agree with the previous findings of Fowler et al. [96] that showed that excited sulfur emits in this range of wavelengths. Difference in equivalence ratio did not pose any significant effect on the spectral emission characteristics.

5.4.2 Effect of Acid Gas Contaminants

As we discussed in section (5.3), carbon dioxide is a common contaminant that accompanies H_2S in the acid gas stream. Case 3 represents the investigation of sulfur deposits collected from (70% H_2S and 30% CO_2) acid gas stream. Figure 5-80 shows the spectrum of sulfur deposits collected under experimental conditions of case 3. Results showed that sulfur peaks are obtained within the same bands as in cases 1 and 2. Presence of CO_2 in the acid gas stream did not show a prominent effect on the quality of deposited sulfur.

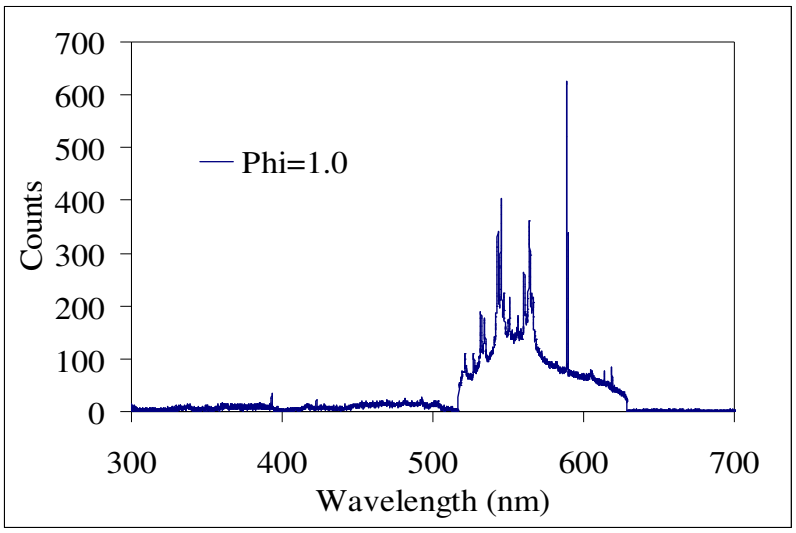

Figure 5-78. Emission spectrum of sulfur deposits collected from of H_2S/O_2 combustion (stoichiometric conditions).

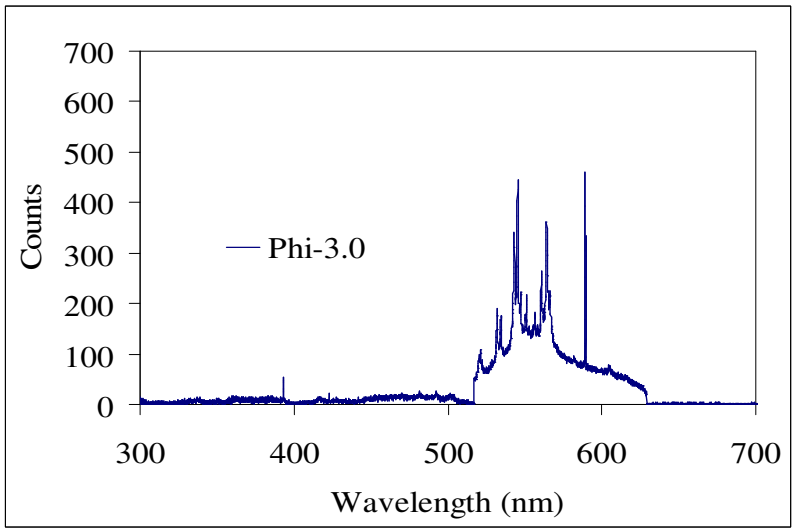

Figure 5-79. Emission spectrum of sulfur deposits collected from of H_2S/O_2 combustion (Claus conditions).

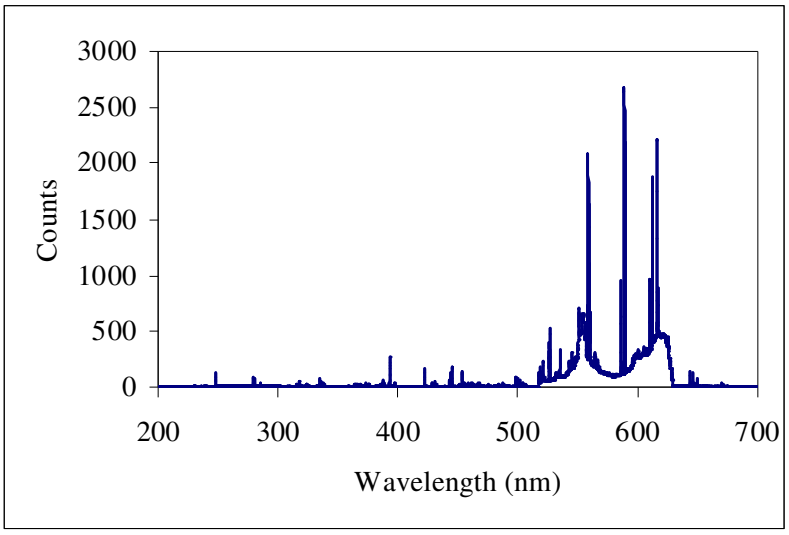

Figure 5-80. Emission spectrum of sulfur deposits collected from $H_2S/O_2/CO_2$ combustion.

5.4.3 Effect of Hydrocarbon Fuels

Presence of hydrocarbon fuels in acid gas stream could be attributed to the imperfect natural gas separation in the amine extraction process. Cases 4 and 5 depict the collection of sulfur deposits in presence of methane (case 4) and propane (case 5). Figure 5-81 shows the emissions spectrum of sulfur deposits collected from case 4. Results assured the presence of

carbon peak at ~ 250nm in addition to sulfur peaks in the range of 547 to 564 nm. This suggests that sulfur deposits collected under these conditions contain trace amounts of carbon to result in low quality of sulfur. On the other hand, figure 5-82 depicts the emissions spectrum of sulfur deposits collected under conditions of case 5. Results show the presence of several carbon peaks (within 250 to 280 nm) due to the formation of soot layer. This indicates that, carbon concentration in captured sulfur is higher than case 4. Figure 5-83 shows a photograph (magnified 30 times) of sulfur deposit collected from case 5 wherein one can clearly see soot layer covers the sulfur deposits.

Chemkin simulations were carried out to justify the presence of carbon (soot) in cases 4 and 5 and absence of carbon in case 3. Figures 5-84 and 5-85 depict carbon net reaction rate in a plug flow reactor under experimental conditions of cases 3 and 4. The results proved that carbon net reaction rate is nine orders of magnitude higher in cases 4 as compared to case 3. This is attributed to the fact that carbon dioxide is unlikely to release the carbon atom thorough chemical reactions. In addition, reaction temperature is relatively low to trigger CO_2 dissociation to carbon and oxygen. However, hydrocarbon reactions are likely to form carbon through the reactions of the alkyl group (CH_3). Chemical channels for carbon formation in case 3 are given via reactions 5-50 up to 5-53 while reactions 5-54 to reaction 5-57 depicts channels for carbon formation in case 4.

$$CO_2 + H \leftrightarrow CO + OH \quad (5\text{-}50)$$

$$CO_2 + (M) \leftrightarrow CO + O + (M) \quad (5\text{-}51)$$

$$H + CO \leftrightarrow C + OH \quad (5\text{-}52)$$

$$CH_4 + O \leftrightarrow OH + CH_3 \quad (5\text{-}53)$$

$$S + CH_4 \leftrightarrow SH + CH_3 \quad (5\text{-}54)$$

$$CH_3 + OH \leftrightarrow CH_2 + H_2O \quad (5\text{-}55)$$

$$CH_2 + H \leftrightarrow CH + H_2 \quad (5\text{-}56)$$

$$H + CH \leftrightarrow C + H_2 \quad (5\text{-}57)$$

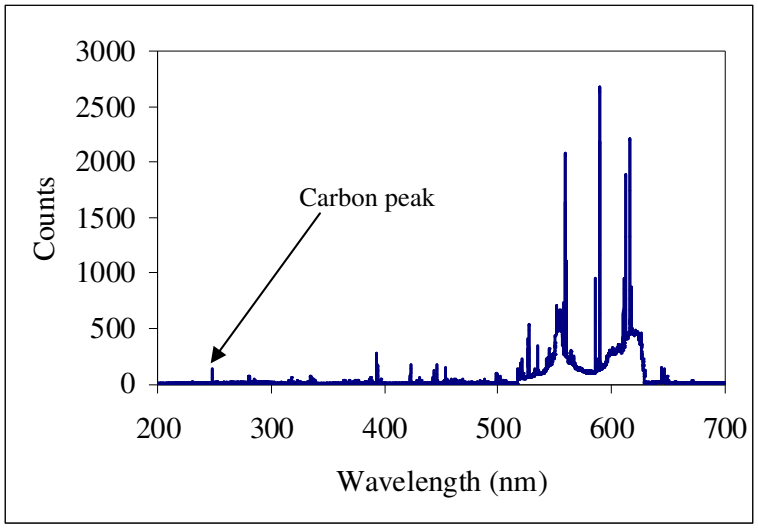

Figure 5-81. Emission spectrum of sulfur deposits collected from $H_2S/O_2/CH_4$ combustion.

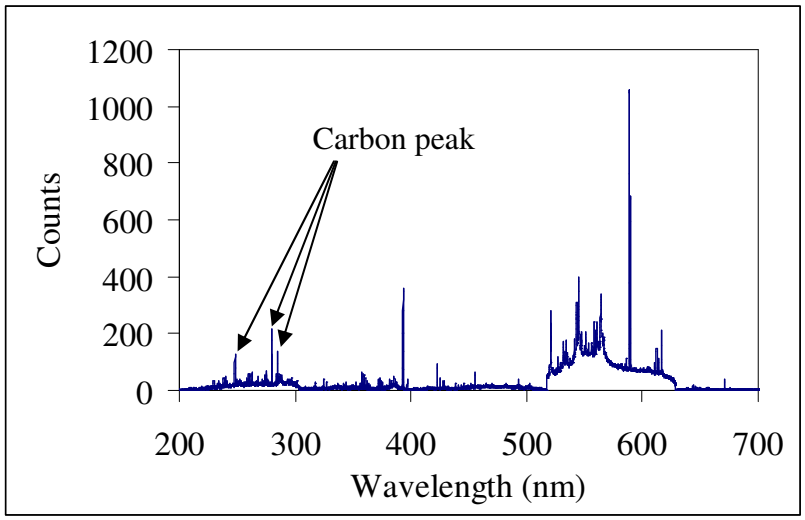

Figure 5-82. Emission spectrum of sulfur deposits collected from $H_2S/O_2/C_3H_8$ combustion.

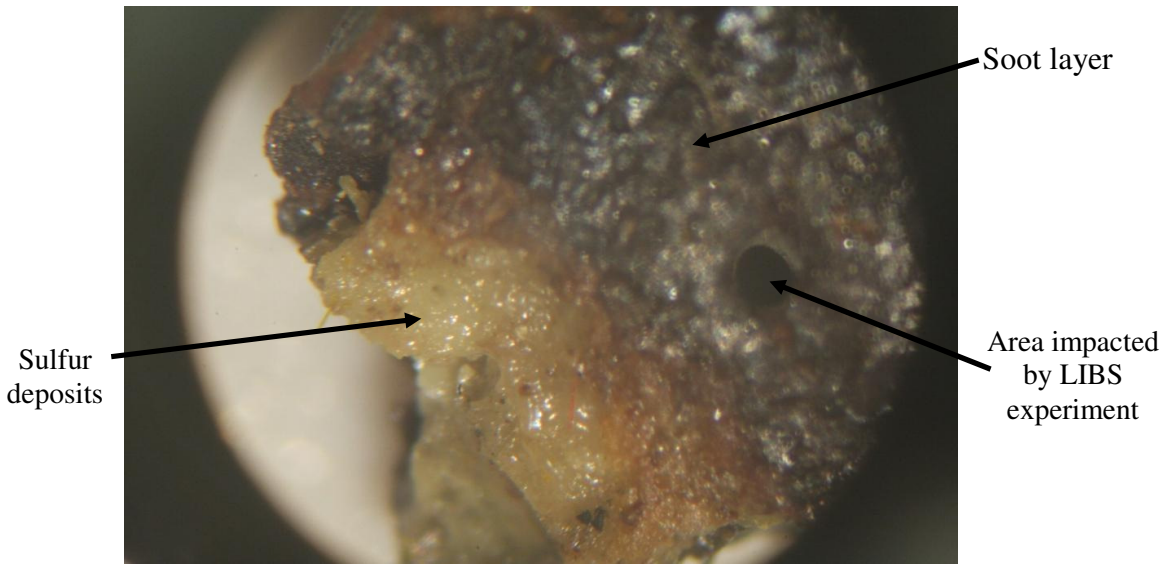

Figure 5-83. Sulfur/soot deposits collected from the combustion of $H_2S/O_2/C_3H_8$.

5.4.4 Summary

Examination of the quality (purity) of sulfur deposits collected from H_2S combustion under Claus conditions has been conducted. Experiments were carried out under different reactor conditions representing practical cases. First and second cases represented the variation of H_2S/O_2 equivalence ratio between rich (Claus) conditions and stoichiometric conditions. Third case represented the presence of CO_2 contaminant in H_2S acid gas stream. Fourth and fifth cases showed the combustion of H_2S with hydrocarbon fuels (methane and propane). Sulfur deposits were collected and analyzed in all cases using X-Ray powder diffraction and laser induced breakdown spectroscopy (LIBS) diagnostics. X-Ray powder diffraction showed that, the allotrope of sulfur deposits is of cyclo-S_8 (α-sulfur) with orthorhombic crystal structure. The LIBS experiments revealed that equivalence ratio of H_2S/O_2 flame did not have any prominent effect on the quality of captured sulfur. Similarly, presence of carbon dioxide in the acid gas stream showed insignificant effect on the deposited sulfur. However, combustion of hydrogen

sulfide in methane and propane flames showed sulfur deposits to contain carbon (soot). Concentration of carbon was higher in case of using propane instead of methane revealing that carbon content in the fuel has a significant effect on the amounts of carbon present in the deposited sulfur.

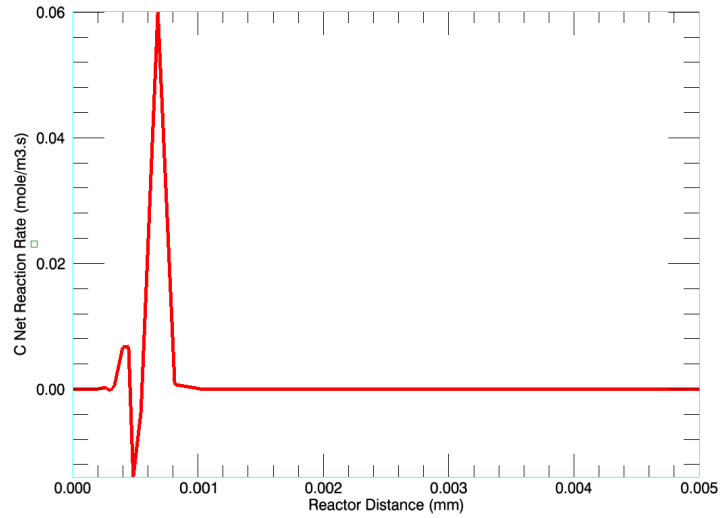

Figure 5-84. Carbon net reaction rate from $H_2S/O_2/CH_4$ flame (Chemkin simulations).

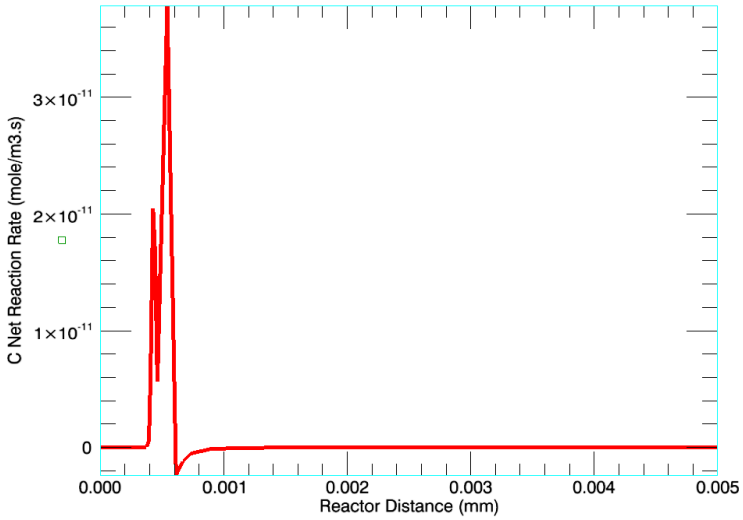

Figure 5-85. Carbon net reaction rate $H_2S/O_2/CH_4$ flame (Chemkin simulations).

CHAPTER 6: EXPERIMENTAL ERROR ANALYSIS

In this chapter we discuss the sources of errors associated with experimental measurements. We firstly present the systematic error in all the measuring/controlling apparatuses, and secondly we discuss the random error presented in our measurements.

6.1 Systematic Error

Sources of systematic error in this research were as follows:

- Traverse mechanisms
- Thermocouple
- Gas chromatograph (TCD and FPD)
- Spectrometer grating
- Flow controllers

Table 6.1 shows the error in all apparatuses used in this research except flow controllers. One can see that, error ranges are very minimal so that they all lie within the experimental data points symbols represented in figures.

Table 6.1. Error range associated with experimental measurements.

Device	Measured quantity	Error
Traverse mechanisms	distance	± 0.0762mm/254mm
Thermocouple	temperature	+ 2.8 K at T=1600 K
TCD	CO, H_2, C_2H_2, C_2H_4, C_2H_6, C_3H_8	<± 0.1 % at concentration of 100 ppm
FPD	H_2S, SO_2, COS, CS_2	<± 0.1 % at concentration of 1 ppm
Spectrometer grating	Wavelengths	± 0.2 nm for 1200 grove/mm grating

Flow controllers error (1.5% of full scale) does not affect the results presented in this dissertation (mole fractions, temperatures, axial distances, and radial distances). However, equivalence ratios given for each experimental condition are affected by the error emanated from the flow controllers. It is important to mention that flow controllers have always been changed in order to efficiently provide the targeted flow rates with the least possible error. For instance, a 400 cm^3/min H_2S flow controller has been used to provide flow rates higher than 100 cm^3/min and less than 300 cm^3/min. On the other hand, a 1000 cm^3/min H_2S flow controller has been used to provide H_2S flow rates higher than 300 cm^3/min. Five flow controllers have been incorporated during this research to provide H_2S flow rates appropriately. The flow controllers had full ranges of (1000, 400, 100, 50, and 20) cm^3/min. On the other hand, two air flow controllers have been used throughout this research with full range of (20 and 10) lit/min. Error appears on the adjusted equivalence ratios (3, 1 and 0.5) varied according to experimental conditions of each investigation. The error range (uncertainty) of equivalence ratios can be calculated as follows:

Equivalence ratio:
$$\phi = \left(\frac{\forall_{H_2S}}{\forall_{O_2}} \right) \times \left(\frac{1}{FA)_{th}} \right) \qquad \text{(Eq.6.1)}$$

where,

$\forall_{H_2S}$: hydrogen sulfide volumetric flow rate

$\forall_{O_2}$: excess oxygen volumetric flow rate

$FA)_{th}$: theoretical equivalence ratio of H_2S/O_2

Excess oxygen volumetric flow rate is, see section (4.1.4):

$$\forall_{O_2} = \left(\frac{Y_{O_2}}{Y_{N_2}} \right) \times \forall_{N_2} \qquad \text{(Eq.6.2)}$$

where,

Y_{O_2} : oxygen mole fraction

Y_{N_2} : nitrogen mole fraction

$\forall_{N_2}$: nitrogen volumetric flow rate

Therefore,

$$\phi = \left(\frac{Y_{N_2}}{Y_{O_2}} \right) \times \left(\frac{1}{FA)_{th}} \right) \times \left(\frac{\forall_{H_2S}}{\forall_{N_2}} \right)$$

(Eq.6.3)

Uncertainty in equivalence ratio ($\delta\phi$) can be calculated from (Eq.6.4) as follows:

$$\delta\phi = \left(\frac{Y_{N_2}}{Y_{O_2}} \right) \times \left(\frac{1}{FA)_{th}} \right) \times \left[\left(\frac{1}{\forall_{N_2}} \Delta_{H_2S} \right)^2 + \left(- \frac{\forall_{H_2S}}{\forall_{N_2}^2} \Delta_{N_2} \right)^2 \right]^{\frac{1}{2}}$$

where,

$\delta\phi$: equivalence ratio uncertainty

Δ_{H_2S} : error in H_2S flow controller

Δ_{N_2} : error in nitrogen flow controller

Uncertainty range in equivalence ratios is given by (Eq.6.5):

$$E_\phi = \frac{\delta\phi}{\phi} \times 100 \quad \% \qquad \text{(Eq.6.5)}$$

Table 6.2 shows the percentage error in equivalence ratios adjusted for experiments presented in chapter 5, sections 5.1.1, 5.1.2, 5.1.3. However, error in equivalence ratios of (section 5.3) is

determined using (Eq.6.1) where the reaction occurred only between H_2S and O_2. It was found that maximum error in equivalence ratio (Φ=3.0) was ± 6.3%.

Table 6.2. Percentage systematic error in experiments.

Investigation	Section 5.1.1	Section 5.1.2	Section 5.1.3	Section 5.3
Equivalence ratio	Uncertainty range (E_Φ) %			
Φ=3	± 5.4	± 6.2	± 3.2	± 6.3
Φ=1.0	± 4.5	± 3.9	± 6.0	—
Φ=0.5	± 4.5	± 3.4	± 3.8	—

The equivalence ratio uncertainty can propagate into reactants flow rates and affect the combustion products mole fractions. We calculated the error propagation of H_2S inlet flow rate into the reaction pool according to the equivalence ratios uncertainty using (Eq.6.1). This error propagates further into H_2S combustion byproducts. In our calculations we took into consideration the effect of density change between the inlet stream and the combustion products in the reaction pool. Density in the reaction pool was calculated based on the assumption that average reactor temperature is 1400K, except for section (5.1.3) where it was assumed to be 1600K. Table 6.3 represents the uncertainty propagation into sulfurous byproducts. It is important to mention that, this uncertainty range represents the error in all H_2S combustion byproducts combined. Moreover, as we mentioned, the error in mole fractions presented in chapter 5 lie within the symbols of experimental data points. However, in case of experiment repetition the possibility of having different byproducts mole fractions is determined by the uncertainty range given in table 6.3.

Table 6.3. Error propagation into H_2S combustion byproducts.

Investigation	Section 5.1.1	Section 5.1.2	Section 5.1.3	Section 5.3
Equivalence ratio	Uncertainty propagation into combustion byproducts (%)			
Φ=3	± 0.76	± 0.48	± 0.54	± 0.76
Φ=1.0	± 1.16	± 0.87	± 1.24	—
Φ=0.5	± 2	± 1.5	± 1.51	—

6.2 Random Error

As we discussed in chapter 4, average time required for each experiment to be performed was 5 hours. Therefore, it was not possible to repeat each experiment enough number of times so that we could calculate the mean and standard deviation for each experiment. Consequently, random error assessment has been achieved via data repeatability check. All experiments performed in this research have been repeated three times and the average value was presented. In section 5.1.1 we have plotted the three sets of data for each experiment, where reliable data reparability was obtained. Maximum standard deviation was observed in H_2 mole fraction under Claus conditions, figure 5-12, to be 1.4%.

CHAPTER 7: CONCLUSIONS AND RESEARCH CONTRIBUTIONS

Research presented in this dissertation revealed several facts about the chemical kinetics of H_2S combustion, conditions under which other sulfurous compounds are formed, and effect of reactor conditions on practical issues for H_2S treatment in Claus process. In this chapter, we discuss the main conclusions drawn out of this research and the research major contributions.

7.1 Conclusions

The presented work started with numerical investigation aiming to obtain a representative reduced mechanism for H_2S oxidation. Experimental approach was then used with specific focus on H_2S combustion in CH_4/air and H_2/air flames in order to determine the behavior of H_2S reaction under different experimental conditions. In addition, non-intrusive flame spectroscopy was performed on H_2S combustion so as to identify intermediate species that could not be identified via gas analysis. Finally, some practical issues regarding H_2S treatment were addressed starting with the effect of other contaminants (CO_2 and N_2) on H_2S treatment in Claus process. Secondly, experiments about the effect of reactor conditions on the quality of captured sulfur were demonstrated.

7.1.1 Reduced Mechanism for H_2S Oxidation

A reduced mechanism for H_2S oxidation was obtained using the direct relation graph and error propagation methodology (DRGEP) coupled with a novel error propagation approach that has been developed in this research. The novel approach was named direct elementary reaction error (DERE) approach. The reduced mechanism consisted of 19 elementary reactions and 14

species while the detailed reaction mechanism of Leeds University contained (111 reactions and 41 species). The reduced reaction underwent comparisons with the detailed reaction mechanism under temperatures range 1400K up to 1800 K. Comparisons were at three equivalence ratios representing fuel-lean, stoichiometric, and fuel-rich conditions. The reduced mechanism successfully captured all reactions details obtained by the detailed mechanism. Moreover, it has been able to track chemical kinetics changes associated with changes in equivalence ratio and reaction temperature. However, some discrepancies were observed, especially on H_2O mole fraction, but they were all within the assigned error threshold (15%). On the other hand, ignition delay time obtained by the reduced mechanism showed good agreement with previous experimental findings. Finally, numerical investigation of mechanistic pathways of Claus process, using the reduced mechanism, was demonstrated at two different stages of the reaction. The pathways gave a reasonable interpretation of the behavior of reactions in Claus process, wherein the dominant reactions differ according to the reactants in the reaction pool.

7.1.2 Hydrogen Sulfide Combustion in Flames

Hydrogen sulfide combustion was examined in CH_4/air flame and H_2/air flame. Three equivalence ratios were studied ranging from Claus conditions (Φ=3.0), stoichiometric conditions (Φ=1.0), and fuel-lean conditions (Φ=0.5). Combustion of H_2S in CH_4/air flame under non-premixed conditions proved that presence of H_2S prevents hydrogen (formed from CH_4/air combustion) oxidation in the burner exit vicinity. However, further down stream H_2 combustion starts to take place. It also proved that, H_2S oxidation results in SO_2 formation in presence of oxygen. However, under rich conditions, e.g. Claus conditions, and with the oxygen depletion, H_2S net reaction shifts towards sulfur formation. Trace amounts of hydrocarbons were formed under Claus conditions; this was attributed to SO_2 role as a coupling catalyst that enhanced the

dimerization of CH_3 radical to form higher series of hydrocarbons, such as acetylene, ethylene, ethane, and propane.

On the other hand, combustion of premixed CH_4/air/H_2S flame showed that sulfur dioxide had a consistent (almost-constant) trend for all the equivalence ratios examined. The fact that reactants were premixed prior to combustion substantiated oxidation competition between H_2S and CH_4, thus reaction of H_2S formed SO_2 rather than S_2. This also validated further the hypothesis of the tendency of H_2S combustion to form SO_2 over S_2. In addition, another sulfur compound (carbon disulfide) was formed under only stoichiometric and Claus conditions. Formation of CS_2 was mainly due to the presence of methane which reacts with sulfur compounds to form CS_2. This also supported the fact that H_2S combustion does not necessarily mean that other harmful sulfurous gases, other than SO_2, are not formed. Finally, hydrocarbons (ethane and ethylene) were observed under Claus conditions away from reactor centerline. This solidified the fact that hydrocarbons formation is attributed to role of SO_2 as a coupling catalyst to the alkyl group (CH_3) where most of CH_3 was consumed before reaching reactor centerline.

Combustion of acid gas (H_2S and CO_2) was examined in H_2/air flames. Examination took place for acid gases of 100% H_2S composition and 50% H_2S/50% CO_2 composition. The role of H_2S as an oxidation inhibitor for hydrogen was proved further as well as the tendency for H_2S combustion to form SO_2 over S_2 in presence of oxygen. Addition of CO_2 proved to promote both decay and production rates for reactants and products. Moreover, CO presence in the reaction pool was distinct evidence on CO_2 role as an oxidation promoter in the reaction pool. It also enhanced the formation of sulfurous-carbonaceous compounds, such as COS and CS_2.

7.1.3 Hydrogen Sulfide Flame Spectroscopy

Spectra of hydrogen sulfide flames have been examined non-intrusively via species chemiluminescent emissions and absorption bands. Examination of typical H_2S/O_2 flame under lean conditions (Φ=0.5) showed strong continuum between 280-460nm which is attributed to singlet and triplet SO_2* afterglow. It was not possible to identify any other excited species due to the strong intensity of this continuum. In order to avoid the presence of SO_2* afterglow trace amounts of H_2S were injected into hydrogen/air flame where formation of a strong bluish inner cone located near to the flame base was observed. The spectrum of the blue cone showed strong group of peaks within 320-470 nm, and no sign of the afterglow continuum was obtained. This allowed us to identify several species either via their chemiluminescent emissions or their absorption emissions. The species identified via chemiluminescent emissions were OH*, SO*, SO_3*, and H* while absorption bands for SH* were obtained.

7.1.4 Practical issues of H_2S Treatment

Finally, practical issues regarding H_2S treatment in Claus process were address. The first issue was to determine effect of contaminants that are likely to exist in the acid gas stream (CO_2 and N_2) on the efficiency of H_2S treatment. The second issue was to identify the effect of different reactor conditions on the quality of collected sulfur from H_2S treatment process.

The results proved that carbon dioxide deteriorates the performance of Claus process drastically with the increase in its concentration in the acid gas stream. On the other hand, nitrogen did not have this prominent effect on Claus process where it was found to act as a diluent into the reactor.

Investigation on purity of sulfur collected from H_2S treatment revealed that equivalence ratio of H_2S/O_2 mixture does not have a substantial effect on the purity of collected sulfur.

Similarly, presence of carbon dioxide in the acid gas stream did not have a significant effect on sulfur deposits quality. However, H_2S combustion in methane or propane flames proved to deteriorate the quality of sulfur, where sulfur deposits analysis proved the presence of carbon. Concentration of carbon was higher in case of propane flame was higher as compared to methane flame assuring that carbon content in fuels has a significant effect the quality of deposited sulfur.

7.2 Research Contributions

Research presented in this dissertation resulted in several contributions in the area of H_2S combustion chemistry as well as H_2S treatment process (Claus process):

- Development of a novel error propagation approach for the reduction of detailed chemical reaction mechanisms.
- Provide an efficiently representative 19-reactions reduced mechanism for H_2S oxidation.
- Determination of the chemical kinetics channels responsible for sulfurous compounds (SO_2, CS_2, and COS) formation from H_2S combustion.
- Identify role of SO_2 as a coupling catalyst that promotes hydrocarbons formation during methane combustion.
- Segregation of SO_2* afterglow continuum in H_2S combustion which allowed us to determine sulfurous species in H_2S flame.
- Determine the effect of contaminants (CO_2 and N_2) in acid gas on the performance of Claus process.
- Determine the effect of reactor conditions on the purity of sulfur collected from H_2S treatment process.

CHAPTER 8: RECOMMENDATIONS FOR FUTURE WORK

The research presented in this dissertation focused on several issues of hydrogen sulfide combustion during its treatment process (Claus process). We managed to provide thorough chemical kinetics description of H_2S combustion at different reactor conditions both numerically and experimentally. In addition, we paid considerable attention to several practical issues that are commonly encountered in H_2S treatment stations. Nevertheless, this work can be extended to new horizons that have been opened through this research.

8.1 Effect of BTX on H_2S Treatment

Several heavy hydrocarbons are proven to naturally exist in crude natural gas wells, depending on the quality of the well. The most famous hydrocarbons are benzene, toluene, and xylene (BTX). Such hydrocarbons, even with slight concentrations, can change the chemical kinetics of H_2S reaction completely. This will cause deviation in Claus process performance from the typical H_2S treatment conditions. In addition, presence of BTX results in faster deterioration of catalytic beds in Claus process due to soot and carbon deposition. Subsequently, it is inevitable to have BTX in the acid gas stream and it is also a must to enhance BTX destruction in prior to the catalytic stages of Claus process. This research point is of pinnacle importance for H_2S treatment enhancement and will require extensive investigations about the chemical kinetics of H_2S/BTX combustion.

8.2 Near-Isothermal Claus Reactor

According to what we concluded in this dissertation, reactor temperature poses a significant role to the formation of sulfurous compounds. Figure (3-1) showed that efficiency of thermal stage of Claus process reaches its peak around temperature of 1600K. Subsequently, if

we managed to sustain reactor temperature around 1600K a noticeable improvement of Claus process performance will be noticed. This requires comprehensive research about H_2S combustion in a near-isothermal reactor at wide range of conditions.

8.3 Hydrogen Separation from H_2S stream

Hydrogen energy has become essential lately with the continuous need to reduce carbon emissions into the environment. It possesses the highest calorific value, on mass basis, as compared to all hydrocarbon fuels, thus it can provide the highest energy release during combustion. On the other hand, hydrogen sulfide treatment relies primarily on the separation of sulfur out of H_2S to prevent the formation of any sulfurous gases. Pyrolysis of hydrogen sulfide can produce considerable amount of hydrogen as well as reduce H_2S amount that needs to be treated. This will lead to a significant reduction in the size of H_2S treatment station as well as the formation of a valuable energy source. This area of research requires attention to provide more details about H_2 separation from H_2S.

8.4 Reforming of Sulfur Compounds in Claus Reactor

According to our discussion in chapter 5, H_2S combustion can release undesirable gases such as SO_2, COS, and CS_2. Typically, tail-gas-treatment stage is installed in H_2S treatment process to recuperate any sulfur-containing gases via a hydrolysis and hydrogenation as shown in reactions (8-1) through (8-3)

$$COS + H_2O \leftrightarrow H_2S + CO_2 \quad (8\text{-}1)$$

$$CS_2 + 2H_2O \leftrightarrow 2\ H_2S + CO_2 \quad (8\text{-}2)$$

$$SO_2 + 2H_2 \leftrightarrow H_2S + 2H_2O \quad (8\text{-}3)$$

In this research we have investigated the experimental conditions under which sulfur byproducts are formed. The next step is to develop a Claus reactor that can alleviate the formation of sulfur byproducts in the reaction pool. This can lead into significant cost savings in form of dispensing the tail-gas-treatment stage.

Research on hydrogen sulfide combustion in presence of BTX has already been started in The Combustion Laboratory at UMD. On the other hand, an experimental setup has been put together to serve the abovementioned research recommendations. The setup consisted of a tubular electrical heater that can provide temperature up to ~1800K. The reactor length is ~30.5 cm and it has a diameter of ~5.1 cm. The reactor if firmly insulated so that temperature variation is very minimal. This will be used to serve the research areas mentioned in section (8.2) and section (8.3).

APPENDIX A: REDUCED MECHANISM FOR H_2S OXIDATION

#	Elementary Reaction	A	n	E/RT
1	$H_2S+M = S+H_2+M$	1.60E+24	-2.61	44800
2	$H_2S+H = SH+H_2$	1.20E+07	2.1	350
3	$H_2S+O = SH+OH$	7.50E+07	1.75	1460
4	$H_2S+OH = SH+H_2O$	2.70E+12	0	0
5	$H_2S+S = 2SH$	8.30E+13	0	3700
6	$H_2S+S = HS_2+H$	2.00E+13	0	3723.84
7	$S+H_2 = SH+H$	1.40E+14	0	9700
8	$SH+O = H+SO$	1.00E+14	0	0
9	$SH+OH = S+H_2O$	1.00E+13	0	0
10	$SH+O_2 = HSO+O$	1.90E+13	0	9000
11	$S+OH = H+SO$	4.00E+13	0	0
12	$S+O_2 = SO+O$	5.20E+06	1.81	-600
13	$SH+S = S_2+H$	1.00E+13	0	0
14	$S_2+H+M = HS_2+M$	1.00E+16	0	0
15	$S_2+O = SO+S$	1.00E+13	0	0
16	$SO+OH = SO_2+H$	1.08E+17	-1.35	0
17	$SO+O_2 = SO_2+O$	7.60E+03	2.37	1500
18	$2SO = SO_2+S$	2.00E+12	0	2000
19	$HSO+O_2 = SO_2+OH$	1.00E+12	0	5000
20	*$2SH = S_2+H_2$*	*1.00E+12*	*0*	*0*
21	*$S_2+M = 2S+M$*	*4.80E+13*	*0*	*38800*
22	*$HS_2+H = S_2+H_2$*	*1.20E+07*	*2.1*	*352.42*
23	*$HS_2+O = S_2+OH$*	*7.50E+07*	*1.8*	*1460*
24	*$HS_2+OH = S_2+H_2O$*	*2.70E+12*	*0*	*0*
25	*$HS_2+S = S_2+SH$*	*8.30E+13*	*0*	*3700*
26	*$SO+O(+M) = SO_2(+M)$*	*3.20E+13*	*0*	*0*
27	*$SO+M = S+O+M$*	*4.00E+14*	*0*	*54000*
28	*$SO+H+M = HSO+M$*	*5.00E+15*	*0*	*0*
29	*$HSO+H = SH+OH$*	*4.90E+19*	*-1.86*	*785*
30	*$HSO+H = S+H_2O$*	*1.60E+09*	*1.37*	*-170*
31	*$HSO+H = H_2S+O$*	*1.10E+06*	*1.03*	*5230*
32	*$HSO+H = SO+H_2$*	*1.00E+13*	*0*	*0*
33	*$HSO+O = SO_2+H$*	*4.50E+14*	*-0.4*	*0*
34	*$HSO+O = OH+SO$*	*1.40E+13*	*0.15*	*150*
35	*$HSO+OH = SO+H_2O$*	*1.70E+09*	*1.03*	*235*
36	*$S+OH = SH+O$*	*6.30E+11*	*0.5*	*4030.55*
37	*$SH+O_2 = SO+OH$*	*1.00E+12*	*503*	*2.48*

APPENDIX B: BRUTE-FORCE ALGORITHM FOR DERE APPROACH

```
import java.io.BufferedReader;
import java.io.FileReader;
import java.io.IOException;
import java.util.Scanner;
import java.util.Vector;


public class Exponential {

    public static void main(String[] args) {
      Scanner keyin = new Scanner(System.in);
      int N=0;
      double total=0;
      String ifname;
      Vector<Vector<Double>> solns = new Vector<Vector<Double>>();
      Vector<Vector<Integer>> solnIdxs = new Vector<Vector<Integer>>();
      double[] a=null;

      System.out.println("File name? > ");
            ifname = keyin.nextLine();
            try
            {
                  BufferedReader infile = new BufferedReader(new
FileReader(ifname));
                  String line;
                  Vector<Double> nums = new Vector<Double>();
                  while((line=infile.readLine())!=null)
                        nums.add(Double.parseDouble(line.trim()));
                  N=nums.size()-1;
                  a = new double[N];
                  for(int i=0; i<N; i++)
                        a[i] =nums.get(i);

            }
            catch (IOException e)
            {
                  System.out.println("File not found -- please re-enter");
            }

      System.out.println("Total Error Limit? > ");
            total = keyin.nextDouble();

        // find subset closest to 0
        double best = 0;
        int max =0;
        for (int n = 1; n < (1 << N); n++)  {
            double sum = 0;
            Vector<Double> sol= new Vector<Double>();
            Vector<Integer> solidx= new Vector<Integer>();
            for (int i = 0; i < N; i++)
                if (((n >> i) & 1) == 1) {
                  sum = sum + a[i];
                  sol.add(a[i]);
```

```
                    solidx.add(i);
                  }
              if ((Math.abs(sum)<=total)&&(Math.abs(sum) >= Math.abs(best))) {
                    best = sum;
                    if(sol.size()>max)
                          max=sol.size();
                    solns.add(sol);
                    solnIdxs.add(solidx);
              }
          }
          for(int i=0; i<solns.size(); i++)
              if(solns.get(i).size()==max){
                    System.out.println("Equations to be removed:
"+solnIdxs.get(i).toString());
                    System.out.println("Corresponding Values:
"+solns.get(i).toString());
              }
          System.out.println("Closest Error Margin = "+best);


      }

}
```

APPENDIX C: LIST OF PUBLICATIONS

Journal Publications

[1] Selim, H., Gupta, A. K., Sassi, M., "Novel Error Propagation Approach for Reducing H_2S/O_2 Reaction Mechanism," The Journal of Applied Energy, 2012; 93:116-124.

[2] Selim, H., Al Shoaibi, A., Gupta, A. K., "Effect of H_2S in methane/air flames on sulfur chemistry and products speciation," The Journal of Applied Energy, 2011; 88(8):2593-2600.

[3] Selim, H., Al Shoaibi, A., Gupta, A. K., "Experimental examination of flame chemistry in hydrogen sulfide-based flames," The Journal of Applied Energy, 2011; 88(8):2601-2611.

[4] Selim, H., Al Shoaibi, A., Gupta, A. K., "Fate of Sulfur with H_2S Injection in Methane/Air Flames," The Journal of Applied Energy, 2012; 92:57-64.

[5] Selim, H., Al Shoaibi, A., Gupta, A. K., "Effect of CO_2 and N_2 Concentration in Acid Gas Stream on H_2S Combustion," The Journal of Applied Energy, http://dx.doi.org/10.1016/j.apenergy.2012.02.072.

[6] Selim, H., Al Shoaibi, A., Gupta, A. K., "Effect of Reaction Parameters on the Quality of Captured Sulfur in Claus Process," Submitted to The Journal of Applied Energy.

[7] Selim, H., Al Shoaibi, A., Gupta, A. K., "Investigation of Sulfur Chemistry with Acid Gas Addition in Hydrogen/Air Flames," Submitted to The Journal of Applied Energy.

Conference Publications

[1] Selim, H., Gupta, A. K., and Sassi, M., "Variation of Optimum Claus Reactor temperature with Acid Gas Composition," 6th International Energy Conversion Engineering Conference (IECEC), Cleveland, OH, July 28-30, 2008, AIAA-2008-5797.

[2] Selim, H., Gupta, A. K., and Sassi, M., "Reduced Mechanism for Hydrogen Sulfide Oxidation," 47th AIAA Aerospace Sciences Meeting (ASM), Orlando, FL, January 5-8, 2009, AIAA-2009-1392.

[3] Selim, H. and Gupta, A. K., "Nonreactive Study for the Reactants Mixing in Claus Reactions," 7th International Energy Conversion Engineering Conference (IECEC), Denver, CO, August 2-5, 2009, AIAA-2009-4506.

[4] Selim, H., Gupta, A. K., and Sassi, M., "Implementation of Novel Error-Propagation-Based Reduction Approach in H_2S/O_2 Reaction Mechanism," 48th AIAA Aerospace Sciences Meeting (ASM), Orlando, FL, January 3-7, 2010, AIAA-2010-1355.

[5] Al Amoodi, N., Selim, H., Gupta, A. K., Sassi, M., and Al Shoaibi, A., "Numerical Simulations of the Thermal Stage in Claus Process: Equilibrium and Kinetic Investigation," 48th AIAA Aerospace Sciences Meeting (ASM), Orlando, FL, January 3-7, 2010, AIAA-2010-1356.

[6] Selim, H., Vijayan, V., Al Shoaibi, A., and Gupta, A. K., "Numerical and Experimental Studies on Mixing and Product Species Distribution in a Claus Reactor," 8th International Energy Conversion Engineering Conference (IECEC), Nashville, TN, August 2-5, 2010, AIAA-2010-7183.

[7] Selim, H., Al Shoaibi, A., and Gupta, A. K., "Examination of Emission Spectra from Hydrogen Sulfide Flames," 49th AIAA Aerospace Sciences Meeting (ASM), Orlando, FL, January 4-7, 2011, AIAA-2011-440.

[8] Selim, H., Al Shoaibi, A., and Gupta, A. K., "Spatial Speciation of H_2S Combustion in Methane/Air Flame," 9th International Energy Conversion Engineering Conference (IECEC), San Diego, CA, July 31-August 3, 2011, AIAA-2011-5668.

[9] Selim, H., Al Shoaibi, A., and Gupta, A. K., "Effect of CO_2 and N_2 Presence in Acid Gas stream on H_2S Combustion," 50th AIAA Aerospace Sciences Meeting (ASM), Nashville, TN, January 9-12, 2012, AIAA-2012-1000.

[10] Selim, H., Al Shoaibi, A., and Gupta, A. K., "Understanding the Quality of Sulfur Deposit Formation in a Claus Reactor," 10th International Energy Conversion Engineering Conference (IECEC), Atlanta, GA, July 29-August 1, 2012, AIAA-2012-3719.

REFERENCES

[1] Wayne, R. P., "Chemistry of Atmospheres: An Introduction to the Chemistry of the Atmospheres of Earth, the Planets, and Their Satellites," Oxford University Press, USA, 1st edition, ISBN: 0198551754, 1985.

[2] Crutzen, P. J., "The possible importance of COS for the sulfate layer of the stratosphere," Geophysical research letters, 1976; 3(2): 73-76.

[3] Tyndall, G., and Ravishankara, A. R., "Atmospheric Oxidation of Reduced Sulfur Species," International Journal of Chemical Kinetics, 1991; 23(6):483-527.

[4] http://www.osha.gov/SLTC/etools/oilandgas/general_safety/h2s_precautions.html#low_hazard_area.

[5] Kohl, A., and Nielsen R., "Gas Purification," Gulf Publishing Company, Houston TX, 5th edition, ISBN: 0884152200, 1997.

[6] Jou, F., Mather, A. E., and Otto, F. D., "Solubility of H_2S and CO_2 in Aqueous Methyldiethanolamine Solutions," Industrial and Engineering Chemistry Process Design and Development, 1982; 21(4):539-544.

[7] Jensen A. B., and Webb C., "Treatment of H_2S-containing gases: A review of microbiological Alternatives," Enzyme and Microbial Technology, 1995; 17(1):2-10.

[8] Haimour, N., and Sandall, O. C., "Absorption of Hydrogen Sulfide into Aqueous Methyldiethanolamine," Chemical Engineering Communications, 1987; 59(1):85-93.

[9] Ball, T., and Veldman, R., "Improve Gas Treating," Chemical Engineering Progress, 1991; 87(1):67-72.

[10] El-Bishtawi, R., and Haimour, N., "Claus Recycle with Double Combustion Process," Fuel Processing Technology, 2004; 86(3):245-260.

[11] Larraz, R., "Influence of Fractal Pore Structure in Claus Catalyst Performance," Chemical Engineering Journal, 2002; 86(3):309-317.

[12] Mora, R. L., "Sulphur Condensation Influence in Claus Catalyst Performance," Journal of Hazardous Materials, 2000; 79(1):103-115.

[13] Khudenko, B. M., Gitman, G. M., and Wechsler, E. P., "Oxygen Based Claus Process for Recovery of Sulfur from H_2S Gases," Journal of Environmental Engineering, 1993; 119(6):1233- 1251.

[14] Chun, S. W., Jang, J. Y., Park, D. W., Woo, H. C., and Chung, J. S., "Selective Oxidation of H_2S to Elemental Sulfur over TiO_2/SiO_2 Catalysts," Applied Catalysis. B, Environmental, 1998; 16(3):235-243.

[15] Levy, A., Merryman, E. L., and Thomas, W., "Mechanisms of Formation of Sulfur Oxides in Combustion," Environmental Science and Technology, 1970; 4(8):653-662.

[16] Cullis, C. F., and Mulcahy, M. F. R., "The Kinetics of Combustion of Gaseous Sulphur Compounds," Combustion and Flame, 1972; 18(2):225-292.

[17] Schofield, K., "The Kinetic Nature of Sulfur's Chemistry in Flames," Combustion and Flame, 2001; 124(1):137-155.

[18] Hynes, A. J., and Wine, P. H., "Kinetics and Mechanism of the Oxidation of Gaseous Sulfur Compounds," Springer, New York NY, 2nd edition, ISBN: 0387988610, Gas-Phase Combustion Chemistry: Chapter 3, p 343, 2000.

[19] Norrish, R. G. W., and Zeelenberg, A. P., "The combustion of Hydrogen Sulphide Studied by Flash Photolysis and Kinetic Spectroscopy," Proceedings of the Royal Society of London, 1957; 240(1222):293-303.

[20] Levy, A., and Merryman, E. L., “The Microstruct"ure of Hydrogen Sulphide Flames,” Combustion and Flame, 1965; 9(3):229-240.

[21] Muller III, C. H., Schofield, K., Steinberg, M., and Broida, H. P., “Sulfur chemistry in flames,” Symposium (International) on Combustion, 1979; 17(1): 867-879.

[22] Muller III, C. H., Schofield, K., and Steinberg, M., “Laser-Induced Fluorescence: A Powerful Tool for the Study of Flame Chemistry,” ACS Publications, Washington DC, Vol. 134, ISBN13: 9780841205703, Laser Probes for Combustion Chemistry: Chapter 2, p. 103, 1980.

[23] Muller III, C. H., Schofield, K., and Steinberg, M., “Near Saturation Laser Induced Chemical Reactions of $Na(3^2P_{3/2,1/2})$ in $H_2/O_2/N_2$ Flames,” Chemical Physics Letters, 1978;57(3):364-368.

[24] Frenklach, M., Lee, J. H., White, J. N., and Gardnier, JR., W. C., “Oxidation of Hydrogen Sulfide,” Combustion and Flame, 1981; 41:1-16.

[25] Bernez-Cambot, J., Vovelle, C., and Delbourgo, R., “Flame Structures of H_2S–Air Diffusion Flames,” Symposium (International) on Combustion, 1981; 18(1): 777-783.

[26] Smith, O. I., Tseregounis, S., and Wang, S.,“High-Temperature Kinetics of the Reactions of SO_2 and SO_3 with Atomic Oxygen,” International Journal of Chemical Kinetics, 1982; 14(6):679-697.

[27] Zachariah, M. R., and Smith O.I., “Experimental and Numerical Studies of Sulfur Chemistry in $H_2/O_2/SO_2$ Flame,” Combustion and Flame, 1987; 69(2):125-139.

[28] Chernysheva, A. V., Basevich, V. Ya., Vedeneev, V. I., and Arutyunov, V. S.,” Mechanism of Gas-Phase Oxidation of Hydrogen Sulfide at High Temperatures,” Translated from Izvestiya Akademii Nauk SSSR, 1990; Vol. 9, p. 1956.

[29] Tsuchiya, K., Kamiya, K., and Matsui, H., "Studies on the Oxidation Mechanism of H_2S Based on Direct Examination of the Key Reactions," International Journal of Chemical Kinetics, 1999; 29(1):57-66.

[30] Glarborg, P., Kubel, D., Dam-Johansen, K., "Impact of SO_2 and NO on CO Oxidation under Post-Flame Conditions," International Journal of Chemical Kinetics, 1996; 28(10):773-790.

[31] Alzueta, M. U., Bilbao, R., and Glarborg, P., "Inhibition and Sensitization of Fuel Oxidation by SO_2," Combustion and Flame, 2001; 127(4):2234-2251.

[32] Dagaut, P., Lecomte, F., Mieritz, J., and Glarborg, P., "Experimental and Kinetic Modeling Study of the Effect of NO and SO_2 on the Oxidation of CO–H_2 Mixtures," International Journal of Chemical Kinetics, 2003; 35(11):564-575.

[33] Sendt, K., Jazbec, M., and Haynes, B. S., "Chemical Kinetic Modeling of the H/S Systems: H_2S Thermolysis and H_2 Sulfidation," Proceedings of the Combustion Institute, 2002; 29(2):2439-2446.

[34] Blitz, M. A., McKee, K. W., and Pilling, M. J., "Temperature Dependence of the Reaction of OH with SO," Proceedings of the Combustion Institute, 2000; 28(2):2491-2497.

[35] Hughes, K. J., Blitz, M. A., Pilling, M. J., and Robertson, S. H., "A Master Equation Model for the Determination of Rate Coefficients in the H + SO_2 Systems," Proceedings of the Combustion Institute, 2002; 29(2):2431-2437.

[36] Hughes, K. J., Tomlin, A. S., Dupont, V. A., and Pourkashanian, M., "Experimental and Modelling Study of Sulfur and Nitrogen Doped Premixed Methane Flames at Low Pressure," Faraday Discussions, 2001; 119:337-352.

[37] Leeds University, Sulfur mechanism extension to the Leeds methane mechanism; May 2002. http://www.chem.leeds.ac.uk/combustion/sox.htm.

[38] Cerru, F., G., Kronenburg, A., Lindstedt, R. P., "Systematically Reduced Chemical Mechanism for Sulfur Oxidation and Pyrolysis," Combustion and Flame, 2006; 146(3):437-455.

[39] Cerru, F., G., Kronenburg, A., Lindstedt, R. P., "A Comparison of Detailed and Reduced Chemical Mechanism for Sulphur Oxidation," Proceeding of the European Combustion Meeting, 2005.

[40] Laakso, D., Smith, C. E., Goumri, A., Rocha, J. R., and Marshall, P., "Theoretical Studies of the RSOO, ROSO, RSO_2 and HOOS (R=H, CH_3) Radicals," Chemical Physics Letters, 1994; 227(4):377-383.

[41] Schofield, K., and Steinberg, M., "Sodium/Sulfur Chemical Behavior in Fuel-Rich and –Lean Flames," The Journal of Physics and Colloid Chemistry, 1992; 96(2):715-726.

[42] Li, S. Y., Rodriguez, J. A., Hrbek, J., Huang, H. H., and Xu, G. -Q., "Reaction of Hydrogen with S/Mo(110) and MoS_x Films: Formation of Hydrogen Sulfide," Surface Science, 1996; 366(1): 29-42.

[43] Sasaoka, E., Taniguchi, K., Hirano, S., Uddin, M., Sasaoka, S., and Sakata, Y., "Catalytic Activity of ZnS Formed from Desulfurization Sorbent ZnO for Conversion of COS to H_2S," Industrial and Engineering Chemistry Research, 1995; 34(4): 1102-1106.

[44] Rodriguez, J. A., Li, S. Y., Hrbek, J., Huang, H. H., Xu, and G. -Q., " Chemical properties of Zn/S/Mo(110) and Co/S/Mo(110) Surfaces: Reaction with Hydrogen and Formation of Hydrogen Sulfide," The Journal of Physics and Colloid Chemistry, 1996; 100(34):14476-14484.

[45] Kaji, A., and McElroy, W. D., "Mechanism of Hydrogen Sulfide Formation from Thiosulfate," Journal of Bacteriology, 1959; 77(5):630-637.

[46] Schütz, M., and Kunkee, R. E., "Formation of Hydrogen Sulfide from Elemental Sulfur during Fermentation by Wine Yeast," American Journal of Enology and Viticulture, 1977; 28(3):137-144.

[47] Persson, S., Edlund, M., Claesson, R., and Carlsson, J., "The formation of Hydrogen Sulfide and Methyl Mercaptan by Oral Bacteria," Oral Microbiology and Immunology, 1990; 5(4):195-201.

[48] Jones, G. W., Yant, W. P., and Berger, L. B., "The Explosibility of Hydrogen Sulfide in Air," Industrial and Engineering Chemistry, 1924; 16(4):353-355.

[49] Coward, H. F., and Jones, G. W., "Limits of Flammability of Gases and Vapors-Bulletin 503," U.S. Government, 1952.

[50] Bradley, J., N., and Dobson, D. C., "Oxidation of Hydrogen Sulfide in Shock Waves. I., Absorption Studies of OH and SO_2 in H_2SO_2Ar Mixtures," The Journal of Chemical Physics, 1967; 46(8):2865-2871.

[51] Bennett, H. A., and Meisen, A., "Hydrogen Sulphide — Air Equilibria under Claus Furnace Conditions," The Canadian Journal of Chemical Engineering, 1973; 51(6):720-724.

[52] Bennett, H. A., and Meisen, A., "Experimental Determination of Air-H_2S Equilibria under Claus Furnace Conditions," The Canadian Journal of Chemical Engineering, 1981; 95(4):532-539.

[53] Chamberlin, D. S., and Clarke, D. R., "Flame Speed of Hydrogen Sulfide," Industrial and Engineering Chemistry, 1928; 20(10):1016-1018.

[54] Kurz, P. F., "Influence of Hydrogen Sulfide on Flame Speed of Propane-Air Mixtures," Industrial and Engineering Chemistry, 1953; 45(10):2361-2366.

[55] Merryman, E. L., and Levy, A., "Kinetics of Sulfur-Oxide Formation in Flames: II. Low Pressure H_2S Flames," Journal of the Air Pollution Control Association, 1967; 17(12): 800-806.

[56] Merryman, E. L., and Levy, A., "Disulfur and the Lower Oxides of Sulfur in Hydrogen Sulfide Flames," The Journal of Physical and Colloid Chemistry, 1972; 76(14):1925-1931.

[57] Merryman, E. L., and Levy, A., "Sulfur Trioxide Flame Chemistry—H_2S and COS Flames," Symposium (International) on Combustion, 1971; 13(1):427-436.

[58] Merryman, E. L., and Levy, A., "Enhanced SO_3 Emissions from Staged Combustion," Symposium (International) on Combustion, 1979; 17(1):727-736.

[59] Merryman, E. L., and Levy, A., "Sulfur-Oxide Formation in Carbonyl Sulfide Flames," Environmental Science and Technology, 1969; 3(1):63-68.

[60] Hedley, A., B., "Factors Affecting the Formation of Sulphur Trioxide in Flame Gases," Journal of the Institute of Fuel, 1967; 40:142-151.

[61] Azatyan, V. V., Gershenson, U. M., Sarkissyan, E. N., Sachyan, G. A., and Nalbandyan, A. B., "Investigation of Low-Pressure Flames of a Number of Compounds Containing Sulfur by the ESR Method," Symposium (International) on Combustion, 1969; 12(1):989-994.

[62] Sachyan, G. A., and Nalbandyan, A. B., Izvestiya Akademii Nauk SSSR, 1964; 7: 1340.

[63] Gershenson, U. M., Nalbandyan, A. B., and Sachyan, G. A., Doklady Akademii Nauk SSSR, 1965; 163: 927.

[64] Sachyan, G. A., and Nalbandyan, A. B., Armyanskii Khimicheskii Zhurnal, 1966; 19: 135.

[65] Sachyan, G. A., Gershenson, U. M., and Nalbandyan, A. B., Doklady Akademii Nauk SSSR, 1967; 175: 1328.

[66] Sachyan, G. A., Gershenson, U. M., and Nalbandyan, A. B., Kinetika i Kataliz, 1967; 8: 949.

[67] Sarkissyan, E. N., Azatyan, V. V., and Nalbandyan, A. B., Doklady Akademii Nauk SSSR, 1964; 158: 179.

[68] Sarkissyan, E. N., Azatyan, V. V., and Nalbandyan, A. B., Doklady Akademii Nauk SSSR, 1966; 168: 1354.

[69] Sharma, A., Padur, J. P., and Warneck, P., "The Chemiluminescent Reactions of Atomic Oxygen with Carbonyl Sulfide and Hydrogen Sulfide," The Journal of Physical Chemistry, 1967; 71(6): 1602-1607.

[70] Liuti, G., Dondes, S., and Harteck, P., "The Reaction of Hydrogen Sulfide and Atomic Oxygen," Journal of the American Chemical Society, 1966; 88(14):3212-3215.

[71] Dowling, N. I., Hyne, J. B., and Brown, D. M., "Kinetics of the Reaction between Hydrogen and Sulfur under High-Temperature Claus Furnace Conditions," Industrial and Engineering Chemistry Research, 1990; 29(12):2327-2332.

[72] Chen, M. S. K., Hegarty, W. P., and Sampat, D. J., "Production of Sulfur from an Oxygen-Enriched Claus System," U.S. Patent 4,632,818, 1986.

[73] Monnery, W. D., Hawboldt, K. A., Pollock, A., and Svrcek, W. Y., "New Experimental Data and Kinetic Rate Expression for the Claus Reaction," Chemical Engineering Science, 2000; 55(21):5141-5148.

[74] Hawboldt, K. A., Monnery, W. D., and Svrcek, W. Y., "New Experimental Data and Kinetic Rate Expression for H_2S Pyrolysis and Re-Association," Chemical Engineering Science, 2000; 55(5):957-966.

[75] Monnery, W. D., Hawboldt, K. A., Pollock, A., and Svrcek, W. Y., "Ammonia Pyrolysis and Oxidation in the Claus France," Industrial and Engineering Chemistry Research, 2001; 40(1):144-151.

[76] Shiina, H., Oya, M., Yamashita, K., Miyoshi, A., and Matsui, H., "Kinetic Studies on the Pyrolysis of H_2S," The Journal of Physical and Colloid Chemistry, 1996; 100(6):2136-2140.

[77] Binoist, M., Labegorre, B., and Monnet, F., "Kinetic Study of the Pyrolysis of H_2S," Industrial and Engineering Chemistry Research, 2003; 42(17):2943-2951.

[78] Harvey, W. S., Davidson, J. H., and Fletcher, E. A., "Thermolysis of Hydrogen Sulfide in the Temperature Range 1350-1600 K," Industrial and Engineering Chemistry Research, 1998; 37(6):2323-2332.

[79] Fukuda, K., Dokiya, M., Kameyama, T., and Kotera, Y., "Catalytic Decomposition of Hydrogen Sulfide," Industrial and Engineering Chemistry Fundamentals, 1978; 17(4):243-248.

[80] Bishara, A., Salman, O. A., Khraishi, N., and Marafi, A., "Thermochemical Decomposition of Hydrogen Sulfide by Solar Energy," International Journal of Hydrogen Energy, 1987; 12(10):679-685.

[81] Slimane, R. B., Lau, F. S., Khinkis, M., Bingue, J. P., Saveliev, A. V., and Kennedy, L. A., "Conversion of Hydrogen Sulfide to Hydrogen by Superadiabatic Partial Oxidation: Thermodynamic Consideration," International Journal of Hydrogen Energy, 2004; 29(14):1471-1477.

[82] Montoya, A., Sendt, K., and Haynes, B. S., "Gas-Phase Interaction of H_2S with O_2: A Kinetic and Quantum Chemistry Study of the Potential Energy Surface," The Journal of Physical and Colloid Chemistry, 2005; 109(6):1057-1062.

[83] Steiger, T., and Steudel, R., "Sulphur Compounds: Part 149. Structures, Relative Stabilities and Vibrational Spectra of Several Isomeric Forms of Sulphoxylic Acid (H_2SO_2) and Its Anion (HSO_2^-): an ab Initio Study," Journal of Molecular Structure: THEOCHEM, 1992; 257(3):313-323.

[84] Laakso, D., and Marshall, P., "An ab Initio Study of Sulfinic Acid and Related Species," The Journal of Physical and Colloid Chemistry, 1992; 96(6):2471-2474.

[85] Gaydon, A. G., "The Spectroscopy of Flames," Chapman and Hall, London, 2nd edition, ISBN: 0470294337, 1974.

[86] Lewis, M., and White, J. U., "The Band Spectrum of HS," Physical Review, 1939; 55(10):894-898.

[87] Fuwa, K., and Vallee, B. L., "Molecular Flame Absorption Spectrometry for Sulfur," Analytical Chemistry, 1969; 41(1):188-190.

[88] Fuwa, K., and Vallee, B. L., "The Physical Basis of Analytical Atomic Absorption Spectrometry," Analytical Chemistry, 1963; 35(8):942-946.

[89] Ding, Y., Naumenko, O., Hu, S., Zhu, Q., Bertseva, E., and Campargue, A., "The Absorption Spectrum of H_2S between 9540 and 10000 cm^{-1} by Intracavity Laser

Absorption Spectroscopy with a Vertical External Cavity Surface Emitting Laser," Journal of Molecular Spectroscopy, 2003; 217(2):222-238.

[90] Naumenko, O., and Campargue, A., "$H_2{}^{32}S$: First Observation of the ($70^{\pm}$,0) Local Mode Pair and Updated Global Effective Vibrational Hamiltonian," Journal of Molecular Spectroscopy, 2001; 210(2):224-232.

[91] Tyuterev, V. G., Tashkun, S. A., and Schwenke, D. W., "An Accurate Isotopically Invariant Potential Function of the Hydrogen Sulphide Molecule," Chemical Physics Letters, 2001; 348(3):223-234.

[92] Syty, A., "Determination of Sulfide by Evolution of Hydrogen Sulfide and Absorption Spectrometry in the Gas Phase," Analytical Chemistry, 1979; 51(7):911-914.

[93] Toyoda, M., Ogawa, T., and Ishibashi, N., "Emission Spectra of Carbon Disulfide, Hydrogen Sulfide, and Thiols by Controlled Electron Impact," Bulletin of the Chemical Society of Japan," 1974; 47(1):95-98.

[94] Wood, R. W., "An Extension of the Balmer Series of Hydrogen and Spectroscopic Phenomena of very Long Vacuum Tubes," Proceedings of the Royal Society of London, 1920; 97(687):455-470.

[95] Parigger, C. G., Plemmons, D. H., and Oks, E., "Balmer Series H_β Measurements in a Laser-Induced Hydrogen Plasma," Applied Optics, 2003; 42(30):5992-6000.

[96] Fowler, A., and Vaidya, W. M., "The Spectrum of the Flame of Carbon Disulphide," Proceedings of the Royal Society of London, 1931; 132(819):310-330.

[97] Gaydon, A. G., and Whittingham, G., "The Spectra of Flames Containing Oxides of Sulphur," Proceedings of the Royal Society of London, 1947; 189(1018):313-325.

[98] Gaydon, A. G., "Spectrum of the Afterglow of Sulphur Dioxide," Proceedings of the Royal Society of London, 1934; 146(859):901-910.

[99] Mulcahy, M. F. R., and Williams, D. J., "Chemiluminescent Emission from the $O(^3P)$-SO_2 System," Chemical Physics Letters, 1970; 7(4):455-458.

[100] Halstead, C. J., Thrush, B. A., "The Kinetics of Elementary Reactions Involving the Oxides of Sulphur. II. Chemical Reactions in the Sulphur Dioxide Afterglow," Proceedings of the Royal Society of London, 1966; 295(1443):363-379.

[101] Pepiot-Desjardins, P., and Pitsch, H., "An Efficient Error-Propagation-Based Reduction Method for Large Chemical Kinetics Mechanisms," Combustion and Flame, 2008; 154(1):67-81.

[102] Lu, T., and Law, C. K., "Linear Time Reduction of Large Kinetic Mechanisms with Directed Relation Graph: n-Heptane and Iso-Octane," Combustion and Flame, 2006; 144(1):24-36.

[103] Korf, R. E., "Depth-First Iterative-Deepening An Optimal Admissible Tree Search," Artificial Intelligence, 1985; 27(1):97-109.

[104] Cullity, B. D., "Elements of X-Ray Diffraction," Prentice Hall, Upper Saddle River NJ, 3rd edition, ISBN: 0201610914, 2011.

[105] Selim, H., Gupta, A. K., and Sassi, M., "Implementation of Novel Error-Propagation-Based Reduction Approach in H_2S/O_2 Reaction Mechanism," 48th AIAA Aerospace Sciences Meeting (ASM), Orlando FL, January 3-7, 2010, AIAA-2010-1355.

[106] Selim, H., Gupta, A. K., and Sassi, M., "Novel Error Propagation Approach for Reducing H_2S/O_2 Reaction Mechanism," The Journal of Applied Energy, 2012; 93:116-124.

[107] Sofranko, J. A., Leonard, J. J., and Jones, C. A., "The Oxidative Conversion of Methane to Higher Hydrocarbons," Journal of Catalysis, 1987; 103(2):302-310.

[108] Selim, H., Al Shoaibi, A., Gupta, A. K., "Effect of H_2S in methane/air flames on sulfur chemistry and products speciation," The Journal of Applied Energy, 2011; 88(8):2593-2600.

[109] Thacker, C. M., and Miller, E., "Carbon Disulfide Production," Industrial and Engineering Chemistry, 1944; 36(2):182-184.

[110] Karan, K., and Behie, L. A., "CS_2 Formation in the Claus Reaction Furnace: A Kinetic Study of Methane–Sulfur and Methane–Hydrogen Sulfide Reactions," Industrial and Engineering Chemistry Research, 2004; 43(13):3304-3313.

[111] Selim, H., Gupta, A. K., and Sassi, M., "Variation of Optimum Claus Reactor temperature with Acid Gas Composition," 6th International Energy Conversion Engineering Conference (IECEC), Cleveland, OH, July 28-30, 2008, AIAA-2008-5797.

[112] Clark, P. D., Dowling, N., Huang, M., Svrcek, W. Y., and Monnery, W. D., "Mechanisms of CO and COS Formation in the Claus Furnace," Industrial and Engineering Chemistry Research, 2001; 40(2):497508.

[113] Murakami, Y., Kosugi, M., Susa, K., Kobayashi, T., and Fujii, N., "Kinetics and Mechanism for the Oxidation of CS_2 and COS at High Temperature," Bulletin of the Chemical Society of Japan, 2001; 74(7):1233-1240.

[114] Gargurevich, I. A., "Hydrogen Sulfide Combustion: Relevant Issues under Claus Furnace Conditions," Industrial and Engineering Chemistry Research, 2005; 44(20):7706-7729.

[115] Halstead, C. J., and Thrush, B. A., "The Kinetics of Elementary Reactions Involving the Oxides of Sulphur. III. The Chemiluminescent Reaction between Sulphur Monoxide and Ozone," Proceedings of the Royal Society of London, 1966; 295(1443):380-398.

[116] Henri, V., and Wolff, F., "Training, Predissociation and Dissociation of Molecules Determined by the Vibrational Spectra. Study of Sulfur Monoxide SO," Journal of Physics. Radium, 1929, English translation; 10(3):81-106.

[117] Clyne, M. A. A., Halstead, C. J., and Thrush, B. A., "The Kinetics of Elementary Reactions Involving the Oxides of Sulphur. I. The Nature of the Sulphur Dioxide Afterglow," Proceedings of the Royal Society of London, 1966; 295(1443):355-362.

[118] Higgins, B., and Siebers, D., "Measurement of the Flame Lift-Off Location on DI Diesel Sprays Using OH Chemiluminescence," SAE Technical Paper, 2001; 2001-01-0918.

[119] Harber, L. C., and Vandsburger, U., "A Global Reaction Model for OH* Chemiluminescence Applied to a Laminar Flat-Flame Burner," Combustion Science and Technology, 2003; 175(10):1859-1891.

[120] Smith, J. D., and Sick, V., "High-Speed Fuel Tracer Fluorescence and OH Radial Chemiluminescence Imaging in a Spark-Ignition Direct-Ignition Engine," Applied Optics, 2005; 44(31):6682-6691.

[121] Walsh, K. T., Long, M. B., Tanoff, M. A., and Smooke, M. D., "Experimental and Computational Study of CH, CH*, and OH* in an Axisymmetric Laminar Diffusion Flame," Symposium (International) on Combustion, 1998; 27(1):615-623.

[122] Gaydon, A. G., "General Discussion," Transactions of the Faraday Society, 1946; 42:363-366.

[123] Dooley, A., and Whittingham, G., "The Oxidation of Sulphur Dioxide in Gas Flames," Transactions of the Faraday Society, 1946; 42:354-362.

[124] Park, J., Lee, K., and Lee, E., "Effects of CO_2 Addition on Flame Structure in Counterflow Diffusion Flames of $H_2/CO_2/N_2$ Fuel," International Journal of Energy Research, 2001; 25(6):469-485.

[125] Hughes, K. J., Turanyi, T., Clague, A. R., and Pilling, M. J., "Development and Testing of a Comprehensive Chemical Mechanism for the Oxidation of Methane," International Journal of Chemical Kinetics, 2001; 33(9):513-538.

[126] http://www.ihs.com/products/chemical/planning/ceh/sulfur.aspx#

[127] Abrahamas, S. C., "The crystal and Molecular Structure of Orthorhombic Sulfur," ACTA Crystallography, 1955; 8:661-671.